Evaluation of Bi-Velocity Methods in Two-Fluid Model for Granular flows: application to fluidized beds

Corey Claire Badger

Submitted for the degree of Doctor of Philosophy

Heriot-Watt University

Institute of Mechanical, Process and Energy Engineering

March 2018

ABSTRACT

Rapid Granular Flows occur in a number of natural and industrial processes therefore the need to accurately describe these flows is apparent. The Euler-Euler based model of Kinetic Theory of Granular Flows is used to model fluidized bed systems within this thesis. Kinetic Theory of Granular Flows is still flawed in its development due to assumptions and simplifications required. This model needs further development to capture other various flow effects. This thesis will further develop the Kinetic Theory of Granular Flows by adding a correction of the Navier-Stokes equations and including non-Newtonian flow characteristics. It has been noted recently that the Navier-Stokes-Fourier equations do not describe compressible flows accurately. This has been attributed to the definition of fluid velocity in the derivation of fluid flow equations. In the incompressible flow regime, the derivation of the fluid flow is based on the velocity of the mass of the fluid. When fluids become compressed the mass flux will not change but the volume flux does change and gives an additional Volume velocity which affects the viscosity of the fluid. Korteweg Stress model provides another route to capture non-Newtonian phenomenon. These corrections to the Navier-Stokes system are extended and investigated into some Rapid Granular-Gas Flow equations in this thesis.

The modifications to the Kinetic Theory of Granular Flows of the compressible volume velocity and the Korteweg approach are considered and tested on simple systems of a fluidized cylinder bed and a recirculating fluidized bed. A six-cyclone recirculating fluidized bed is then used as a larger and more complex system. It been found that by combining both modifications the overall results were improved.

DEDICATION

I would like to dedicate this work to my partner in life and to my close friends and family for all their support through the ups and downs that is the life of a PhD.

ACKNOWLEDGEMENTS

I would like to give my thanks and acknowledgements to Dr S. Kokou Dadzie and Professor Raffaella Ocone at Heriot-Watt University, and Professor Jason Reese and Dr Matthew Borg at the University of Edinburgh for their help and support throughout my time at both universities.

ACADEMIC REGISTRY

Research Thesis Submission

Name*:*			
School:			
Version: *(i.e. First, Resubmission, Final)*		Degree Sought:	

Declaration

In accordance with the appropriate regulations I hereby submit my thesis and I declare that:

1) the thesis embodies the results of my own work and has been composed by myself
2) where appropriate, I have made acknowledgement of the work of others and have made reference to work carried out in collaboration with other persons
3) the thesis is the correct version of the thesis for submission and is the same version as any electronic versions submitted*.
4) my thesis for the award referred to, deposited in the Heriot-Watt University Library, should be made available for loan or photocopying and be available via the Institutional Repository, subject to such conditions as the Librarian may require
5) I understand that as a student of the University I am required to abide by the Regulations of the University and to conform to its discipline.
6) I confirm that the thesis has been verified against plagiarism via an approved plagiarism detection application e.g. Turnitin.

* *Please note that it is the responsibility of the candidate to ensure that the correct version of the thesis is submitted.*

Signature of Candidate*:*		Date:	

Submission

Submitted By *(name in capitals):*	
Signature of Individual Submitting:	
Date Submitted:	

For Completion in the Student Service Centre (SSC)

Received in the SSC by *(name in capitals):*			
1.1 Method of Submission *(Handed in to SSC; posted through internal/external mail):*			
1.2 E-thesis Submitted (mandatory for final theses)			
Signature:		Date:	

Please note this form should be bound into the submitted thesis.

TABLE OF CONTENTS

LISTS OF TABLES

LISTS OF FIGURES

NOMENCLATURE

A	Area, m^2
C_D	Drag coefficient
C_p	Specific Heat Capacity, J/kgK
D_i	Shear tensor
D_p	Particle diameter, m
D_{vs}	Solid Phase Volume Diffusion Coefficient, m^2/s
e	Coefficient of Restitution
F	Force, N
g	Gravity, $9.81 m/s^2$
g_0	Radial Distribution
I	Identity Matrix
J_i	Volume Diffusivity Flux Density of Phase i, m/s
J_v	Volume Diffusivity Flux Density, m/s
k	Thermal Conductivity, check
P	Pressure, N/m^2 (Pa)
P_s	Solid phase pressure, N/m^2 (Pa)
Re_p	Particle Reynolds number
t	Time, s
T	Korteweg Stress tensor, N/m^2 (Pa)
U	Velocity, m/s
U_m	Mass Velocity, m/s
U_v	Volume Velocity, m/s
$\bar{v}$	Partial specific volume, m^3/kg
v_t	Particle terminal velocity, m/s
w	Mass fraction

Greek Letters

α_g	Gas phase volume fraction
α_s	Solid phase volume fraction
β	Interphase momentum exchange, (need to check)
β_0	Tangential Coefficient of Restitution
θ	Granular Temperature, m^2/s^2
λ	Bulk viscosity, Pa.s
μ	Shear viscosity, Pa,s
μ_f	Friction Coefficient
μ_g	Gas phase dynamic viscosity, Pa.s
ν	Kinematic viscosity, m^2/s
ρ	Density, kg/m^3
τ	Stress tensor, Pa

Subscripts

g	Gas phase
i	i^{th} phase
m	Mass
s	Solid phase
v	Volume

Chapter 1: Introduction

Multiphase flows occur in many natural and industrial processes which can range from avalanches and volcanic eruptions to industrial reactors and food production. As these flows can be found in such a wide range of situations from natural mud flows and domestic vacuum cleaners to jet engines and manufacturing pharmaceuticals that the ability for understanding these systems of flow and modelling them accurately is needed.

A multiphase system consists of two or more fluids, known as phases of the flow and can be a mixture of solids, liquids and gases. The solid phase generally consists of many solid particles such as sand or powder. The solid particles have unique properties in which the particles can be agitated to act like a liquid. If enough agitation occurs and the particles are moving sufficiently, it can also be described as moving like a gas. But unlike two fluids, the interaction between the particle phase and a fluid phase is affected by each other in a unique way. This work is limited to rapid granular-gas flows, which generally consist of a gas phase and a granular phase made up of many solid particles.

Rapid granular-gas flows can be abrasive against surfaces, which needs to be understood. For applications such as sand blasting the correct ratios of particles to fluid as well as the machinery needed to combine and deliver the flow to the desired area needs to be considered. The abrasion effect can also damage and wear down equipment and machinery used for the rapid granular flows. One example is that within a fluidized bed reactor the particles are constantly moving against parts within the reactor, and will be in contact with some parts more than others such as the walls within cyclone separators or cooling pipes within the reactors. This abrasive action could lead to damage to the surfaces, causing leaks to occur, which can be catastrophic if dangerous chemicals were able to escape and contaminate the environment or mix with other chemicals present causing unwanted reactions. Therefore, by modelling the fluidized bed reactor it would be possible to asses in the design stage where abrasion damage could be occurring and design against it effectively.

In this chapter an introduction to the methods for modelling multiphase flows is discussed, followed by the main application studied in this thesis, which is the fluidized bed system. The software is discussed in its current form, and its advantages and disadvantages are briefly described. Finally, the scope of this thesis will be outlined, with the goals of the research and development.

1.1 Multiphase Modelling Methods

There are two methods for solving multiphase flows; Eulerian based methods and Lagrangian based methods. Eulerian based methods assume that all phases act like fluids and have momentum and energy interphase exchanges accordingly. For the granular phase it will involve the simplification of the granular phase interactions and averaging the granular phase material properties, with the drawback that information on the particle scale is lost and not all flow characteristics or particle interactions are able to be accounted for. This method is normally used for large simulations as the simplifications make it computationally cost-effective. The Lagrangian based methods track the speed and direction of each individual particle and can capture the effects of collisions easily. However, with the increased particle level information comes a significantly large computing cost in terms of time and processing power. This has limited these kinds of solver methods to lab-scale flow investigations and other model validations. In an ideal situation Lagrangian based methods would be used, as they can accurately capture the flow characteristics and particle interactions, but due to the high computing cost it is not practical for most large-scale flows that occur in both industry and with natural phenomenon.

The Eulerian method for multiphase flows is typically known as the Two Fluid Model (TFM) where two fluids are interpenetrating continua, such as air bubbles up a water column. For rapid granular gas flows, the granular phase is considered to act like a fluid, therefore the governing equations have a similar form to the Navier-Stokes hydrodynamic equations called the Kinetic Theory of Granular Flow (KTGF). This method is based on molecular dynamics but differs as collisions between particles are considered to be dissipative due to the particles' inelastic properties (whereas molecular collisions are fully elastic). Additional particle interactions are included such as particle stresses and interparticle friction. From the literature there are numerous formulations for different aspects of KTGF as no single method can account for the full range of flow densities. Many model formulations are based on empirical data, as opposed to a true understanding of the flow characteristics. Part of this problem is due to the treatment of the granular phase as a fluid with additional interactions added in to the original KTGF.

There are advantages and disadvantages for using either Eulerian or Lagrangian based methods for solving multiphase flows, and this is a very large area of active research. There are many areas within each method that have been further refined and these will be discussed further in the literature review in Chapter 2.

1.2 Fluidized Bed System Characteristics

Fluidized beds are used primarily in the chemical processing industries for mixing, reaction and drying processes. For Rapid Granular Gas flows there is an advantage to using fine particulates as the smaller the particle size, the greater the surface area that can be in contact with the gas passing through the fluidized bed system for a given mass of particles. A fluidized bed generally consists of a vessel containing a large quantity of solid particles, with an inlet at the base of the vessel where a gas phase is introduced to move the particles.

There are a number of fluidized bed configurations and only a few will be described here for brevity. The most useful variations in the fluidized bed are due to the type of gas inlet at the base of the vessel. In Figure 1, the first is a uniformly distributed gas inlet, where a porous plate at the base of the vessel allows the gas phase to pass through and not the solids phase. Small bubbles are produced near the base of the vessel and rise up while coalescing into larger bubbles. The second is known as the jet inlet, where one or more small inlets are at the base of the vessel and have a very high gas phase inlet velocity. An issue with this inlet orientation is that the particles near the base on either side of the inlet tend not to move so are not circulated in the system. The third is a spouting fluidized bed, where the base of the vessel slants towards a small gas inlet with a small porous plate or screen to allow for the gas phase to enter the vessel and the particles not to leave through the base. The funnel shape at the base of the vessel allows for particles to move towards the gas inlet to be entrained into the main flow, enabling all the particles to be circulated in the system.

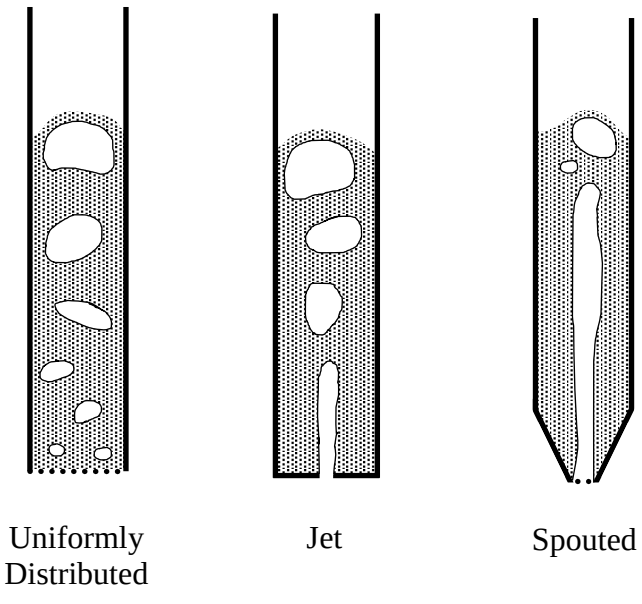

Figure 1 - Fluidized bed inlet types.

Another consideration for the fluidized bed is the rate of gas flow into the vessel can affect its fluidizing behaviour. Figure 2 shows a range of fluidizing behaviours in a vessel with a uniformly distributed inlet. For very fine particles in a vessel it is possible to have delayed bubble formation occurring at a gas inlet velocity above the minimum fluidization velocity. The minimum fluidization velocity is the minimum gas inlet velocity that can sustain fluidization. In a bubbling flow, small bubbles are formed and rise towards the top of the solids bed and by this action move the particles in a liquid-like state. Slugging flow occurs with much larger and heavier particles than the bubbling regime, and bubbles can coalesce into large bubbles across the width of the fluidized bed, generating slug-like movements of gas and particles. Rapid or fast fluidizing flow occurs when the gas velocity becomes sufficiently large enough to suspend and carry the particles towards the top of the fluidized bed. In this regime the particles can be said to be acting more like a gas. Once the particles reach the top of the vessel they are separated from the gas flow by a cyclone separator and returned to the main vessel near the base. This particular fluidized bed configuration is known as a recirculating fluidized bed as the particles are recirculated throughout the whole system.

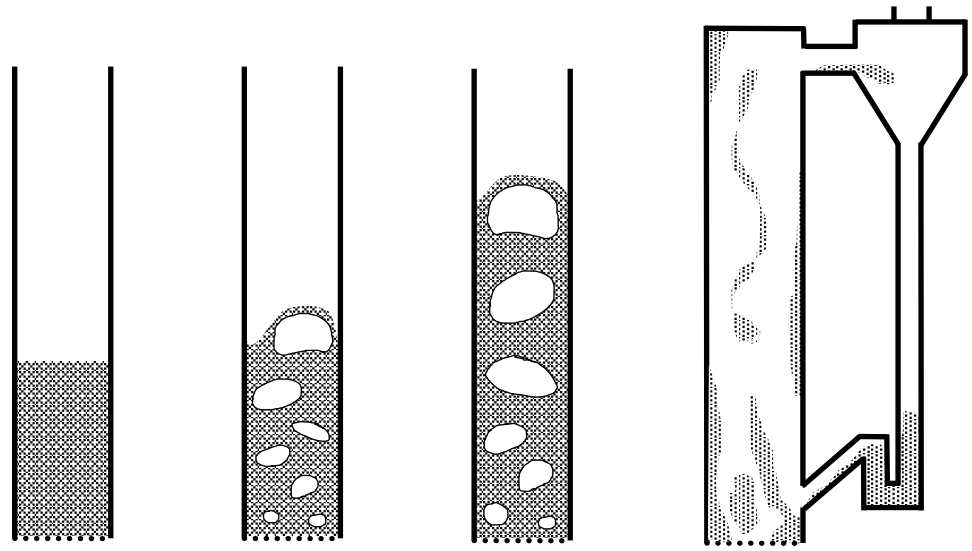

Figure 2 - Fluidizing regimes.

While it is possible to create lab-scale experimental models, these cannot be scaled to industrial dimensions due to the nonlinear nature of fluidized flows. This is because the systems are very chaotic and are still not very well understood. Therefore, there is a need to model industrial-scale systems to better design and predict the performance of the system.

1.3 Scope of Thesis

The scope of this thesis is to research, develop and test a novel way of improving the current Kinetic Theory of Granular Flows (KTGF) method to better describe the hydrodynamic motion of rapid-granular flows. Brenner (2005) has suggested that for compressible flows two different velocities need to be considered. The reason for this is that the velocity of the fluid considered in the Navier-Stokes equations are based on the mass flux only. When flows are compressible, the mass flux will not change but the volume flux will. Therefore, two different velocities need to be considered; the mass velocity of the fluid and the volume velocity of the fluid. This affects the shear viscosity of the fluid as it is dependent on the volume velocity as opposed to the mass velocity typically used. By considering the compressible effects within KTGF it would be possible to extend the range of flows that could be simulated using this method. Another consideration for the compressibility is adding the well-known Korteweg stress, as first developed by Korteweg (1901) for multiple phase flows in which phase transitional phenomena in fluids can be simulated. It was noted that when there are two fluids with different densities and viscosities, additional stresses are created. By testing and combining these into the KTGF for the granular phase it is hoped to create a more well-founded model for rapid granular gas flows. These modifications will be made to the KTGF model and tested on 3 different fluidized bed systems. The use of fluidized beds is due to there being a significant amount of both experimental and simulation data available for a range of fluidized beds to compare and validate this new model. Also, fluidized bed systems are needed for a number of industrial processes and so understanding the behaviour of particulates is crucial for good design and efficient processes.

This thesis is arranged in the following manner; a literature review of the current issues and considerations of modelling rapid granular gas flows and their applications is presented, followed by a detailed discussion of the equations involved in KTGF and the modifications for both Volume Diffusion Flux and Korteweg Stress are laid out. For each modification there are two different models presented, each will be tested individually before deciding on a single model for that modification. Simulations in simple geometries are presented in Chapter 4, with a comparative study between different solver software available. This will allow for the modifications to be tested individually in two different flow regimes. Chapter 5 presents a complex fluidized bed case for each modification individually, from which results will determine the best performing model and combine

into a single solver and compared. The final chapter summarizes the research completed and the simulation analysis. The conclusion discusses whether the modifications of Volume Diffusion Flux and Korteweg Stress were successful in better predicting the overall flow, and whether they are useful.

Chapter 2: Literature Review

In this chapter a literature review is conducted and forms the basis of understanding of rapid granular flows. Firstly, understanding the different flow regimes and their impact on the way in which the solvers are interpreted is followed by a discussion of the ways in which granular-gas flows can be modelled. This moves on to a comparison of the different ways in which the particle-particle and particle-fluid interactions can be dealt with. The final section is a brief discussion of realistic particle distributions with multiple phases, and the applications for granular-gas modelling are presented.

2.1 Flow Regimes

Granular flows can be classed into various flow regimes that describe different aspects of granular-gas flows such as particle density or solid volume fraction. The first flow regime to be discussed differentiates granular flows by how they act, e.g. like a solid, liquid or gas. This behaviour is determined by the particle concentration and the degree of excitation the particles are subjected to. The regime focussed on in this work is the gas-like regime known as rapid granular flows. This regime has been described using the Kinetic Theory of Granular Flow (KTGF), which is based on the dynamical description of gases. This and other methods will be discussed in the following sections. There are other flow regimes, but these will only be briefly discussed here.

Elghobashi (1994) has defined a set of flow regimes through the solid volume fraction. This method allows for the determination of which particle/gas coupling scheme is expected. The first is known as the dilute regime, when the solid volume fraction is less than 0.1% and experiences one-way coupling. In this regime, the particles have a negligible effect on the gas phase, but the gas phase influences the particle phase. The second regime is known as the dense regime where the solid volume fraction is greater than 0.1%. In this regime, the gas phase is affected by the presence of the particles, and the gas phase affects the particles, so two-way coupling is required. The final regime is the very dense regime and occurs at solid volume fractions of much greater than 0.1%, where particle collisions start to affect the gas phase as well as the solid phase, this is known as four-way coupling. It is possible that if the solid volume fraction is high enough the gas phase can be neglected, but this does not apply to rapid granular flows. This is because the interparticle forces will become dominant in such flows as chutes or hopper flows. The particles are moving very independently of the gas phase.

The determination of whether a flow is governed by gas turbulence or particle collisions uses the characteristic time scale as described by Zhang and Reese (2001), who define 3 different time scales; the characteristic time scale of eddies, the mean particle relaxation time and the mean particle collision time. If the mean particle relaxation time is much less than the characteristic time scale of the eddies, then the particle motion is controlled by the gas flow. If the mean particle collision time is much smaller than the mean particle relaxation time, then the flow is controlled by the particle collisions. When the mean particle relaxation time is not much larger than the mean particle collision time, the gas turbulence affects the flow.

Geldart (1973) classifies 4 distinct regimes which describe different flow characteristics within fluidized bed systems. These are classified by the relative density between the solid and fluid phases, and the particle diameters, as can be seen in Figure 3.

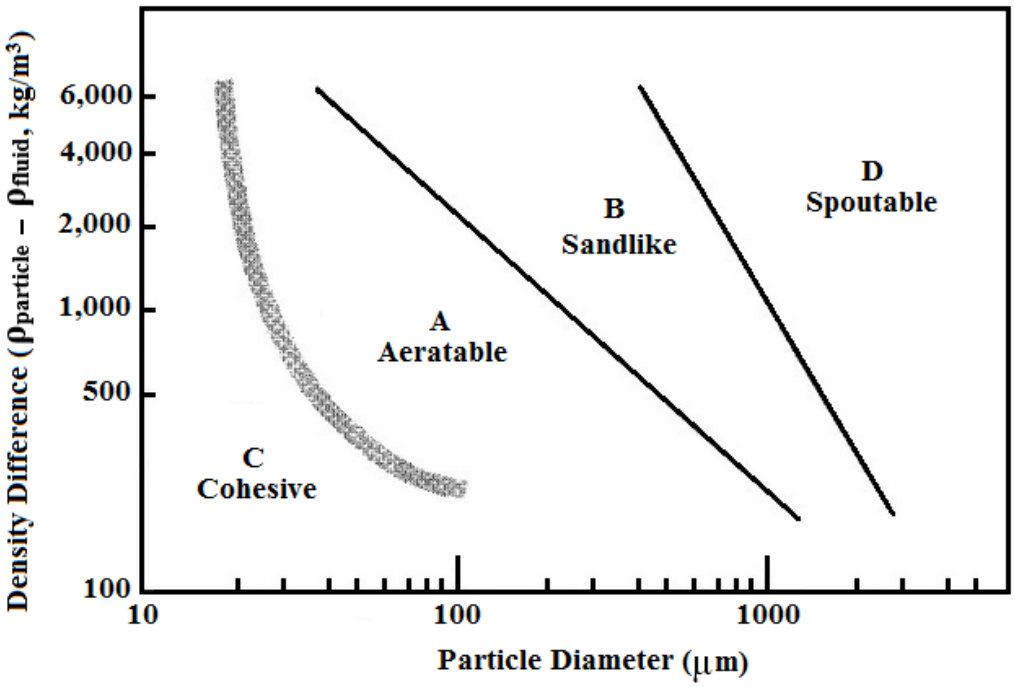

Figure 3- Geldarts classifications (Geldart, 1973).

The four groups are described as follows:

Group A – Aeratable

When the gas is first introduced to the system the bed first expands with a large initial bubble rising towards the top of the solid phase in the vessel where the bubble then breaks and then a regular formation of bubbles can be seen. This group can have either a small mean diameter or a low particle density.

Group B – Sand-like

In this group, there is not as much bed expansion as found with group A type particles and bubbles are formed more readily when just above the minimum fluidization velocity. A large proportion of materials come under this group.

Group C – Cohesive

The particle size is small enough so that inter-particle forces, such as Van der Waals and liquid bridge force, are large enough to prevent the fluid forces moving the particles easily, resulting in poor mixing. Instead either the bed lifts in a single slug in small diameter beds or creates small holes that go from the distributor plate to the surface in larger fluidized beds. Normally mechanical mixers are used to help aid fluidization and mixing.

Group D – Spoutable

These are typically either the heaviest or biggest particles which require very high fluidization velocities and mix poorly, though these particles are easily spouted. This group is named for its ability to move particles with a lot of momentum.

Another way to define the flow regimes is to relate to the Knudsen number. The Knudsen number helps to determine when rarefication effects occur. In terms of a gas system the Knudsen number (*Kn*) is the ratio of the mean free path (λ) of a gas molecule and a characteristic length scale (*L*). For example, the characteristic length scale used for microchannel flows is the width or across the streamwise length of the channel. The Knudsen number for gas flows is given as:

$$Kn = \frac{\lambda}{L}.$$

If $Kn << 1$, then the gas is acting like a continuum fluid on the characteristic length scale, *L*. If $Kn >> 1$, the flow is considered to be in the Knudsen regime and rarefied gas dynamics are applied.

To determine the Knudsen number for a granular-gas flow system the characteristic length scale is based on the diameter of the particle and the mean free path on the distance before a gas molecule encounters another gas molecule. Therefore, the Knudsen number is defined as:

$$Kn = \frac{\lambda}{D_p},$$

where *Kn* is the Knudsen number, λ is the mean free path of the gas phase and D_p is the diameter of the particle. If the particle diameter is much larger than the mean free path of the gas molecule (Kn < 0.01) then the gas phase can be treated as a continuum flow and is therefore in the continuum regime. If the mean free path of the gas molecule is much larger than the particle radius (Kn > 1) the particle appears to the gas molecules like another gas molecule and this known as the free molecular or kinetic regime. In between these regimes is the transition regime (0.01< Kn < 1). So, if a granular gas flow has particles with very small diameters, continuum-based modelling cannot be applied. There has been work been done on modelling these dilute, large Knudsen number flows with success (Passalacqua and Fox, 2010; Passalacqua and Fox, 2011).

Throughout the literature, there is an emphasis on one-way coupled flows as these are the simplest to model, however most flows are in the dense regime or in a variable flow where two or more regimes exist in a single system, such as fluidized beds. Therefore, further research is needed to understand dense flow regimes with two- and four-way coupled flows. There have been attempts to deal with the transition between one regime and another (Khalilitehrani, Abrahamsson and Rasmuson, 2014). Dilute flows do occur, but many industrial and natural phenomena occur more frequently in the dense regime or are across a range of regimes. For further research, the dense regime has a number of interesting characteristics that are not fully understood and require more complex models to describe. As particle phenomena play an important role in dense flows, particles and their influence will be discussed further in this chapter.

2.2 Lagrangian Method vs. Eulerian Method

In principle there are two ways in which the granular phase can be solved, the first is the Lagrangian method. Every particle is tracked throughout the simulation by its position, velocity and material properties. This gives an advantage in studying microscopic flows, but unfortunately has a large computing cost in time and resources to simulate, even with simple flow systems. The second method is known as the Eulerian method and treats the particle phase as a continuous fluid with properties that are averaged over either time or volume. The computing cost of this method is much less than the Lagrangian method due to no longer needing to track every molecule or particle and averages the characteristics of a large number of molecules or particles. Therefore, an Eulerian based method is able

to simulate large and complex flow geometries with a relatively small computing cost but loses particle level details such as the particle velocity. A summary of the 3 main ways in which a multiphase system is modelled by combinations of Eulerian and Lagrangian methods are shown in the Table 1.

Table 1 - Multiphase modelling methods comparison.

	Direct Numerical Method	Eulerian-Eulerian Method	Eulerian-Lagrangian Method
Fluid Phase Model	Direct Numerical Method	Eulerian Method	Eulerian Method
Particle Phase Model	Lagrangian Method	Eulerian Method	Lagrangian Method
Computing Cost	Very high	Low	High
Level of Information	Very high	Low	High
Typical Use	Small particle numbers, laminar flows	Industrial (large) scale, large number of particles	Small lab scale, Investigation on the particle scale
Examples	Direct Numerical Simulation – Discrete Element Method (DNS-DEM)	Kinetic Theory of Granular Flows (KTGF), Two Fluid Model (TFM)	Discrete Element Method – Computational Fluid Dynamics (CFD-DEM), Computational Particle Fluid Dynamic (CPFD)

For the particle phase the Lagrangian method is used to track individual particles velocity, position and the collisions that occur between them. The most commonly used method for modelling the particle flow is the Discrete Element Method (DEM). This is a discrete method where every particle is tracked, and Newton's laws of motion are applied to the particles' motion and the interactions between them. A general review on DEM-based methods can be found in Zhu *et al.* (2007) and a review of their applications can be found in Zhu *et al.* (2008). They separate each combination of Eulerian-Lagrangian method into 3 categories: sub-particle, pseudo-particle and computational cell. The sub-particle class has such models as LB-DEM (Lattice Boltzmann – Discrete Element Method) or DNS-DEM (Direct Numerical Simulation – Discrete Element Method) where both phases are at the particle scale. In pseudo-particle methods the particles are treated as pseudo particles, such as parcels of particles, with their own attributes. The Two Fluid Model (TFM) can be classed as computational cell method where the particle and fluid phase information are averaged over the whole cell.

Computational Fluid Dynamics – Discrete Element Method (CFD-DEM) combines the DEM for the particle phase and a continuous method for the fluid phase, and was first

realised for fluidized beds by Xu and Yu (1997). There are two different formulations of CFD-DEM known as model A and model B and a review of their formulations has been done by Zhou *et al.* (2010). For fluidized beds the main difference between these two models is that model A's pressure drop is shared by both phases while model B assumes the pressure drop applies to the gas phase only. It was found by Feng and Yu (2004a) that for a single solid phase there was not much difference between the models, but with multiple particle phases model B was most appropriate; this has been confirmed in subsequent journal publications (Feng and Yu, 2004b; Zhou *et al.*, 2010). CFD-DEM is one of several combinations of different scale models, although it is the most popular for determining the validity of other models (Deen *et al.*, 2007; Chen and Wang, 2014). Other models exist where DEM is combined with other methods, such as the Lattice Boltzmann method, but these are not as well developed as CFD-DEM and need further development and validation of their own. Another model has been used by Jiang *et al.* (2014) which is the Computational Particle Fluid Dynamic (CPFD) model where the fluid phase is described using the Eulerian method and the solid phase is treated as 'parcels' of numerous particles with their own properties.

An advantage in using this kind of method is that detail on the microscopic scale can be achieved more easily than in experimental conditions such as 3D flows within a cylinder. The disadvantage of using this method is its high computational cost, which means currently it is restricted to small, lab-scale systems. To overcome the high computational cost, Braun *et al.* (2012) have continued to develop the Dense Discrete Particle Model (DDPM) that can deal with large dense particle flow systems. This works by assuming "parcels" of particles, instead of individual particles, which reduces the overall computational time. Chen and Wang (2014) have conducted a study to compare DDPM and CFD-DEM with the Eulerian based Two Fluid Model (TFM). This shows that CFD-DEM can capture the full detail, while both DDPM and TFM can capture some effects in the flow but are lacking in such areas as accurately describing the particle interactions.

Since each particle is tracked, the computational cost of using CFD-DEM is high, which means this method is only currently used for small investigations of flow properties on a laboratory scale. With the cost of computing coming down it is possible to complete a reasonably sized simulation on a workstation. Overall, the CFD-DEM method is a good tool for investigating particle effects that would not otherwise be possible to measure in experiments. As it has been established in the literature, this method is a useful tool to compare against newly developed methods.

The Two Fluid Model (TFM) is based on all phases of a system being treated as interpenetrating continua, based on the Eulerian method. There are 3 possible procedures used for averaging the continuous phase equations: time, volume and ensemble averaging. The time averaging procedure is the average of flow properties over time at a specific point in the flow. The time interval needs to be less than the time for the system to change significantly but large enough for local fluctuations to occur. This means that this method can only realistically be used in a steady flow system as otherwise significant changes will not accurately be accounted for. The volume averaging procedure averages the flow properties within a defined volume at an instant in time. The volume must be larger than the distance between particles but smaller than the length in which spatial changes occur. Therefore, the drawback is that this procedure only works for a homogeneous flow. The final procedure combines the advantages of both of these procedures with none of the disadvantage; this procedure is based on the probability of a flow field flow being at a particular configuration at a known time. This method is very difficult to implement therefore volume averaging is typically used.

For Rapid Granular Flows the granular phase is considered to act like a fluid, so the governing equations can have a similar form to hydrodynamic equations. The granular phase is described using the Kinetic Theory of Granular Flow (KTGF). This method is based on the dynamics of gases but differs as collisions between particles are considered to be dissipative due to their inelastic properties (whereas molecular collisions are fully elastic). To apply kinetic theory to granular flows, some similar assumptions to gas dynamics must be made. The main assumption is that only binary collisions occur, which can only happen if the flow is dilute enough that multiple particle collisions are highly improbable. Also, collisions need to be of short duration to avoid multiple collisions. This requires particles that are hard and only slightly inelastic. The final assumption made is that the particles are smooth and frictionless. KTGF methods using these assumptions agree well for dilute flows, but not all flows work with these assumptions. In dense flow systems it can be observed that particles can have long and enduring contacts, particle shape and roughness have been shown to significantly affect flows (Oschmann, Hold and Kruggel-Emden, 2014; Njobuenwu and Fairweather, 2015; Zhao, Lu and Zhong, 2015).

The problem with this method is the need for additional closure equations for the granular phase. This has been done for many different flow regimes and, so far, there is no accepted theory that is applicable to all flow regimes. Due to the averaging procedure, information on the particle scale is lost, as well as creating additional terms in the momentum equation

which require additional closure equations. There is no consensus on how the closure equations should be dealt with as there are several assumptions made that can only apply to certain situations. There are a number of Kinetic Theories (KT) being developed which work for individual situations, e.g. dense granular flow (Berzi, 2014), frictional particles (Chialvo and Sundaresan, 2013) or development of KT models for fluidized bed flows as discussed by Peirano and Leckner (1998). Zhang and Reese (2000) developed a KT model that includes the effect of the interstitial gas that is shown to affect chute flows. Another model developed that includes the effects of volume fraction gradients has been proposed by Massoudi and Boyle (2001). Much effort has been focused on the dilute regime as the assumption of only binary collisions occurring between particles is the simplest to model. Due to separate models being developed for different flow regimes there have been problems when modelling variable regime situations, such as fluidized beds and pneumatic conveying. Chialvo and Sundaresan (2013) developed a method to account for both the dilute and dense flow regimes as well as including friction. Another method to combine these flows by using two models that switch between the dense and dilute regimes has been shown by Khalilitehrani, Abrahamsson and Rasmuson (2014). These methods still need to be further developed and tested but are a first step to a single method for all flow regimes.

Advantages of using the Eulerian based method with KTGF are that it has a low computational cost so is able to simulate a large system or a large number of particles. Disadvantages of using this method are that the detail at the particle scale is lost. There has been a suggestion that using KT to model multiphase flows is flawed. Campbell (2006) suggests that the current developments of models for rapid granular flow are very limited in their use outside of a laboratory experiment. There is some truth in this as there is no consensus on a method or a set of methods that can include the effects of shape, friction, and contact types for all flow regimes.

In conclusion there is no general consensus on the development of the kinetic theory method, and this is still an active area of research. Therefore, more research should continue in this area to develop a consistent method which can be applied to real flows. The EE methods are a good tool for analysing flows that are quite large in a computationally cost-effective way. Future research developing these tools should include such characteristics as enduring contacts, particle shape and inter-particle forces.

2.3 Particle-Particle Interactions

In this section the particles' properties and their interactions are discussed. This is an important area of research especially for the study of dense flows. As has been discussed previously, particle interactions play an important role in dense flows so their characteristics need to be modelled appropriately. To keep within the scope of this thesis, the particles in this study are considered not to break up or change in mass (e.g. through burning) and all particles are assumed to be of the same density and diameter.

The following sections deal with a number of these aspects and their effects on the flow. The first section discusses the collisions that occur between particles and, this is followed by a discussion on the effects of particle shapes. From there, the interparticle friction effects and their models are detailed.

2.3.1 Particle Collisions

Particle collisions are important, certainly when four-way coupling occurs. There are a number of contact types. The first is the simple binary collision. These collisions assume that a particle will only be colliding with one other particle. This assumption can be made for most rapid granular flows in the dilute regime due to the high probability of only this kind of collision occurring. This kind of collision is the least computationally expensive as it only has to detect if a pair is in contact and then resolve the forces. The second kind of contact is the multiple contact, which occurs in the medium to dense regime, and is where a particle can come in to contact with several other particles at the same time. These are more computationally expensive due to the increased number of detections required and the need to resolve a more complex system. The third kind of contact is an enduring contact in which the particle will not have an instantaneous contact with another particle but will be in contact for some time. This occurs most often in dense flows such as fluidized beds.

The Coefficient of Restitution (e) describes the ratio of particle velocities before and after between two particles in a collision. It takes into account the dissipation that can occur in a collision. The equation for the coefficient of restitution is:

$$e = \frac{u_a - v_a}{u_i - v_i}, \tag{1}$$

where (u_i-v_i) is the initial speed difference between the particles before the collision and (u_a-v_a) is the difference after the collision. If e = 1, then the collision is fully elastic and

the speed before the collision is the same as after the collision. When e = 0.99, it is considered to be a slightly inelastic collision, and only a small amount of energy is lost. If e is much less than one, then plastic deformation has occurred. There are a number of factors that can affect the coefficient of restitution, such as roughness, fracture and particle shape.

One way of measuring the Coefficient of Restitution is to assess the impact of a single particle onto a surface of a known material. This has been reported by Gorham and Kharaz (2000), and Kharaz, Gorham and Salman (2001), where a particle of known size and material is dropped onto a surface and the speed and duration of the contact are measured from images taken during the experiment. From these images, using image processing software, the speed and rotation of the particle can also be calculated before and after the impact, giving the coefficient of restitution and other useful material properties.

Another method is to use the material properties, which allows for effects of certain types of deformation to be included. Particles can go through several stages of deformation during a collision, depending on the material properties and speed of the collision. If the particles are large enough, there are three phases of the collision. When the initial collision occurs, causing a small indentation, the collision produces elastic deformation. Further indentation will produce elastic-plastic deformation in the material. This is when the material just under the contact point deforms plastically, while the surface is still elastically deformed. The final phase is when the material on the surface and underneath both deform plastically. These phases have been incorporated into a model by Kosinski *et al.* (2014) and compared with a simple model that assumes that the collision occurs only in the fully plastic phase. This showed that the simplified assumptions cannot be made for particle collisions that end in the plastic-elastic phase at low velocity impacts.

The effect of the coefficient of restitution on a fluidized system has been studied by Goldschmidt *et al.* (2001) with multiple particle phases within the system. They show that dense regime systems strongly depend on the dissipation of energy caused by the particle-particle collisions. The greater the departure of the coefficient of restitution from the ideal (e = 1), the more vigorous the bubbling that occurs, which in turn causes binary particle systems to segregate faster than the experimental measurements show. Another study by Loha *et al*. (2014) showed that the formation of bubbles is affected by the coefficient of restitution. For elastic particles with e = 1, few or no bubbles formed, but e < 1 bubbles are formed. Therefore, the correct coefficient of restitution is important in predicting flow patterns properly.

2.3.2 Particle Shape

For dilute flows, the particle collisions are considered to be instantaneous and it is also normally assumed that non-spherical particles act in the same manner as spherical particles. But for dense flows, it has been noted that particle shape can affect a number of flow characteristics, such as mixing and segregation effects (Oschmann, Hold and Kruggel-Emden, 2014) and minimum fluidization velocity (Zhou *et al.*, 2011).

There have been a few studies on particle shape effects within a fluidized bed, which is a dense flow regime and in most processes the particles are not spherical. Ellipsoidal particles in fluidized beds have been investigated by Zhao and van Wachem (2013); they found that the particle orientation was not specific in the centre of the bed but was aligned in the streamwise direction near the walls and, in turn, affected the mixing in the wall regions. Zhou *et al.* (2011) also investigated ellipsoidal particles in fluidized beds and found that, when compared to spherical particles, the ellipsoid particles do make a significant difference in the flow characteristics. The minimum fluidization for ellipsoid particles is much less than for spherical particles. Oschmann *et al.* (2014) completed a comprehensive study of non-spherical particles in fluidized beds, which showed the significance of shape characteristics. Kruggel-Emden and Oschmann (2014) studied non-spherical particles in pneumatic conveying. Other studies of particle shape have included shear flows and highlighted the effects of shape on flows (Guo *et al.*, 2012b; Guo *et al.*, 2013). Particle shape has only recently been studied in more detail as computing costs have come down. Investigations are still limited due to there not being much experimental data currently to be able to validate models.

Non-spherical particle simulations can often be very time consuming compared to those with spherical particles due to the need for not only detecting if there is a contact but in what position each of the particles is. Also, there can be an error if there is a contact detected with large particle aspect ratios due to using methods based on spherical particles (which can give false detections). Particle contact detection for non-spherical particles has been developed for large aspect ratio particles in Guo *et al.* (2012a).

The interphase momentum exchange is greatly influenced by the drag effects on non-spherical shapes. Drag is usually dependent on the cross-sectional area of a particle in the streamwise direction. For non-spherical particles, rotation is easily generated due to sharp edges, which means the cross-sectional area is not constant in the streamwise direction of the flow. There have been several studies in which new drag models have been developed

(Hölzer and Sommerfeld, 2008; Hölzer and Sommerfeld, 2009; Zastawny *et al.*, 2012). Accuracy has yet to be achieved, as can be seen in a comparison of models in Hölzer and Sommerfeld (2008), in which the best model compared to experimental values still has an error of 14.1%.

All the above studies for particle shape have been accomplished using CFD-DEM simulations, as there are no other methods that can deal comprehensively with non-spherical particles. As can be seen from the literature, particle shape tends to affect dense flows that are computationally expensive to fully simulate. Therefore, there is room for developing a continuum-based method which could incorporate the effects discussed above. Kodam *et al.* (2009) does suggest that a kinetic theory should be developed to account for particle shape effects for both dilute and dense flows. Ozahi *et al*. (2008) has proposed a modification to Ergun's correlation for non-spherical particles, in which an equivalent particle diameter is used and this can predict the overall pressure drop of the granular system well.

2.3.3 Particle Friction

For some KTGF models, friction is neglected, but it has been shown that for dense flows friction cannot be ignored. Dilute flows tend to have short duration particle-particle collisions, but friction tends to only occur when there are enduring contacts. In addition, the rate at which collisions occur in dilute flows tends to be small, therefore friction is generally ignored in this regime. However, in dense flow regimes, enduring contacts do occur often so that particle-particle contact mechanics, such as sliding and sticking, become important. Makkawi *et al.* (2006) studied the effects of cohesion-based friction on a fluidized bed and found that when compared to no-friction there was a significant difference in the flow characteristics, such as dissipation of energy and movement of particles throughout the system. Another study by *Guo et al.* (2013) for rod- and disk-shaped particles found that friction in the dense regime significantly increases the interparticle stress, while in the dilute regime less stress occurs. This is believed to be due to the dissipation that friction causes during collisions. In terms of flow stability, Mitrano *et al.* (2013) have shown that high levels of friction cause a decrease in the instability of the flow system when compared to frictionless flows. The system sensitivity to friction has been examined by Shuai *et al.* (2012): they showed that the flow system is highly affected by the friction added to it.

The ways in which friction has been studied and included into the KTGF model can be split into two groups. The first is based on incorporating frictional particles with both rotational and translational motion into the continuum equations for the KTGF model. The second group only modifies the particle stress to include an additional frictional stress term. The first group is based on the idea that if particles have enduring contacts it is possible to have the particles rotate due to sliding and tangential forces during collisions, which means that rotation of the particles cannot be neglected in the dense regime. Jenkins and Zhang (2002) first developed this method for frictional, slightly inelastic particles in which both rotational and translational motions are taken into account. The frictional collision is described using the normal Coefficient of Restitution (e), the tangential Coefficient of Restitution (β_0), and a friction coefficient (μ_f) based on the cohesion forces between particles. By relating the translational and rotational fluctuations in particle velocity, an effective coefficient of restitution is given. Using this simple model, Sun and Battaglia (2006) simulated rotational particles in a simple fluidized bed. By including the rotational particle model for friction, they found that for a single particle phase in the fluidized bed the bubble intensity and bed expansion was higher than for particles without rotation, due to the increase in energy dissipation which better agreed with experimental results. For binary particle mixtures the particle segregation effects were quite different in that less segregation occurred with rotation included, which agreed with experimental results when compared to non-rotational particles.

Zhao *et al.* (2013) further developed the work of Jenkins and Zhang (2002) to include both sticking and sliding collisions between particles. There is a critical angle of impact between the particles at which either sliding or sticking occurs. When the impact angle is larger than a critical angle it is considered to have a sliding collision and when it is smaller than the critical angle then it is a sticking collision. From this they developed an equivalent roughness coefficient that accounts for a more realistic range of collision types. A study was then carried out on a fluidized bed system, and a range of friction restitution coefficients were tested (Zhao, Lu and Zhong, 2015), which showed that there is sensitivity to this parameter in the system. This model was then developed further by Yang *et al.* (2016) who incorporated rotational and translational motion using the Chapman-Enskog solution to derive a new particle velocity distribution and new closures for the momentum, mass and energy equations. Very recently, Yang *et al.* (2017) compared this model to the Jenkins and Zhang (2002) model using a Discrete Particle Model (DPM). Their results showed that by explicitly including particle friction there

was a greater rise in the energy dissipation which, again, led to better agreement with the DPM results.

The second method to incorporate frictional stress is to add the additional frictional stress to the stress tensor within KTGF. There have been a number of models of friction that follow this path. These models are typically based in some part on empirical data through experiments, and then tested against different particle systems. Johnson and Jackson (1987) proposed a semi-empirical equation that has been used often in simulating flows, although it has been observed by Van Wachem (2000) that at a solid volume fraction close to the random packing limit the stress becomes very high. Another model that is based on very dense flows by Syamlal *et al.* (1993) better describes the stress at the random packing limit, however, there is a significant difference at the solid volume fraction friction cut-off limit. These two models are very popular for simulating particulate flows and both are built into commercial and non-commercial software (Syamlal, Rogers and O'Brien, 1993; Van Wachem, 2000; ANSYS® Academic Research Mechanical, 2017). Other models have been developed, such as the viscosity divergent model by Bocquet *et al.* (2001) in which they observed that close to the random packing limit the shear viscosity will behave differently when compared to other transport properties. The shear viscosity is related to the particle motion fluctuations, as opposed to the mean motion that other models are based on. Therefore, they proposed a model dependent on the volume fraction. Abrahamsson *et al.* (2014) compared the Bocquet *et al.* (2001) model to the Johnson and Jackson (1987) model and found that the viscosity divergent model better represents the transition between liquid-like and gas-like particle behaviour. Another model by Jop *et al.* (2006) treats the particle phase as a visco-plastic fluid. The friction coefficient is a value between two empirical minimum and maximum friction related through the shear rate. Farzaneh *et al.* (2015) used a simple fluidized bed to compare the Jop *et al.* (2006) model with the earlier mentioned Syamlal *et al.* (1993) model. They showed that the Jop *et al.* (2006) model better captures the flow characteristics of the particles when the particles can get stuck due to high interparticle friction in close packing occurring at the walls. The time taken for particles to complete a single circulation of the fluidized bed is better represented.

2.4 Particle-Fluid Interactions

The particle-fluid interactions are described by the momentum transfer between each phase through forces such as drag, lift and other unsteady forces. The force coupling is achieved through the interphase term in the momentum equation for each phase. A

number of these interphase forces have been discussed in detail by Crowe *et al.* (1998) and discussed in the context of modelling by Zhu *et al.* (2007). Each of these forces will be briefly discussed here, as they can have significant impact on modelling flows correctly.

Unsteady forces are due to the acceleration of the particles relative to the fluid and can be considered in two parts. The first is known as the virtual or apparent mass. This is a mass additional to the particles own mass due to the resistance to acceleration by the surrounding fluid. The second part is the Basset force, in which the fluid boundary layer around a particle is slow to react to the acceleration of the particle and creates an additional viscosity effect. Lift forces are generated by the rotation of the particles in the fluid. Two of these lift forces that are typically considered are the Saffman force and the Magnus force. The first is caused by a velocity gradient in the surrounding fluid causing rotation of the particle, in turn causing a pressure distribution across the particle. Larger velocity on the top of the particle will produce a lower pressure than on the bottom of a particle, which has a lower velocity and higher pressure. A lift force is generated from this pressure difference, in the direction of the lower pressure. The Magnus lift force is caused by the particle itself rotating and creating the velocity gradient in the surrounding fluid, and thereby creating a pressure difference from one side to the other. Other forces, such as pressure gradient and buoyancy forces, are typically disregarded in particle-gas flows as the material density ratio of the gas phase to the particle phase is sufficiently large that these forces become insignificant. The lift and unsteady forces are also disregarded in most cases of rapid granular flows, as the dominant force in the interphase momentum transfer is the drag force.

One common drag model was developed by Gidaspow (1994), which combined the formulations of Ergun (1952) and Wen and Yu (1966). The Ergun (1952) formulation is based on empirical data from the pressure drop through a fixed bed of particles at the solids packing limit, while Wen and Yu (1966) conducted experiments on particles settling in a bed at various solid volume fractions. It has been noted by Zhang and Reese (2003) that these correlations do not take into account other influences, such as the solid volume fraction in the Ergun (1952) drag model and the relative random motion of the particles by Wen and Yu (1966), both of which occur in rapid granular flows. They proposed a new formulation of the drag model that takes these additional influences into account, and this was tested on a pneumatic conveying system, showing better qualitative agreement with experimental data.

Another common drag model was developed by Syamlal *et al.* (1993), based on correlations of terminal velocities in fluidized beds and settled bed experiments with respect to the solids volume fraction and particle Reynolds number. Taghipour *et al.* (2005) compared Wen and Yu (1966), Gidaspow (1994) and Syamlal *et al.* (1993) drag models with a pseudo 2D fluidized bed and found that all three models agree with experimental data above the minimum fluidization velocity. Gao *et al.* (2012) also compared the Gidaspow (1994) and Syamlal *et al.* (1993) drag models with their own model based on using different drag models for different solids volume fractions. In the very dilute regime ($0.99 < \alpha_g \leq 1.0$) the drag model of Schiller and Naumann (1935) is used. For the dilute regime ($0.94 < \alpha_g \leq 0.99$), the Wen and Yu (1966) drag model is used, and the Mckeen and Puglsey (2003) drag model is used for the dense regime ($\alpha_g \leq 0.94$). They also included a smooth transition term to move between the different drag models, as opposed to the Gidaspow (1994) model in which there is a discontinuous transition between the regimes. The results showed that the Gidaspow (1994) and Syamlal *et al.* (1993) drag models both over-predict the amount of particle entrainment occurring throughout the height of the fluidized bed, causing a more even distribution of the particles across the full height of the bed. The new drag model was significantly better when compared to the experimental results, due to there being less momentum transfer through the drag and, consequently, particles did not travel as high up the height of the vessel as the other models.

There are several fluid-particle interactions that have been identified and drag force modelling is an active area of research. No model has so far been generally regarded as a good basis for the drag force modelling in all flow regimes. Certain models do work well for certain flow regimes, but due to the complex nature of particulate flows not all drag models are suitable for all flows.

2.5 Multiple Particle Phases

A number of the methods discussed so far have not dealt with more than one solid phase. This is not realistic in real processes, so will need to be discussed. It can affect such aspects as segregation and mixing, as well as aeolian transport. Any real system will have multiple particle sizes of one material, or a mixture of materials that will change local flow patterns in ways that a single solid phase cannot account for.

Mathiesen *et al.* (2000) studied three phases with different particle diameters, which were the averaged sections of a real particle size distribution with a standard deviation. Murray

et al. (2012) have investigated several distribution methods to find the optimum number of particle phases. It was found that relatively few particle phases are needed to represent a moderately sized distribution, although many more phases are needed for much wider distributions.

With multiple solid phase systems, the mixing and segregation changes from that of single solid phase systems. A number of binary mixtures have been studied to investigate the effects of size and density differences between various solid phases. Hoomans *et al.* (2000) used CFD DEM to investigate particles with the same density but different sizes in a fluidized bed. When the particles were perfectly elastic, it was observed that there was full segregation of the different solid phases, with the large particles at the base of the bed and smaller particles at the top. When more realistic particles were used (slightly inelastic and frictional) the segregation still occurred but was not complete due to the mixing action of the bubbles moving the larger particles upwards. Goldschmidt *et al.* (2003) conducted experiments on fluidized beds to investigate particle properties, such as size, shape, densities and collision properties. Bokkers *et al.* (2004) compared the DPM CFD model to experimental values by Goldschmidt *et al.* (2003) and found agreement with the segregation rates and the movement of large and small particles. Sun and Battaglia (2006) modified the kinetic theory model to include particle rotation for the investigation of segregation and mixing in fluidized beds. It was found that the addition of rotation gave better agreement with experimental values. A study of channel flows using KTGF by Liu *et al.* (2008) showed that particles of the same density but different diameters tend to have higher segregation rates.

There is still much to investigate, such as whether having more than two phases with differing densities and particle sizes will better represent a true granular material. This will be important in such industries as food and pharmaceuticals as these need to be able to be mix materials effectively.

2.6 Applications

As previously discussed in this chapter, effective continuum modelling of granular-gas flows will allow for large scale and more complex systems to be simulated before building the facilities. This will reduce the overall cost of a system and will enable system issues to be identified and rectified early in the design process. In this section, the application of using Kinetic Theory of Granular Flows for realistic flow systems will be discussed, and

how current models are able to predict flows and produce useful data for engineers and designers.

The most common granular gas system that is used for testing and verifying new models is the pseudo 2D fluidized bed. This is because experimental measurements, such as imaging flow characteristics like bubble formation, can be done easily. Using this system is typically the first step in comparing and validating solvers such as Kinetic Theory of Granular Flow (KTGF) and CFD-DEM. Several studies have repeatedly found that Lagrangian solvers such as CFD-DEM outperform KTGF when compared to experimental results. Goldschmidt *et al.* (2004) found this when comparing a discrete particle model (DPM) with the KTGF model and concluded that DPM did produce better results than KTGF, although KTGF did still agree reasonably well. Deen *et al.* (2007) has found that DPM performed well for multiple solid phases, and Almohammed *et al.* (2014) used a discrete element model (DEM) to compare KTGF with experiments on a spouted fluidized bed and found that KTGF did not capture all the flow characteristics. Other flow systems have been modelled, including impinging particle flows in a channel by Chen and Wang (2014) where, again, CFD-DEM captured most of the flow characteristics while KTGF was only able to deal with a limited range of particle mass flows.

More complex geometries and flows have been modelled, including both spherical and non-spherical particles in a tapered fluidized bed (Sau and Biswal, 2011). Zhou *et al.* (2010) compared several formulations of CFD-DEM and simulated three flow systems; pseudo 2D fluidized bed, pneumatic conveying, and a cyclone separator. Both the fluidized bed and the pneumatic conveying were well represented, while the cyclone needed more careful modelling choices. Li *et al.* (2014) conducted a study on the differences in modelling 2D and 3D geometries of risers in circulating fluidized bed (CFB) systems. They found that 2D would only be useful for qualitative comparison while 3D modelling enables a more complete realistic description of the complex flow structures. The inlet and outlet boundaries could not be properly described in a 2D model.

From the literature it is clear that there is still a gap in producing accurate information from KTGF models in small-l and lab-scale simulations. These have been identified as problems with accurately predicting flow characteristics, such as particle rotation. Much model validation and comparison is for a pseudo 2D fluidized bed, but as Li *et al.* (2014) have shown that there is a significant difference between 2D and 3D model geometries and these need to be kept in mind when comparing models.

2.7 Literature Discussion

The current issues surrounding KTGF is that it is based on gas dynamics. It assumes that energy is not lost in collisions between particles and that all collisions are perfectly elastic. This is not true for granular flows, which have characteristics such as deformation, varying size and shape, as well as other particle-particle forces. However, the original method can be used for granular flows that have a very low solids volume fraction, this is because nearly all the assumptions are reasonable in this situation. Most granular flows that exist outside of a laboratory are denser and have variations in their solid volume fraction, particles can be inelastic and can have different collision dynamics, such as sliding and sticking, which have been shown to change the flow characteristics greatly (Bokkers, van Sint Annaland and Kuipers, 2004; Sun and Battaglia, 2006; Chialvo and Sundaresan, 2013; Loha, Chattopadhyay and Chatterjee, 2014). Several methods that have been developed specifically for either dense or dilute flows have been successful, but these methods will not work on their own for the whole flow spectrum. This suggests that there is a fundamental problem with the KTGF model formulation. There have been attempts to combine methods or develop new methods which can deal with a range of flows. But these have numerous variants which will work for specific situations (e.g. rapid, dense pipe flow etc.) but no one has yet been able to produce single method.

Some of these shortcomings have been highlighted when KTGF has been compared with Lagrangian-based models. These show that generally the description of the particle phase is incomplete, and more research and development need to be done to improve this. This is important, as currently the models that have a better overall comparability to experimental results are based on more computationally demanding solvers, such as CFD-DEM and direct numerical models. An accurate KTGF solver would still be preferred in order to reduce computing costs. Currently, there is a trade-off between the accuracy needed and the efficiency of a solver. These issues are being addressed with more detailed investigations of the ways that particles interact in different flow regimes. By simulating flows with solvers such as CFD-DEM it can become clear at which point certain interactions become important, such as particle rotation and its role in friction and energy dissipation. More recently, studies of differing particle shape are bringing forward the need to include particle shape effects into the KTGF for more realistic flows, and this is an expanding area of research. Overall, there are many individual areas of research in which more integration is needed, and more complex and realistic flows need to be tested and their simulations validated.

Chapter 3: Theoretical Development

This Chapter will focus on the theoretical development of continuum equations for use in multiphase flows. In this chapter, the basis of the Kinetic Theory of Granular Flows (KTGF) is set out, alongside some model variations, such as the drag model. Volume Diffusion Flux is introduced as a variation of the continuum model that includes the effects of compressibility in fluids. This is further developed here for rapid granular gas flows by modifying Volume Diffusion Flux to work within the KTGF framework. Another modification is made based on Korteweg Stress, which is developed here for the solid phase. Several variations of each modification are also made and discussed.

3.1 Kinetic Theory of Granular Flow

For Rapid Granular Flows, the granular phase is considered to act like a fluid, so the governing equations have a similar form to the hydrodynamic equations. The granular phase is described using the Kinetic Theory of Granular Flow (KTGF). This method is based on gas dynamic models but differs as collisions between particles are dissipative due to their inelastic properties. The Two-Fluid Model will be used to describe the interactions occurring between the granular and gas phases. In this section, the Eulerian based Two-Fluid Model with the KTGF is described and forms the basis for the models and modifications that will be made to improve its suitability for simulating Rapid Granular Gas flows.

For this thesis the basis of the Two-Fluid model is as described within the OpenFOAM software, specifically the solver called twoPhaseEulerFoam. The Two-Fluid model with KTGF as developed by Enwald, Periano and Almstedt (1996) for the continuity and momentum balance equations are:

Continuity equations

Gas Phase
$$\frac{\partial \alpha_g}{\partial t} + \nabla \cdot \left(\alpha_g U_g\right) = 0\,, \tag{2}$$

Solid Phase
$$\frac{\partial \alpha_s}{\partial t} + \nabla \cdot \left(\alpha_s U_s\right) = 0\,, \tag{3}$$

Momentum equations

$$\text{Gas Phase} \quad \rho_g \alpha_g \left[\frac{\partial U_g}{\partial t} + U_g \cdot \nabla U_g\right] = -\alpha_g \nabla P + \nabla \cdot \alpha_g \tau_g + \alpha_g \rho_g g - \beta\left(U_g - U_s\right), \tag{4}$$

$$\text{Solid Phase} \quad \rho_s \alpha_s \left[\frac{\partial U_s}{\partial t} + U_s \cdot \nabla U_s\right] = -\alpha_s \nabla P + \nabla \cdot \alpha_s \tau_s - \nabla P_s + \alpha_g \rho_g g + \beta\left(U_g - U_s\right). \tag{5}$$

The first term on the right side of the momentum equation (5) describes the pressure of the solid phase and the second term is the particle viscous stress, while the third term is the interparticle pressure caused by the collisions between particles (which is significant in dense flow systems). The fourth term is the effect of gravity on the solid phase, and the final term is the interphase momentum exchange primarily occurring through the drag force on the particles moving through the gas fluid phase.

The closure relations of the momentum equations require a full description of the solid phase stress. In the dense regime, particle collisions dominate the flow and, by using Gas Kinetic Theory, it is possible to describe the stresses caused by these interactions. The solids phase stress can be described as having a collisional contribution in which momentum exchange occurs directly from particle collisions, and a kinetic contribution from particles moving through planes of shear in the flow. Firstly, the concept of granular temperature is introduced here as the fluctuations in particle velocity, given as:

$$\theta = \frac{1}{3} < U_s'^2 >, \tag{6}$$

where θ is the granular temperature and U_s' is the fluctuation in the solid phase velocity. An additional balance is then created to supplement the momentum and continuum balances to relate the granular temperature to the solid phase stress as:

$$\frac{3}{2}\left[\frac{\partial}{\partial t}(\alpha_s \rho_s \theta) + \nabla \cdot (\alpha_s \rho_s \theta U_s)\right] = (-\nabla P_s I + \tau_s) : \nabla U_s - \nabla \cdot (\kappa_s \nabla \theta) - \gamma_s - J_s, \tag{7}$$

where κ_s is the solids thermal conductivity, γ_s is the dissipation of granular energy through inelastic particle collisions, and J_s is the dissipation generated by the fluctuating force caused by the gas phase through the fluctuation of the solid phase velocity. The first term on the right side characterises the creation of fluctuating energy due to shear in the solid phase, and the second term is the diffusion of fluctuating energy along gradients of granular temperature.

The solids pressure has been described by Lun *et al.* (1984) as:

$$P_s = \rho_s \alpha_s \Theta + 2 g_0 \rho_s \alpha_s^2 \theta (1 + e) \,, \tag{8}$$

where ρ_s is the density of the solid phase, α_s is the solid volume fraction, g_0 is the particle radial distribution and e is the Coefficient of Restitution. The first term on the right side represents the kinetic contribution to the pressure by considering the momentum transfer through the solid phase as particles move through planes of shear in the flow. The second term is the collisional contribution and stems from the momentum transfer within particle-particle collisions. This form of the solid phase pressure is typically used in both commercial and non-commercial flow solvers.

The viscous stress tensor for the solid phase is:

$$\tau_s = 2\mu_s D_s + \left(\lambda_s - \frac{2}{3}\mu_s\right) tr(D_s) I \,, \tag{9}$$

where μ_s is the solids shear viscosity stress tensor, λ_s is the solids bulk viscosity, I is the identity matrix and D_s is:

$$D_s = \frac{1}{2}(\nabla U_s + (\nabla U_s)^T) \,. \tag{10}$$

The solids bulk viscosity is, again, typically described by Lun *et al.* (1984) as:

$$\lambda_s = \frac{4}{3}\alpha_s^2 \rho_s g_0 (1 + e) \sqrt{\frac{\theta}{\pi}} \,. \tag{11}$$

The description of the solids shear viscosity stress, μ_s, has a number of variations, two of which will be discussed here as they are used within this work. The first was developed by Gidaspow (1994) in which the inelastic nature of the particles is not taken into account. This makes this method better suited to very slightly inelastic particles (e.g. glass beads) and, as shown by Van Wachem (2000), tends to agreement with other stress models at

the packing limit of the solid phase. Another method was developed by Syamlal *et al.* (1993) and, when compared to the Gidaspow (1994) model, has a significant difference in the stress at low solids volume fraction. Each of these models are listed in Table 2.

Table 2 - Solids shear viscosity models.

Model	Description	
Gidaspow (1994)	$\mu_s = \frac{4}{5}\alpha_s^2\rho_s d_s g_0(1+e)\sqrt{\frac{\theta}{\pi}} + \frac{2\frac{5\sqrt{\pi}}{96}\rho_s d_s\sqrt{\theta}}{(1+e)g_0}\cdot\left[1+\frac{4}{5}g_0\alpha_s(1+e)\right]^2$	(12)
Syamlal *et al.* (1993)	$\mu_s = \frac{4}{5}\alpha_s^2\rho_s d_s g_0(1+e)\sqrt{\frac{\theta}{\pi}} + \frac{\alpha_s d_s\rho_s\sqrt{\pi\theta}}{6(3-e)}\left[1+\frac{2}{5}(1+e)(3e-1)\alpha_s g_0\right]$	(13)

The conductivity of granular energy has a similar form to the shear stress in that there is a collisional part and a kinetic part. The conductivity model used in this work has been developed by Gidaspow (1994):

$$\kappa_s = \frac{2}{(1+e)g_0}\left[1+\frac{6}{5}(1+e)g_0\alpha_s\right]^2\kappa_{dil} + 2\alpha_s^2\rho_s d_s g_0(1+e)\sqrt{\frac{\theta}{\pi}}, \quad (14)$$

with the dilute form of the conductivity of granular energy given as:

$$\kappa_{dil} = \frac{75}{384}\rho_s d_s\sqrt{\pi\theta}\,. \quad (15)$$

The dissipation due to the inelastic inter-particle collisions are considered by Lun *et al.* (1984) as:

$$\gamma_s = 12(1-e^2)\frac{\alpha_s^2\rho_s g_0}{d_p\sqrt{\pi}}\theta^{3/2}\,. \quad (16)$$

The rate of energy dissipation per m^3, as an effect of the fluctuating force caused by the gas phase through the fluctuation of the solid phase velocity, has been described by Louge *et al.* (1991) as:

$$J_s = \beta\left(3\theta - \frac{\beta d_p(U_g-U_s)^2}{4\alpha_s\rho_s\sqrt{\pi\theta}}\right). \quad (17)$$

This correlation, however, does not tend to zero as it reaches the solids packing limit therefore Van Wachem (2000) divided J_s by the radial distribution function, and this will be used in this work.

The solids stress is dependent on the radial distribution to determine the number of collisions occurring for a given solid volume fraction. Lun and Savage (1986) developed a radial distribution function:

$$g_0 = \left[1 - \left(\frac{\alpha_s}{\alpha_{s,max}}\right)^{\frac{1}{3}}\right]^{-1} . \tag{18}$$

The frictional stress is caused by particles in a very dense regime in which particles have enduring contacts. To account for this additional stress, they are simply added to their respective parts of the solids stress equations as:

$$P_{s,total} = P_s + P_{s,f} , \tag{19}$$

$$\mu_{s,total} = \mu_s + \mu_{s,f} . \tag{20}$$

Johnson and Jackson (1987) developed a semi-empirical model for the frictional solids pressure ($P_{s,f}$):

$$P_{s,f} = Fr \frac{\left(\alpha_s - \alpha_{s,min}\right)^n}{\left(\alpha_{s,max} - \alpha_s\right)^p} , \tag{21}$$

where Fr, n and p are empirical material constants, and $\alpha_{s,min}$ is the minimum volume fraction of which friction will become important within the system. The additional viscous stress due to friction ($\mu_{s,f}$) is related to the frictional solids pressure through Coulomb's law:

$$\mu_{s,f} = P_{s,f} \sin \Phi , \tag{22}$$

where Φ is the internal angle of friction of the particle.

The interphase momentum exchange occurs primarily through the drag force between the phases. Other forces such as lift do occur, but this is neglected in many systems as the lift force is significantly small enough not to be included. There are many drag models that have been developed specifically for KTGF flows, and each have their own merit. A discussion on the formulation and variation of these models has been set out in the literature review in section 2.4; therefore, only the two models that have been used in this work will be described here. The first and most commonly used, as it is typically available in most commercial and non-commercial software, is by Gidaspow (1994), which combines the low solids volume fraction drag model of Wen and Yu (1966) with the

higher solids volume fraction drag model of Ergun (1952). The second model used in this thesis is by Syamlal *et al.* (1993), which is based on empirical correlations of the terminal velocity in fluidized bed systems related to the solids volume fraction and particle Reynolds number. Each of these drag models is listed in the Table 3 below.

Table 3- Interphase momentum transfer, drag models.

Model	Description
Gidaspow(1994) (based on Ergun(1952) and Wen & Yu(1966))	$\beta = \begin{cases} 150\frac{(1-\alpha_g)^2\mu_g}{\alpha_g d_p^2} + 1.75\frac{\rho_g\lvert U_g - U_s\rvert(1-\alpha_g)}{d_p}, & \alpha_g \le 0.8 \\ \frac{3}{4}C_D\frac{\alpha_g\rho_g\lvert U_g - U_s\rvert(1-\alpha_g)}{d_p}\alpha_g^{-2.65}, & \alpha_g > 0.8 \end{cases}$ $C_D = \begin{cases} \frac{24}{Re_p}\left(1 + 0.15Re_p^{0.687}\right), & Re_p < 1000 \\ 0.44, & Re_p \ge 1000 \end{cases}$ $Re_p = \frac{\alpha_g\rho_g d_p\lvert U_g - U_s\rvert}{\mu_g}$
Syamlal *et al.* (1993)	$\beta = \frac{3}{4}C_D\frac{\alpha_g(1-\alpha_g)\rho_g}{V_r^2 d_p}\lvert U_g - U_s\rvert$ $C_D = \left(0.63 + 4.8\sqrt{\frac{V_r}{Re_m}}\right)^2$ $V_r = \frac{1}{2}\left(a - 0.06Re_m + \sqrt{(0.06Re_m)^2 + 0.12Re_m(2b-a) + a^2}\right)$ $a = (1-\alpha_s)^{4.14}$ $b = \begin{cases} 0.8(1-\alpha_s)^{1.28}, & \alpha_g \ge 0.15 \\ (1-\alpha_s)^{2.65}, & \alpha_g < 0.15 \end{cases}$ $Re_m = \frac{\rho_g d_p\lvert U_g - U_s\rvert}{\mu_g}$

The Two-Fluid Model with the Kinetic Theory of Granular flows as described above will be used as the basis on which modifications will be made to improve accuracy and suitability for Rapid Granular Gas Flows. In the following sections these changes to this model will be described.

3.2 Volume Diffusion Flux

For compressible fluid flows, Brenner (2005) developed the hypothesis of there being not one but two different velocities that need to be considered, based on the flux of both mass and volume. The reason for this is that the velocity of the fluid considered in the Navier-Stokes equations is based on the mass flux only. When flows become compressible, the mass flux will not change but the volume flux will. This affects the shear viscosity of the fluid, therefore two different velocities need to be considered; mass velocity of the fluid, and volume velocity of the fluid.

In compressible flows the Volume (V) and the Mass (M) of a fluid at any point in space can be described by the relationship:

$$dV = \frac{dM}{\rho}. \tag{23}$$

However, this does not constitute the relationship of their flux i.e.

$$n_v \neq \frac{n_m}{\rho}, \tag{24}$$

where n_v is the volume flux and n_m is the mass flux. The flux as described by Brenner (2005) is:

$$n_v = \frac{n_m}{\rho} + J_v, \tag{25}$$

where J_v is the Volume Diffusion Flux. The velocities for both the mass and volume can be related using the Volume Diffusion Flux as:

$$U_v = U_m + J_v, \tag{26}$$

where U_v and U_m are the Volume and Mass velocities of the fluid respectively and J_v is:

$$J_v = D_v \nabla \ln\rho, \tag{27}$$

where D_v is the volume diffusivity coefficient. For single phase fluids the volume diffusion coefficient is related to the thermometric diffusivity α_v (Brenner, 2010a):

$$D_v = \alpha_v = \frac{k}{C_p \rho}, \tag{28}$$

where k is the thermal conductivity and C_p is the specific heat capacity. This model can be used for both incompressible and compressible flows; as the flow becomes incompressible ($\nabla\rho = 0$), the volume diffusion term J_v disappears and the Navier-Stokes Equations are reduced to their incompressible form. This makes this method better for describing mixed density flows with the same set of equations. Brenner suggests that the Navier-stokes equations are fundamentally flawed due to the assumptions made that the velocity of the mass should be used. While this method has been continuously developed by Brenner (2005; 2009a; 2009b; 2010a; 2010b; 2012; 2013) there has also been an increase in interest in testing and using this method.

3.2.1 Single Phase Granular Modification of Volume Diffusion Flux

As the formulation of the Two-Fluid Model with the Kinetic Theory of Granular Flows is based on the same hydrodynamic equations that only consider mass flux in compressible flows, it is possible that Volume Diffusion Flux can be modified for a granular flow. The first modification made in this thesis is to formulate a single-phase adaptation of equation (27) to be in terms of the volume fraction instead of density. As the density of the solid phase does not itself have compressible properties it can be recast in terms of volume fraction change. This changes equations (27) and (28) to:

$$J_{vs} = D_{vs}\nabla\alpha_s \,, \tag{29}$$

where the volume diffusion coefficient is found through dimensional analysis to be:

$$D_{vs} = \frac{\rho_s \nu_s}{(\alpha_s\rho_s) + (\alpha_g\rho_g)}. \tag{30}$$

This single granular phase modification only considers the compressibility of the solids phase. Therefore, a multiphase form of the Volume Diffusion Flux will be considered in this thesis as well as the single granular phase form.

3.2.2 Multiphase Granular Modification of Volume Diffusion Flux

A further modification of the volume diffusion flux is to consider the solid volume fraction in terms of a varying mass fraction, *w*. This will allow for the total mass of both phases in the system to be considered. For multiphase flows, Fick's diffusion law (Bird, Stewart and Lightfoot, 2002) is used to determine each phase's diffusion volume flux as (Brenner, 2010a):

$$J_i = -\rho D\nabla w_i \,, \tag{31}$$

where D is the binary diffusion coefficient and w_i is the mass fraction of phase i. For the volume diffusion coefficient, Brenner (2010a) has shown that D=D_{vs}, as D_{vs} is the binary diffusion coefficient for the solid phase in terms of volume. In terms of KTGF for the solid phase, the mass fraction w_i becomes:

$$w_s = \frac{\alpha_s\rho_s}{\alpha_s\rho_s + \alpha_g\rho_g}, \tag{32}$$

where w_s is the specific density of the solid phase divided by the total density of both phases.

For the solid phase J_s is:

$$J_s = -\rho_s D_{vs} \nabla w_s \,, \tag{33}$$

and is related to the solids Volume Diffusion Flux, J_{vs} by:

$$J_{vs} = \left(\bar{v}_s - \bar{v}_g\right) J_s \,, \tag{34}$$

where $\bar{v}$ is the partial specific volume of each phase (i):

$$\bar{v}_i = \frac{\alpha_i}{\rho_i} \,. \tag{35}$$

3.2.4 Summary of Volume Diffusion Flux Modifications

A summary of the Volume Diffusion Flux Modifications is shown in Table 4.

Table 4 - Summary of Volume Diffusion Flux Modifications.

Label	Volume Diffusion Flux Modification	
Single Phase	$D_{vs} = \frac{\rho_s \nu_s}{(\alpha_s \rho_s) + (\alpha_g \rho_g)}$	(36)
	$J_{vs} = D_{vs} \nabla \alpha_s$	(29)
Multiphase	$D_{vs} = \frac{\rho_s \nu_s}{(\alpha_s \rho_s) + (\alpha_g \rho_g)}$	(36)
	$w_s = \frac{\alpha_s \rho_s}{\alpha_s \rho_s + \alpha_g \rho_g}$	(32)
	$J_s = -\rho_s D_{vs} \nabla w_s$	(33)
	$J_{vs} = \left(\bar{v}_s - \bar{v}_g\right) J_s$	(34)

There are two main ways to modify the momentum equations to include volume diffusivity; the first is to recast the entire equation set in terms of volume velocity U_v instead of mass velocity U_m, but this is time-consuming. The second method only changes the term within the viscous stress tensor, as done by Greenshields and Reese (2007). This method will be implemented here to clearly illustrate the difference in implementation between the original method and the new modified method for the solid phase. Therefore, the stress tensor equation (10) will become:

$$D_s = \frac{1}{2} \left(\nabla U_{vs} + (\nabla U_{vs})^T \right) \,, \tag{36}$$

where the volume velocity of the solid phase velocity is:

$$U_{vs} = U_{ms} + J_{vs} \,. \tag{37}$$

Both the single phase and the multiphase forms of the Volume Diffusion Flux for the solid phase will be tested to see whether considering both phases compressibility is required when considering the viscosity of the fluid.

3.3 Korteweg Stress

Korteweg (1901) proposed a model in which phase transitional phenomena in fluids can be simulated. He noted that when there are two fluids with different densities and viscosities, additional stresses are created. This model relies on the stress tensor being dependent on the gradient of both the density and velocity of the fluid. The Korteweg stress is added to the Navier-Stokes equations as an additional stress tensor, *T*. This tensor can act like an effective interfacial tension between the fluids. It is generally known that the Korteweg Stress tensor model has the ability to capture non-Newtonian phenomenon. This could allow for non-Newtonian effects to be modelled in granular flows. Heida and Málek (2010) showed that using Korteweg stress within compressible flow systems is thermodynamically consistent. A review of miscible fluids by Truzzolillo and Cipelletti (2017) concluded that the additional stress as first suggested by Korteweg (1901) has been found in experimental data.

The Korteweg Stress tensor, as described by Anderson *et al.* (1997) is:

$$T = \left[-P + K\rho\nabla^2\rho + \frac{1}{2}K|\nabla\rho|^2\right]I - K\nabla\rho \otimes \nabla\rho\,, \tag{38}$$

where *K* is based on the material properties of the fluid, such as density and viscosity.

3.3.1 Single Phase Granular Modification of Korteweg Stress

To incorporate the Korteweg Stress for the solids phase in the KTGF model, a similar approach is followed as in the previous section on the Volume Diffusion Flux modification for a single solid phase, and considering equation (38) in terms of volume fraction leads to:

$$T = \left[-P + K\rho\nabla^2\alpha_s + \frac{1}{2}K|\nabla\alpha_s|^2\right]I - K\nabla\alpha_s \otimes \nabla\alpha_s\,, \tag{39}$$

where *K* can be found through dimensional analysis to be:

$$K = \frac{\mu_s^2}{\rho_s}. \tag{40}$$

3.3.2 Multiphase Granular Modification of Korteweg Stress

Anderson *et al.* (1997) also proposed that the Korteweg Stress should be written in terms of a mass fraction for binary mixtures. Taking the same approach as with the Volume Diffusion Flux, and modifying the mass fraction to be in terms of specific density, equation (38) becomes:

$$T = \left[-P + K\rho\nabla^2 w_s + \frac{1}{2}K|\nabla w_s|^2\right] I - K\nabla w_s \otimes \nabla w_s \,, \tag{41}$$

where the solid phase mass fraction w_s is:

$$w_s = \frac{\alpha_s \rho_s}{\alpha_s \rho_s + \alpha_g \rho_g} \,. \tag{32}$$

3.3.3 Summary of Korteweg Stress Modifications

To incorporate the Korteweg Stress into the Kinetic Theory of Granular Flows, the solid phase momentum equation (4) becomes:

$$\begin{aligned} \rho_s \alpha_s \left[\frac{\partial U_s}{\partial t} + U_s \cdot \nabla U_s\right] \\ = \; -\alpha_s \nabla \mathrm{P} + \nabla \cdot \alpha_s \tau_s - \nabla \mathrm{T} + \alpha_g \rho_g g + \beta\left(U_g - U_s\right), \end{aligned} \tag{42}$$

where the solid phase pressure, P_s is included within the Korteweg Stress term, T. A summary of the Korteweg Stress modifications is shown in Table 5 below.

Table 5 - Summery of Korteweg Stress Modifications.

Label	Equations for Original and Korteweg Stress Modifications	
Single Phase	$T = \left[-P + K\rho\nabla^2\alpha_s + \frac{1}{2}K\lvert\nabla\alpha_s\rvert^2\right] I - K\nabla\alpha_s \otimes \nabla\alpha_s$	(39)
	$K = \frac{\mu_s^2}{\rho_s}$	(40)
Multiphase	$T = \left[-P + K\rho\nabla^2 w_s + \frac{1}{2}K\lvert\nabla w_s\rvert^2\right] I - K\nabla w_s \otimes \nabla w_s$ (41)	(40)
	$K = \frac{\mu_s^2}{\rho_s}$	(40)
	$w_s = \frac{\alpha_s\rho_s}{\alpha_s\rho_s + \alpha_g\rho_g}$	(32)

3.4 Discussion

In this chapter the standard equations that will form the basis of our solver have been described. The Two-Fluid Model with the Kinetic Theory of Granular Flows (KTGF) have been described, along with models within the KTGF that are better suited for

different flow regimes. Each of the Bi-Velocity and Korteweg Stress model variations that have been described will be compared using existing experimental and simulation data.

Two additional modifications have been developed; the first is the Volume Diffusion Flux, and the second is from adding the Korteweg Stress to the KTGF. Volume Diffusion Flux has been developed to better account for the effects of compressible flows, and in this thesis is modified for use with the granular phase and KTGF. Two variations have been developed; the first is reliant on the gradient of the solids volume fraction as the density of the solid phase does not change, the second is more reliant on the properties of both phases by a mass fraction of the solid phase and the overall combined solid and gas phases. For the Korteweg Stress, the same approach has been taken, with appropriate formulation of the material constant K found through dimensional analysis. Again, a single-phase form is developed using the gradient of the solids volume fraction as was done with the Bi-Velocity modification. The second variation also uses the mass fraction so both phases have been considered, which is dependent on volume fraction and density of the solid phase to give a mass fraction (w_s).

Each of these modifications will be tested by comparison to both experimental and other reported simulation results, as well as comparing with an unmodified version of the granular flow model. Once this has been completed, their usefulness will be discussed and the possibility examined of combining both volume diffusion flux and Korteweg stress models to create a more complete description of a compressible granular-gas system.

Chapter 4: Simple Fluidized Bed Simulations

In this chapter the first set of simulations on simple fluidized bed geometries will be carried out. A discussion of the various commercial and non-commercial solver software will be discussed and compared throughout this section. The models, as set out in Chapter 3, will be implemented into a solver code and tested using the different simple fluidized bed systems. The first simulated fluidized bed system will be a cylinder fluidized bed, and the second will be a more complex flow in a recirculating fluidized bed. The first task will be to simulate the cylinder fluidized bed case with the existing commercial software Fluent and with the open source software OpenFOAM. Results will be compared to experimental data and other numerical results as reported in the literature. This will allow for the validation of OpenFOAM as a tool that can be used to test the modifications described in the previous chapter. Once that is complete, the sensitivity of OpenFOAM will be tested to further validate the software. Both the Volume Diffuse Flux models and the Korteweg Stress models will then be tested on the cylinder fluidized bed. For the recirculating fluidized bed problem, simulations will be run using both the un-modified and modified OpenFOAM solver and compared with experimental and other reported simulation results. Finally, a discussion of the performance of OpenFOAM as a granular flow solver and the effects of each of the modifications will be made.

4.1 Simulation Software

There are several commercial and non-commercial software packages available for simulating multiphase flows. Commercial software can be limited by its license, for example, as a maximum number of cells may be used in a single simulation. In the past decade the use of open source software has been increasing by researchers due to its ability to be readily modified to include new models. This gives an advantage over commercial software in that there are no licensing issues, or limitations in the functionality of the solver. One well known and established software for modelling multiphase flows is OpenFOAM, which is open source and freely available to be downloaded and modified. OpenFOAM is written in C++ which allows it to be easily changed to add new models or create new solvers. A number of solvers are already available to use and the full list is available in the OpenFOAM User Guide. The OpenFOAM solver used in this thesis is called twoPhaseEulerFoam (v2.4, OpenFOAM Foundation), and is based on the Eulerian method and only considers two phases: one continuous phase and one dispersed phase, and is based on the two fluid method as

presented by Rusche (2002) that has been modified to be able to use the KTGF as set out by Van Wachem (2000). The OpenFOAM software uses the finite volume method to discretize and solve the flow equations.

MFix is another open source code that has been developed by the National Energy Technology Lab (NETL) as part of the US Department of Energy (DoE). MFix stands for "Multiphase Flow with Interphase eXchanges" and is primarily for multiphase flows (while OpenFOAM in which is designed for a wide range of flow systems that include multiphase flows). This is based on Fortran code, which also allows for changes to the solvers to be made easily.

The final software used is Ansys Fluent, which is a commercially available program. Solver code modification cannot be made directly but can be done indirectly by adding macros as a User Defined Function. A full list of its functionality and available solvers can be found in the ANSYS Fluent 17.0 Theory Guide (2017). For the purposes of this work Fluent will be used as it currently stands at version 17.0 and will not be modified to include the Volume Diffusion Flux and Korteweg Stress; it will be primarily used to help validate the open source solvers MFix and OpenFOAM.

4.2 Cylinder Fluidized Bed Case

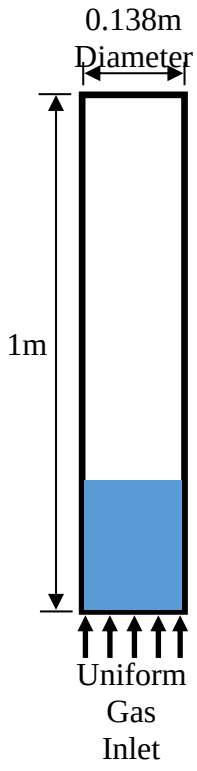

Figure 4 - Geometry of a Simple Cylinder Fluidized Bed.

The first case for which the OpenFOAM software will be compared and validated is based on the paper by Makkawi *et al.* (2006): a simple cylindical fluidized bed. This case will be used to compare the OpenFOAM and Fluent software with experimental and MFix data as reported by Makkawi *et al.* (2006). The simulations consist of six different experimental conditions: Geldart group A/B particles of diameter 125µm at gas inlet velocities 0.13m/s, 0.26m/s and 0.4m/s; and Geldart group B particles of diameter 350µm at gas inlet velocities of 0.26m/s, 0.54m/s and 0.8m/s. The gas is evenly distributed into the base of the cylinder and the top is open to the atmosphere. The full description of the parameters and geometry used in the simulations are given in Figure 4 and Table 6.

To keep the simulation consistent with the MFix simulations as described in the original work, the boundary conditions at the inlet will be an evenly distributed gas inlet that is impenetrable by the particle phase, and the outlet boundary will be a pressure boundary

at atmospheric pressure (1.013 bar). The walls will be described using the Johnson and Jackson (1987) boundary condition in which the gas phase has no slip at the walls and the solid phase will have partial slip. The drag model used will be the Syamlal *et al.* (1993) drag model as described in the MFix solver.

A mesh independence test was carried out to ensure the correct mesh size is used. This was also done for both OpenFOAM and Fluent, which were found to have very similar results from this test therefore the same mesh size was used for both solvers. Four mesh sizes were tested: a very rough mesh of 19,575 cells, a rough mesh of 48,000 cells, a medium mesh of 88,125 cells and a fine mesh of 199,680 cells. Through comparison of the total pressure drop between the inlet and outlet, a mesh of 88,125 cells is used in which the minimum cell dimensions are 4mm in all directions. This gave the best results and increasing the mesh density did not significantly improve the results beyond the medium mesh.

The initial condition simulation will consist of a static bed of particles up to a height of 0.2m, at the maximum random packing solids volume fraction of 0.65. To avoid large fluctuations during the start-up of the system, the time-averaging will start after an initial period after which the system can be said to be in a stable state. For this simulation it was observed that after 10 seconds of run time the particle fluctuations did not change significantly; from then, an additional 14 seconds were run to find the time-averaged properties.

Table 6 – Cylinder Fluidized Bed Parameters (Makkawi, Wright and Ocone, 2006).

Parameters	
Cylinder	Diameter 0.138m, Height 1m
Particles	Group A/B D_p=125µm, Density 2500kg/m^3 Group B D_p=350µm, Density 2500kg/m^3
Particle-Particle Coefficient of Restitution	0.8
Particle-Wall Coefficient of Restitution	0.8
Internal angle of friction	0.5 (degrees)
Max solid volume fraction	0.65
Critical solid volume fraction	0.58
Gas	Air, Density 1.4kg/m^3, μ_g = 1.8 x 10^{-5}N/m^{2}s
Gas Inlet Velocities	Group A/B: 0.13m/s, 0.26m/s and 0.4m/s Group B: 0.26m/s, 0.54m/s and 0.8m/s
Simulation time	24s
Static Bed Height	0.2m
Measuring height at cross section	Between 0.143m and 0.181m

In this work, simulations were carried out using two different simulation software; Fluent and OpenFOAM. This is to compare the OpenFOAM software to other known solver software to help validate it, and then will enable us to use OpenFOAM to develop and test the new solver models as described in Chapter 3. Both OpenFOAM and Fluent will

be used to simulate the cylinder fluidized bed, and results compared to the MFix and experimental results as originally reported by Makkawi *et al.* (2006).

4.2.1 Software Comparison and Validation

The OpenFOAM and Fluent solvers are compared against the experimental and MFix results from the original paper for both particle diameters and all gas inlet velocities set out in Table 6. Figure 5 shows the time-averaged cross section results between cylinder heights of 0.143m and 0.181m of the solid volume fraction to match the experimental measurement range. Also, the time-averaged solid volume fraction across the full height of the cylinder is reported and compared for each case.

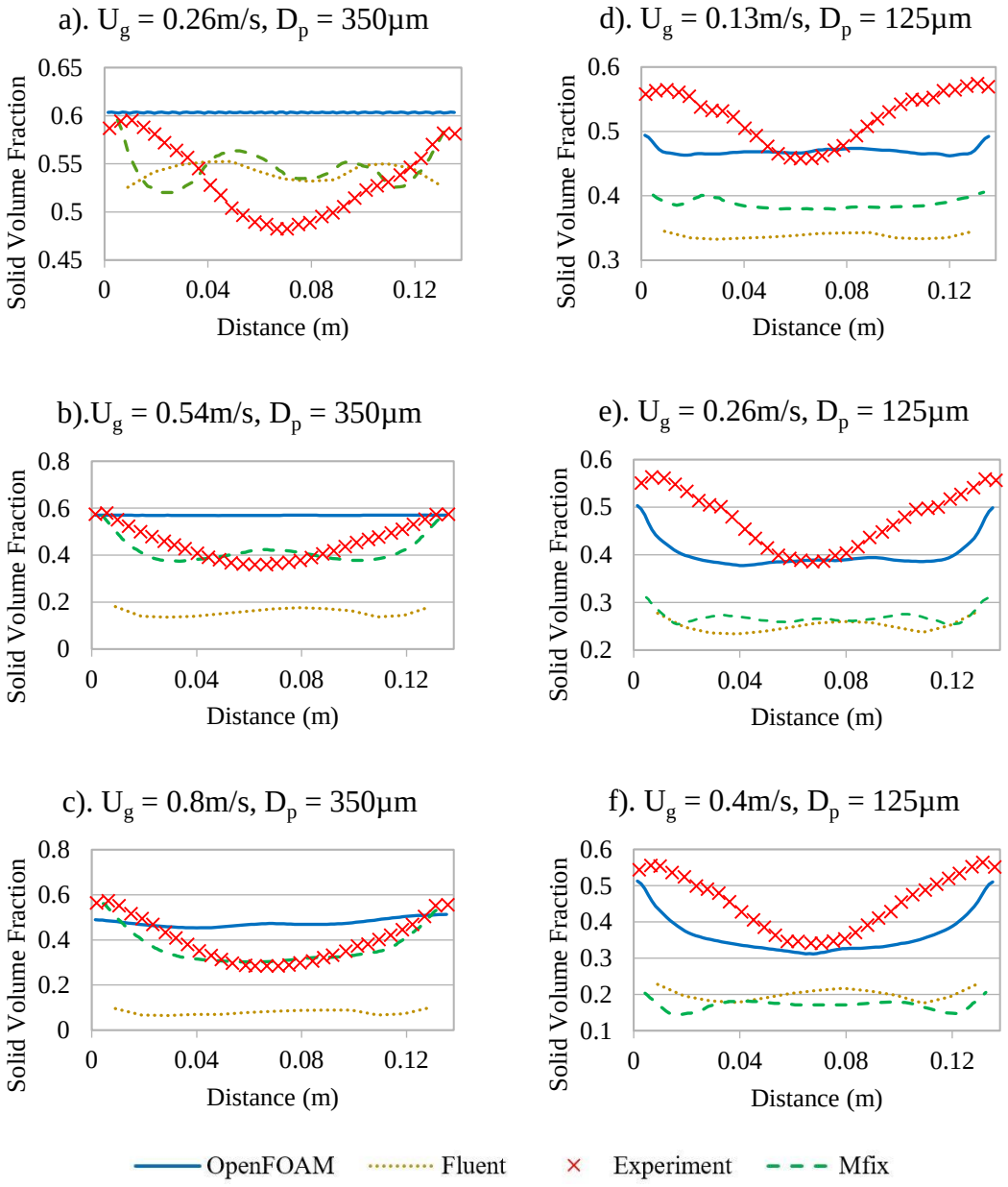

Figure 5 – Time-averaged solid volume fraction profile cross-section averaged between heights of 0.143m and 0.181m for the cylinder fluidized bed case.

In Figure 5 the time averaged cross-sectional results are shown for both particle diameters and all inlet gas velocities. For the 350μm diameter particles (Geldart group B) in Figure 5a) MFix, Fluent and OpenFOAM do not compare well to the experimental results reported. This could be due to shortcomings in these solvers to accurately model fluidizing behaviour at close to the minimum fluidization velocity at the inlet for larger particles. For higher inlet velocities, in Figure 5b) and c), the MFix and experimental results do compare very well, as was originally reported. OpenFOAM, however, does not fluidize at the lowest inlet gas velocity and only shows signs of fluidizing behaviour at the highest inlet gas velocity of 0.8m/s. Similar behaviour has been reported before by Herzog *et al.* (2012) in which OpenFOAM reported a much higher minimum fluidization for very large particles which are Geldart group D type particles, when compared to both their own MFix and Fluent results. For the particles with a diameter of 125μm, and at all three inlet gas velocities, Figure 5d), e) and f) show that OpenFOAM compares better with the experimental results than with both Fluent and MFix simulation results. Although the Fluent and MFix results match well with each other, both report much lower solids volume fraction.

The time-averaged solid volume fraction across the full height of the cylinder, averaged across the cylinder diameter at each height, can be seen in Figure 6, though no experimental results were reported. For the particles of diameter 350μm there are significant differences in the overall bed height predicted by each solver. The Fluent solver results for the higher inlet gas velocities in Figure 6b) and c) show that the particle entrainment is too high, causing a greater distribution of the solids phase throughout the height of the cylinder, with some particles leaving the system through the outlet at the top of the cylinder. This suggests that Fluent may be predicting gas phase velocities around the particles being close to or greater than the particles' terminal velocity. The OpenFOAM results are quite different to Fluent and MFix results, as can be seen in Figure 6a) where the solid phase is sitting at its maximum random packing limit of 0.63, and up to a height of around 0.2m no fluidization is occurring. At increasing inlet gas velocities, the OpenFOAM solver results show very little bed height increase, with little to no bubble formation. This suggests that OpenFOAM cannot predict bubble formation or fluidization behaviour for close to the minimum fluidization velocity for larger particles. For the smaller particles, Figure 6d) and e) show that the average bed heights predicted by all three solvers are significantly different. The OpenFOAM results for diameter 125μm in Figure 5 suggests the solids volume fraction profile across the cylinders height is closer

to the possible real profile. This also suggests that both MFix and Fluent both predict a more distributed solid phase up the cylinders height.

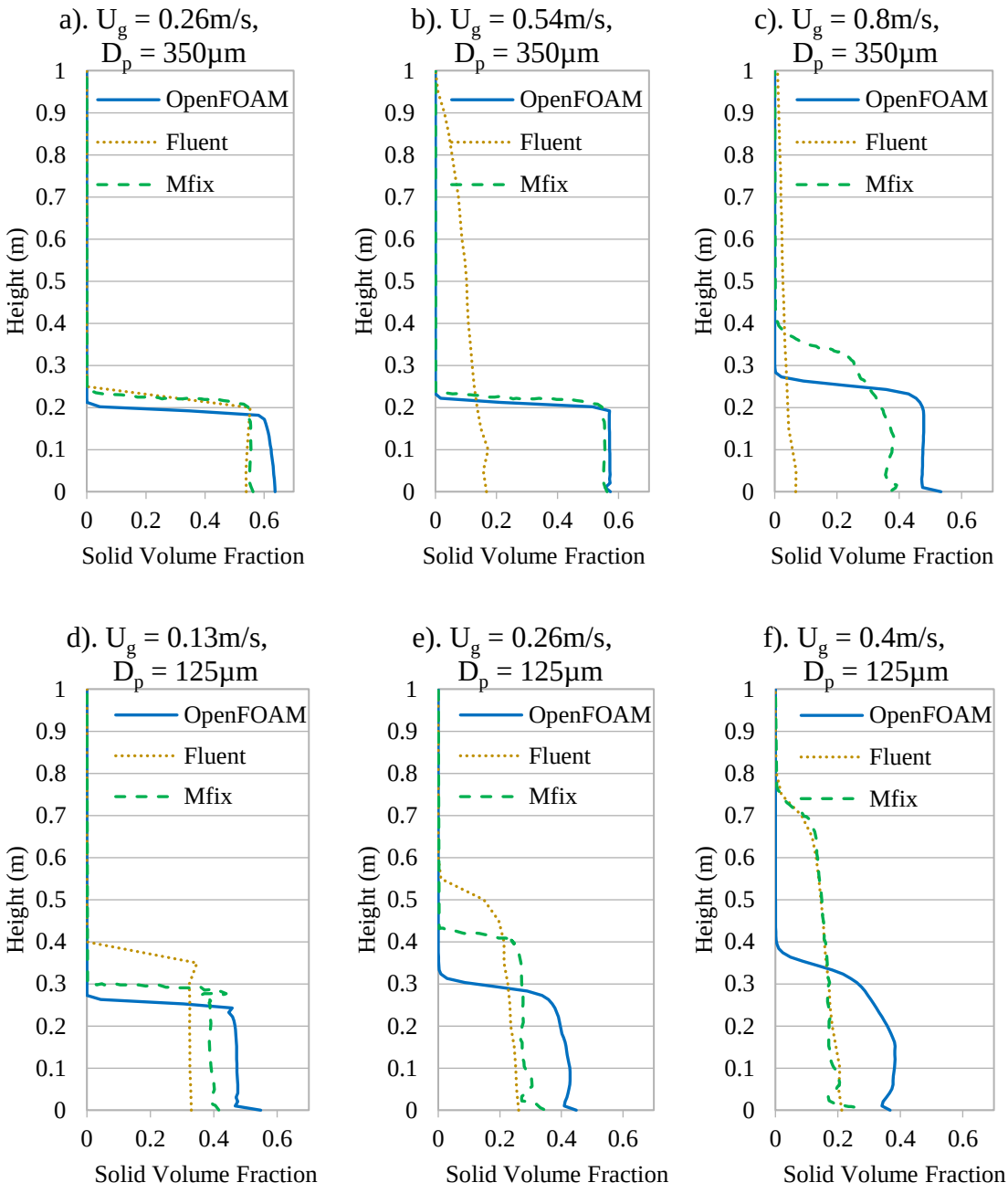

Figure 6 – Time-averaged solid volume fraction profile averaged across the cylinder diameter for the full height of the cylinder fluidized bed case.

The results from this comparison between the OpenFOAM, MFix and Fluent solvers show that each solver requires improvement in the modelling to account for all Geldart group particles. The OpenFOAM solver seemed to perform best for the smaller Geldart group A/B particles while overpredicting the minimum fluidization for the larger Group B particles. This has been reported before by Herzog *et al.* (2012) for much larger particles in the Geldart Group D range. This suggests that the OpenFOAM solver in its

current form does not work well for larger particles, while the MFix solver predicts the larger-particle flows better.

4.2.2 Coefficient of Restitution Sensitivity Analysis

The Coefficient of Restitution (CoR) plays an important role in granular-gas flows as it can affect flow structures such as bubble formation and particle velocities (Loha, Chattopadhyay and Chatterjee, 2014). Now we will vary the CoR to observe the sensitivity of the OpenFOAM solver. As the OpenFOAM solver performs best with 125µm diameter particles, this will be used as the basis for the sensitivity analysis. Gas inlet velocities of 0.13m/s and 0.4m/s will be compared to show how the inlet gas velocity also affects the results. A CoR of 0.7 and 0.9 will be simulated and compared to the original CoR of 0.8 and experimental results.

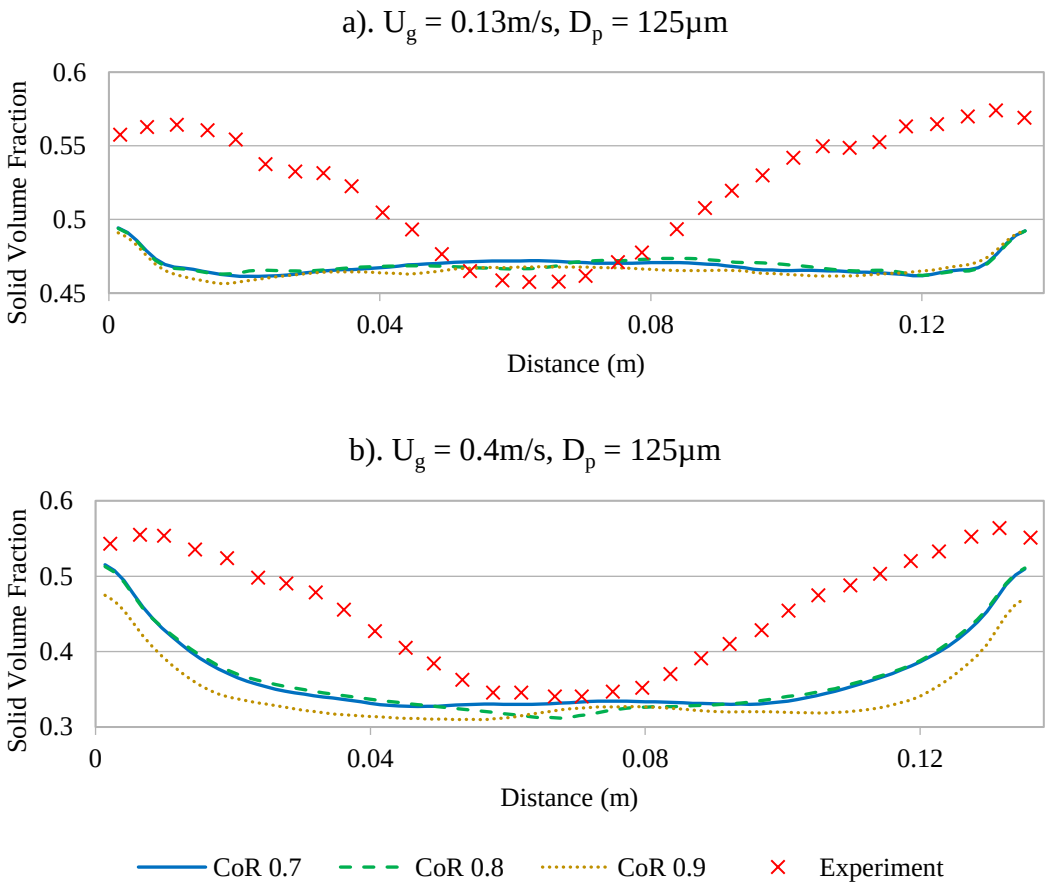

Figure 7 - CoR comparison, time-averaged solid volume fraction profile cross-section averaged between heights of 0.143m and 0.181m for the cylinder fluidized bed case.

For the impact of CoR for the lower inlet gas velocity of 0.13m/s in Figure 7a), it can be seen that there is only a small difference in the core of the flow, and the CoRs of 0.9 and 0.8 have a slightly lower solids volume fractions have, with no differences at the walls. The impact of CoR can be better seen with the higher inlet gas inlet velocity of 0.4m/s in

Figure 7b). The largest difference occurs with a CoR of 0.9 across the full width of the cylinder. This suggest that there are more bubbles forming and more particle entrainment, which is counter to what was reported by Loha *et al.* (2014) i.e. that the bubble formation is supressed with increasing CoR. For the cross-sectional profiles of the solids volume fraction it can be seen that as the CoR increases towards more elastic particle collisions, the profiles become flatter, with a lower solids volume fraction.

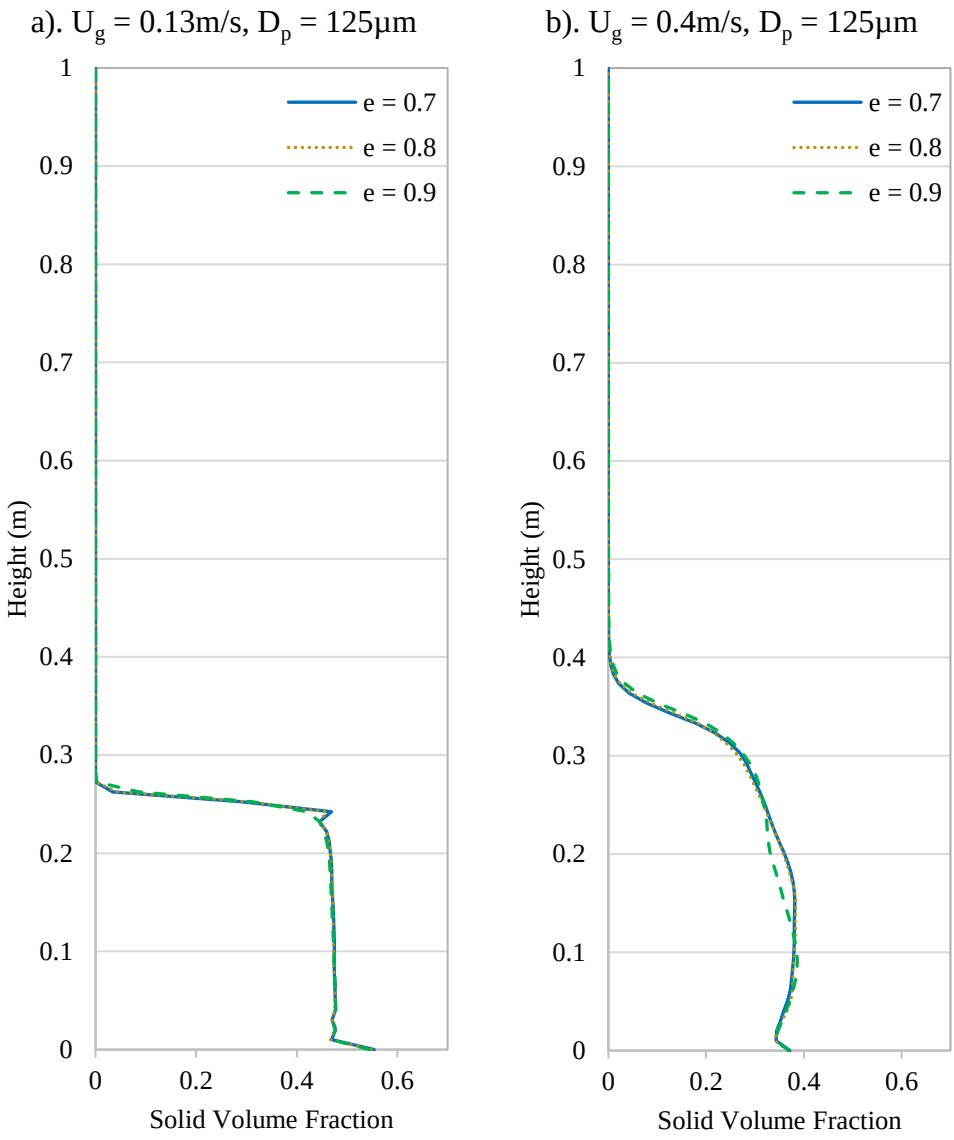

Figure 8 - CoR comparison, time-averaged solid volume fraction profile averaged across the cylinder diameter for the full height of the cylinder fluidized bed case.

Figure 8a) also shows very little variation between the different CoR values, other than a very small variation in solids volume fraction near the top of the solids region of the fluidized bed in which bubbles breaking the surface create the small difference observed. The results with a CoR of 0.9 do not show bubbles breaking near the surface of the solids region as clearly, which is expected from previous results in the literature. For the larger inlet gas velocity of 0.4m/s in Figure 8b), the results with a CoR of 0.9 have a higher

solids volume fraction near the base of the bed and then a much lower section of solids volume fraction where the cross-section average occurs between 0.143m and 0.181m. This is where the apparent contradiction occurs in Figure 7b) with the averaged cross-section only capturing the lower solids volume fraction region where the bubble formation is not as clear. Therefore, it does not contradict the findings by Loha *et al.* (2014) in that as the particles become nearly elastic the formation of bubbles is suppressed.

The overall results show that OpenFOAM acts as expected in terms of its sensitivity to the Coefficient of Restitution. As the particles became more inelastic, bubbles are more readily formed. The specified CoR of 0.8 in the original paper by Makkawi *et al.* (2006) is confirmed in this analysis to be the best suited for the cylinder fluidized bed, as the subsequent numerical results best match the experimental results.

4.2.3 Volume Diffusion Flux Models

From the results of the previous sections on the cylinder fluidized bed case, only the case of 125μm diameter particles at a gas inlet velocity of 0.4m/s will be used, as the OpenFOAM solver results in this case best matched with the experimental data. Now the cylinder fluidized bed case will be used to test and compare both the single and multiphase forms of the Volume Diffusion Flux models. For ease of understanding the single phase model as described in section 3.2, equations (29) and (35) will be referred to as Model A, and the multiphase model as described also in section 3.2, equations (35), (32), (33) and (34), will be Model B. The original solver in OpenFOAM will be referred to by its name, which is twoPhaseEulerFoam. A summary of each model can be seen in Table 7 below.

Table 7 - Volume Diffusion Flux model descriptions for cylinder fluidized bed case.

Label	Equations for Original and Volume Diffusion Flux Modifications	
twoPhaseEulerFoam	$\tau_s = 2\mu_s D_s + \left(\lambda_i - \frac{2}{3}\mu_s\right) tr(D_s) I$	(9)
	$D_s = \frac{1}{2}(\nabla U_s + (\nabla U_s)^T$	(10)
Model A	$U_{vs} = U_m + J_{vs}$, to replace U_s in equation (10)	(26)
	$D_{vs} = \frac{\rho_s \nu_s}{(\alpha_s \rho_s) + (\alpha_g \rho_g)}$	(35)
	$J_{vs} = D_{vs} \nabla \alpha_s$	(29)
Model B	$U_{vs} = U_m + J_{vs}$, to replace U_s in equation (10)	(26)
	$D_{vs} = \frac{\rho_s \nu_s}{(\alpha_s \rho_s) + (\alpha_g \rho_g)}$	(35)
	$w_s = \frac{\alpha_s \rho_s}{\alpha_s \rho_s + \alpha_g \rho_g}$	(32)
	$J_s = -\rho_s D_{vs} \nabla w_s$	(33)
	$J_{vs} = (\bar{v}_s - \bar{v}_g) J_s$,	(34)

Firstly, the time-averaged solids volume fraction across the width of the cylinder in Figure 9 shows that there is very little difference between the original twoPhaseEulerFoam model and Model A. However, Model B produces a lower solids volume fraction profile across the cylinder, which means it does not compare as well to the experimental results as twoPhaseEulerFoam and Model A. This suggests that in the measured cross section there may be larger bubbles or a greater number of small bubbles, being produced. In the centre of cylinder there is essentially no difference between any of the models, while the profile differs for Model B away from the centre of the flow.

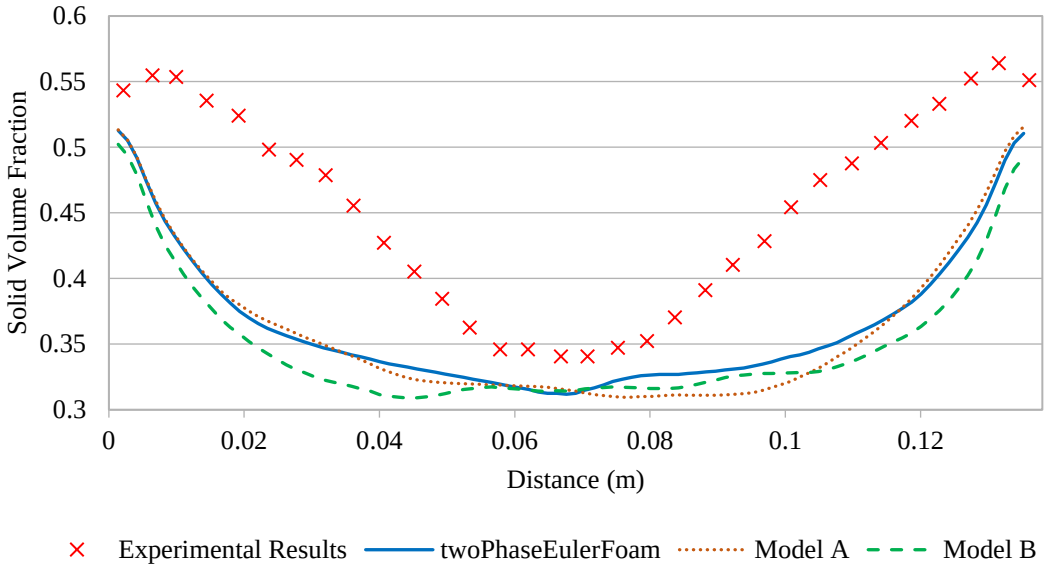

Figure 9 – Time-averaged solid volume fraction across the width of the cylinder, for the Volume Diffusion Flux models.

Figure 10 shows that results from Model A and from twoPhaseEulerFoam are not as similar as first appears in Figure 9. Both models A and B have a slightly higher time-averaged solid volume fraction. The region where the cross section is averaged over (between 0.143m and 0.181m across the full diameter) there is very little difference between twoPhaseEulerFoam and Model A, which reflects the cross-section profile comparison of Figure 9. Just below this region, twoPhaseEulerFoam and Model B have very similar solids volume fraction, while Model A has a slightly smaller solids volume fraction in comparison. Below 0.1m, models A and B predict the same solids volume fraction, which is smaller than twoPhaseEulerFoam. This suggests that there are larger bubbles or more bubbles being produced at the base of the bed than predicted in twoPhaseEulerFoam. Overall, from the time-averaged solids volume fractions in Figure 9 and Figure 10, there is a small difference in the progression of the solid phase flow up the cylinder, which can be characterised as larger bubbles or more bubbles being

produced at the base of the cylinder, producing an overall higher average particle bed height.

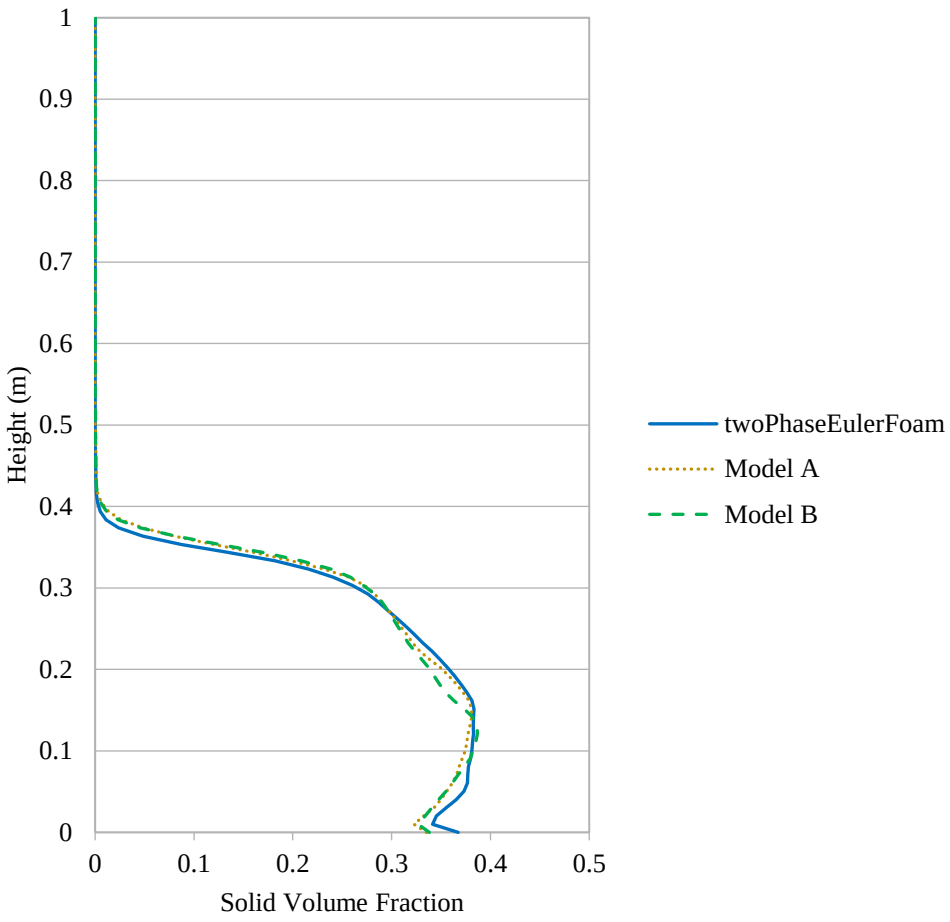

Figure 10 – Time-averaged solid volume fraction through the height of the cylinder, for the Volume Diffusion Flux Models.

The overall pressure drop of the system has not been reported for this experiment, therefore the pressure drop between the inlet and outlet over the full time of the simulation will only be looked at for qualitative results. In Figure 11 the largest fluctuation in the pressure drop occurs with Model B, while both twoPhaseEulerFoam and model A show similar changes in the pressure drop. This supports our presumption that Model B produces greater bubble formation and breaking at the surface with additional stresses due to the Volume Diffusion Flux. Initially the pressure drop is lower in models A and B than twoPhaseEulerFoam, which can be attributed to the lower viscosity causing less stress to occur in the start-up of the system. The total pressure drop through the bed for each model also showed some minor differences: Model A has a slightly lower pressure drop than twoPhaseEulerFoam, and Model B has a larger drop off. However, the largest difference between twoPhaseEulerFoam and the models is only 22Pa, which is very small compared to the overall pressure drop of around 2800Pa on average.

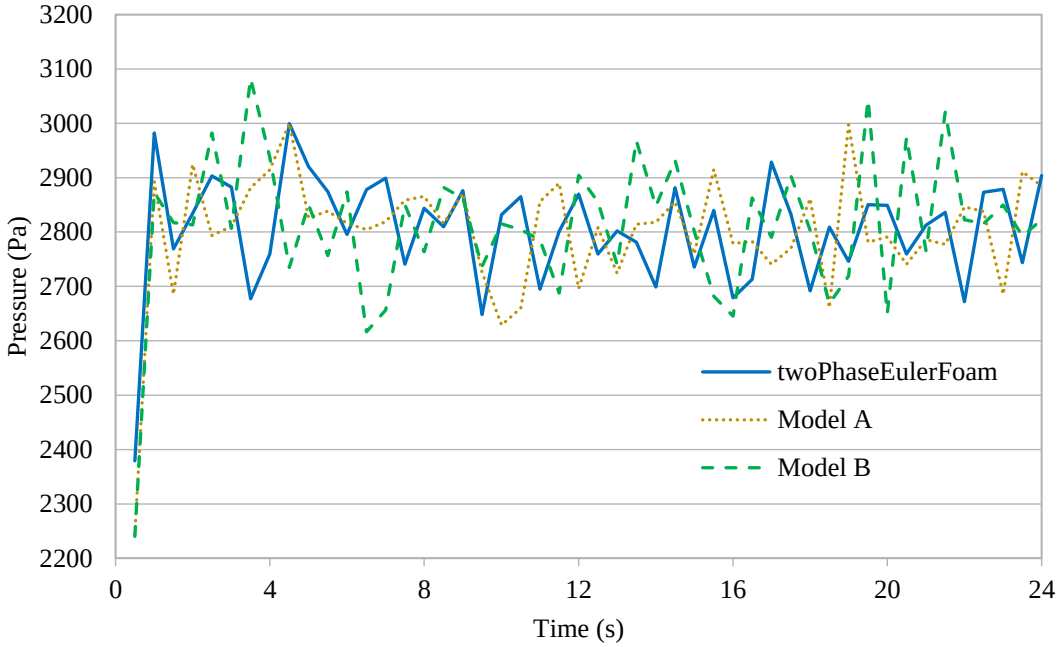

Figure 11 - Pressure Drop along cylinder, for the Volume Diffusion Flux models.

The solid phase velocity in the y vertical (axial) direction of the cylinder can be seen in Figure 12. There is a significant difference in the velocity profile of Model B compared to the other models. It produces a larger positive (upwards) velocity in the centre and larger negative (downwards) velocity closer to the walls. The profiles are all similar in shape, but the differences between Model B and twoPhaseEulerFoam mean that particles circulate more quickly in the fluidized bed. Model A, when compared to twoPhaseEulerFoam, has a slightly slower circulating action but is not significantly different.

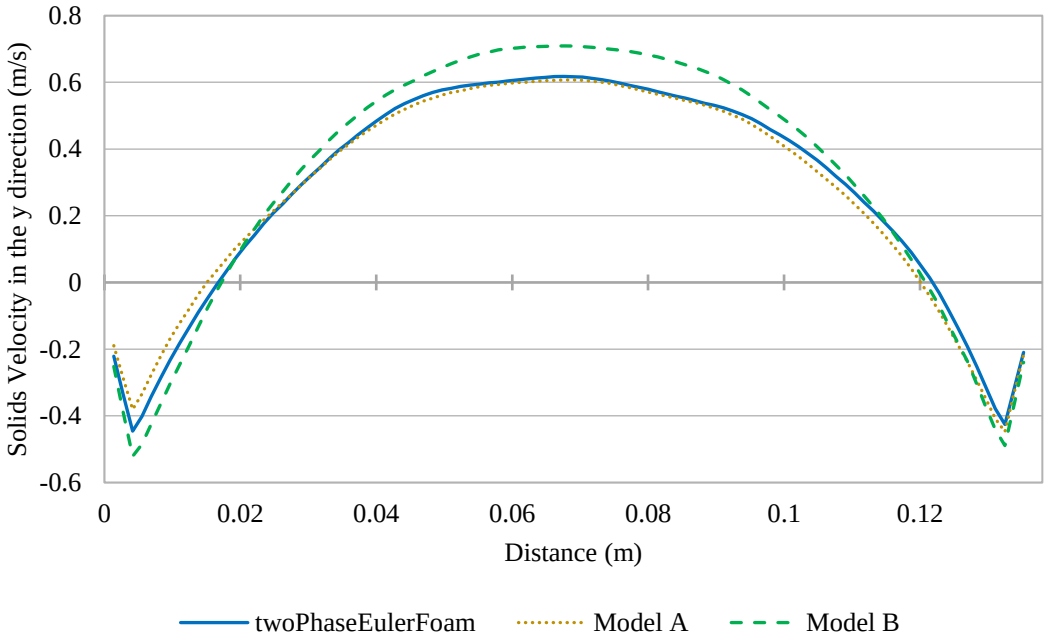

Figure 12 – Time-averaged solids velocity in the vertical direction, for the Volume Diffusion Flux models.

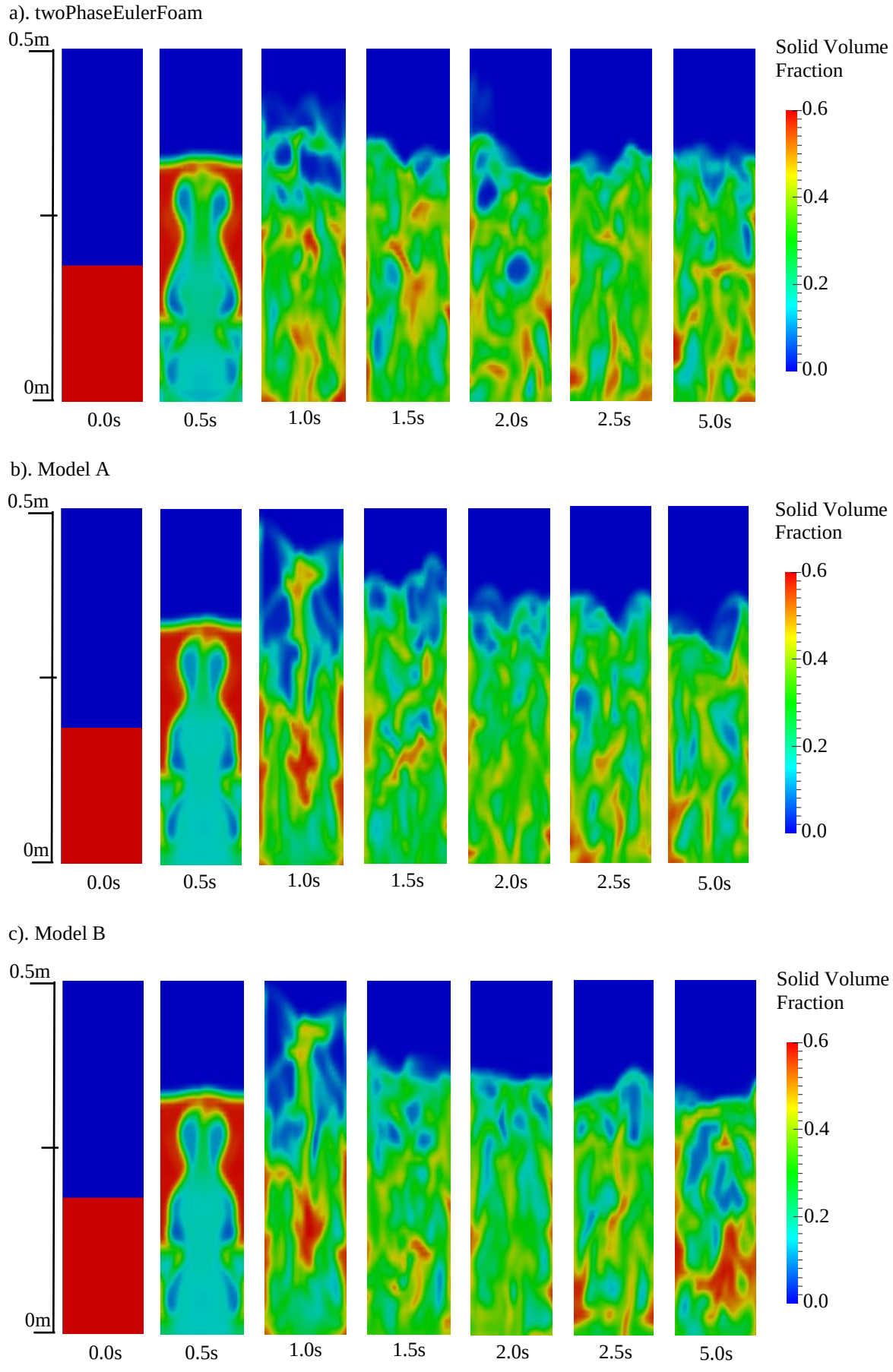

Figure 13 - Solid Volume fraction in the cross-section of the cylinder, from 0 to 5 seconds, for the Volume Diffusion Flux models.

The initial conditions of the simulation, with a static bed of particles, can be seen in Figure 13 for each of the models. Both models A and B produce a higher initial bed expansion but a similar initial bubble shape to twoPhaseEulerFoam. The time taken for the collapse of the initial bubble takes longer in models A and B, as can be seen at 1 second with the descent of the initial top layer of particles still occurring. Model A predicts smaller bubbles are formed, with more dilute regions than for twoPhaseEulerFoam and clearer and more distinct bubbles. Model B seems to produce bubbles that are larger than those in Model A, while they are less distinct than with twoPhaseEulerFoam.

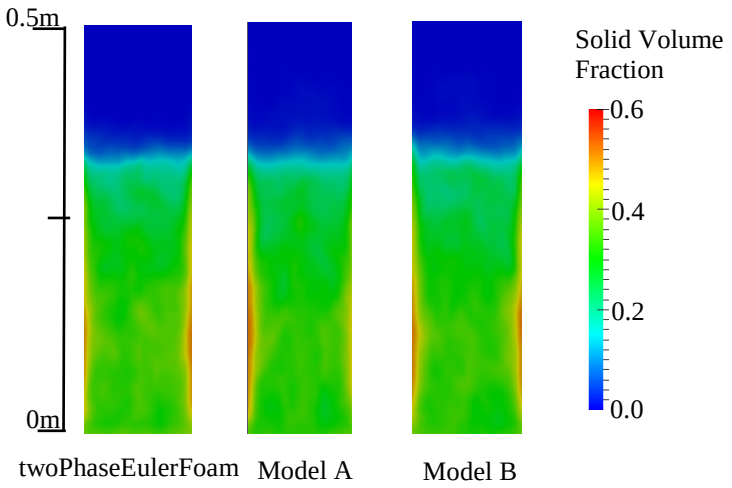

Figure 14 – Time-averaged solid Volume Fraction longitudinal cross-section of the cylinder fluidized bed, for the Volume Diffusion Flux models.

The time-averaged cross section images in Figure 14 show there are not large qualitative differences between the models' except near the walls where Model A produces some bias, with a higher solids volume fraction on one side than the other. However, this bias could be due to the simulation not running long enough to produce a better average across the cylinder. Models A and B show higher solids volume fractions at the cylinder walls, but there are no other significant differences observed.

The images in Figure 15 are of the time-averaged solids velocity in a longitudinal cross-section of the cylinder. All three models show that there is circulation occurring, with a large upward velocity in the centre and a downward velocity near the walls of the cylinder. The maximum velocity in Model B is much higher than the other two models and occurs over a greater part of the centre of the cylinder, which agrees with the cross-sectional solids velocity results in Figure 12. Both models show a larger region where there is little to no movement near the walls with there being more solids velocity being in the direction towards the centre while a slightly larger region each side of the centre flow for the returning particles as they fall.

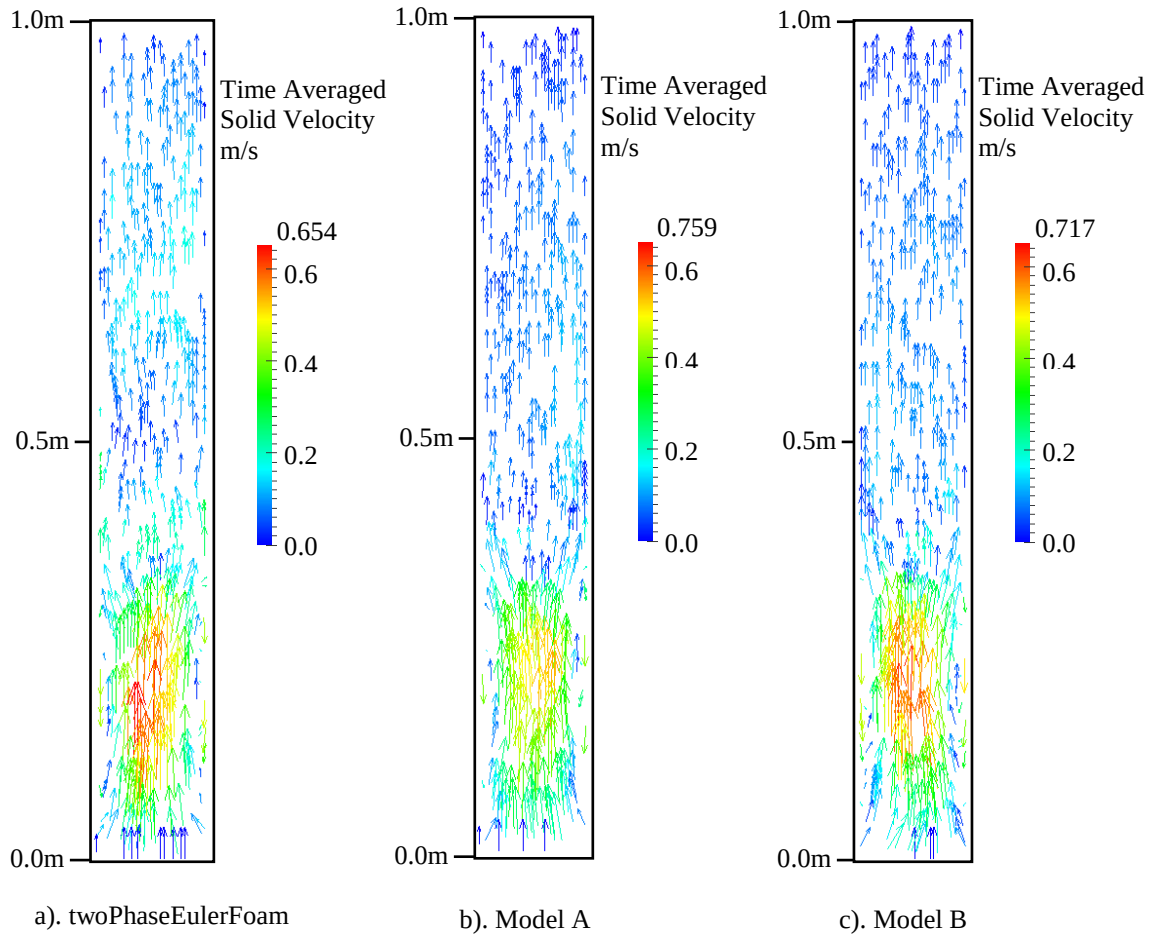

a). twoPhaseEulerFoam b). Model A c). Model B

Figure 15 - Time-averaged solids velocity over the full height of the cylinder, for the Volume Diffusion Flux.

From these results for the Volume Diffusion Flux modifications in the cylinder fluidized bed fluidized bed case it can be seen that there is not a significant difference between the original solver and the modifications. However, there were some differences for Model B in flow characteristics such as the solids velocity, and start-up effects in the solids volume fraction. Neither Model A or B improved upon the results from the original solver twoPhaseEulerFoam when compared to experimental data. This could be due to these modifications not necessarily being appropriate for this particular set of flow conditions. Therefore, it would be useful to test these modifications with another fluidized system.

4.2.4 Korteweg Stress Models

The case with particle diameters of 125μm and an inlet gas velocity of 0.4m/s will also be used to test both the Korteweg stress modifications. This enables us to observe additional effects of the Korteweg stress modifications and the mass fraction (w_s). As in the previous section, the original OpenFOAM model (twoPhaseEulerFoam) will be compared to the two modifications of the Korteweg Stress model that will be called Model C and Model D. A summary of these models is shown in Table 8.

Table 8 – Korteweg Stress model descriptions foe the cylinder fluidized bed case.

Label	Equations for Original and Korteweg Stress Modifications	
twoPhaseEulerFoam	$\rho_s\alpha_s\left[\frac{\partial U_s}{\partial t}+U_s\cdot\nabla U_s\right]=-\alpha_s\nabla P+\nabla\cdot\alpha_s\tau_s-\nabla P_s+\alpha_g\rho_g g+\beta(U_g-U_s)$	(5)
Model C	$\rho_s\alpha_s\left[\frac{\partial U_s}{\partial t}+U_s\cdot\nabla U_s\right]=-\alpha_s\nabla \mathrm{P}+\nabla\cdot\alpha_s\tau_s-\nabla \mathrm{T}+\alpha_g\rho_g g+\beta(U_g-U_s)$	(42)
	$T=\left[-P+K\rho\nabla^2\alpha_s+\frac{1}{2}K\lvert\nabla\alpha_s\rvert^2\right]I-K\nabla\alpha_s\otimes\nabla\alpha_s$	(39)
	$K=\frac{\mu_s^2}{\rho_s}$	(40)
Model D	$\rho_s\alpha_s\left[\frac{\partial U_s}{\partial t}+U_s\cdot\nabla U_s\right]=-\alpha_s\nabla \mathrm{P}+\nabla\cdot\alpha_s\tau_s-\nabla \mathrm{T}+\alpha_g\rho_g g+\beta(U_g-U_s)$	(42)
	$T=\left[-P+K\rho\nabla^2 w_s+\frac{1}{2}K\lvert\nabla w_s\rvert^2\right]I-K\nabla w_s\otimes\nabla w_s$	(41)
	$K=\frac{\mu_s^2}{\rho_s}$	(40)
	$w_s=\frac{\alpha_s\rho_s}{\alpha_s\rho_s+\alpha_g\rho_g}$	(32)

In Figure 16, the time-averaged solids volume fraction profiles across the width of the cylinder are seen to be distinctly different for each model. Model C has the greatest difference in its over profile, with a lower solids volume fraction away from the centre while the centre is higher (and in this region closer to the experimental results). Model D does not have as large a difference from the twoPhaseEulerFoam model. Again, there is a smaller solids volume fraction away from the centre of the flow, while being similar to Model C results near the walls and closer to twoPhaseEulerFoam results at the centre. Overall, Model C does not improve the solids volume fraction profile. Model D produces better results but it still is not an improvement over twoPhaseEulerFoam when compared to the experimental results.

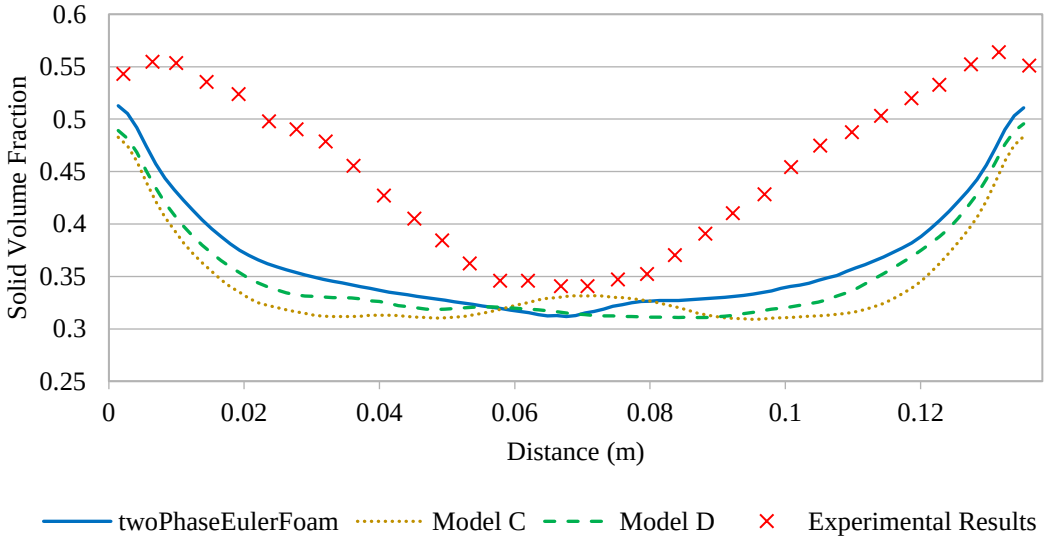

Figure 16 – Time-averaged solid volume fraction across the width of the cylinder, for Korteweg Stress models.

The solids volume fraction through the height of the cylinder is given in Figure 17 and shows that both models C and D have a greater time-averaged bed expansion than the twoPhaseEulerFoam model predicts. The similarities between models C and D continue further down the cylinder, with smaller solids volume fractions compared to twoPhaseEulerFoam. Then a sharp increase occurs in the solids volume fraction around 0.1m. This could be due to the particles falling and the bubbles forming at the base of the bed: at this point the particles slow in their decent and are circulated back up the cylinder by the action of the gas phase. The twoPhaseEulerFoam model has a greater height range over which this occurs, and Model D has the largest increase in the solids volume fraction at 0.1m. At the base of the cylinder, models C and D both seem to produce either larger bubbles or more bubbles then twoPhaseEulerFoam, with Model D having the smallest solids volume fraction at the base of the cylinder. Between Figures 17 and 18 the solids volume fraction for Model D provides the closest match to the experimental data of the two Korteweg Stress models. Both models' C and D do show that there are some differences compared to twoPhaseEulerFoam results in the distribution of flows through the cylinder.

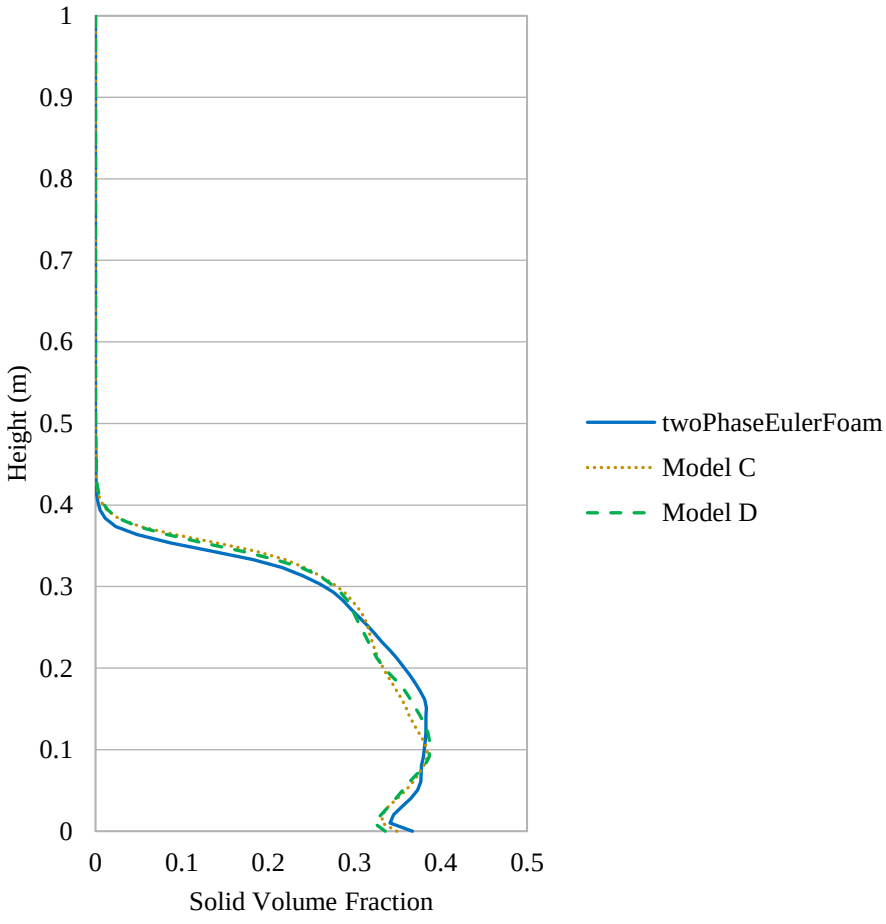

Figure 17 – Time-averaged solid volume fraction through the height of the cylinder, for the Korteweg Stress models.

As in the Volume Diffusion Flux discussion, the overall pressure drop between the inlet and outlet over the full time of the simulation will be examined qualitatively. In Figure 18 the initial pressure drop is the highest in Model C, while Model D closely matches twoPhaseEulerFoam. Overall, and given the fluctuations, there is a slightly larger pressure drop using Model C, due to the bubble formation and breaking at the surface of the solid phase region. Both models C and D have a slightly larger overall time averaged pressure drop with Model C being the largest, however, the difference between the twoPhaseEulerFoam and Model C is 37 Pa which is not particularly significant.

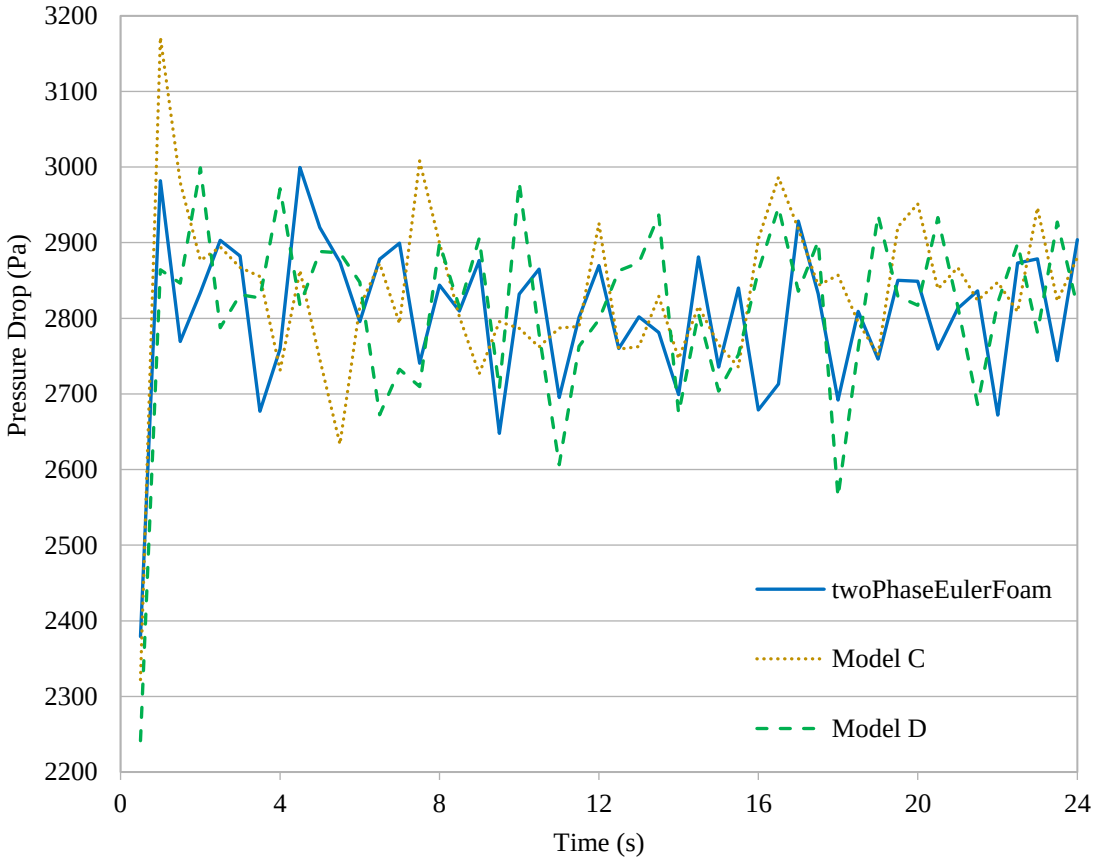

Figure 18 - Pressure Drop along cylinder for the Korteweg Stress models.

A more significant difference between the models can be seen in the solid velocities in Figure 19. Both models C and D have a higher solids velocity in the centre of the cylinder. The profiles differ across the cylinder, as Model C peaks at a slightly lower velocity than Model D and in general has a larger negative (downward) velocity of the particles near the walls. There is some bias towards one side of the cylinder, which could be due to the length of time over which the flow is averaged; a larger time period might negate this effect.

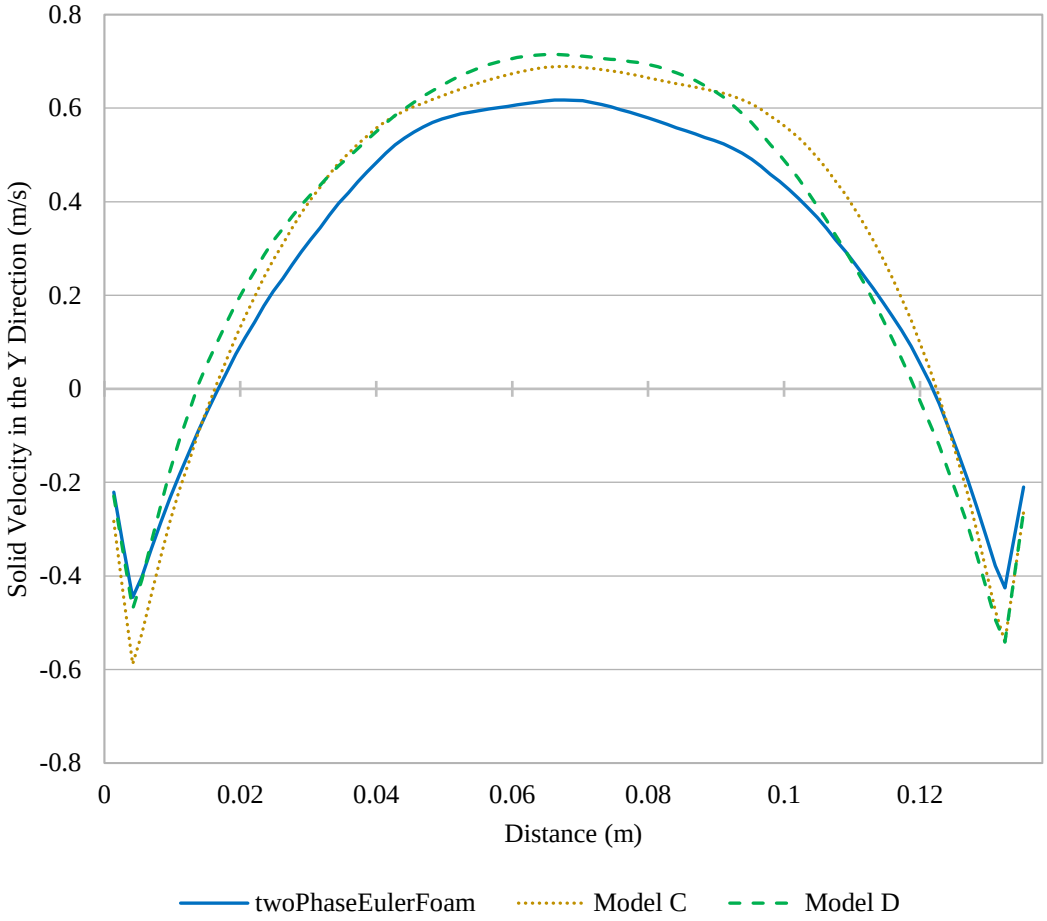

Figure 19 – Time-averaged solids velocity in the vertical direction, for the Korteweg Stress models.

The initial formation of the first bubble and the bed expansion can be seen in Figure 20 where all three models produce similar flow structures. The collapse of the initial bed expansion occurs more slowly for models C and D than in twoPhaseEulerFoam, and the solid phase is suspended for longer (as can be seen in Figure 20 for the time of 1.0 seconds). As the simulation progresses, Model C produces larger, more distinct bubbles than Model D, which could account for the lower solids velocity and lower solids volume fraction observed with Model C.

The time-averaged solids volume fraction cross section is shown in Figure 21. It is very clear that models C and D both have a larger region of time-averaged solids volume fraction in the cylinder compared to twoPhaseEulerFoam, which confirms what was observed in Figure 17 for the time-averaged solids volume fraction. Model C has a slightly higher maximum solids volume fraction at the walls, compared to the other two models. Again, this could be due to the higher solids velocity producing a higher rate of particles hitting the walls and slowing down in that region, resulting in, on average, a higher solids volume fraction to.

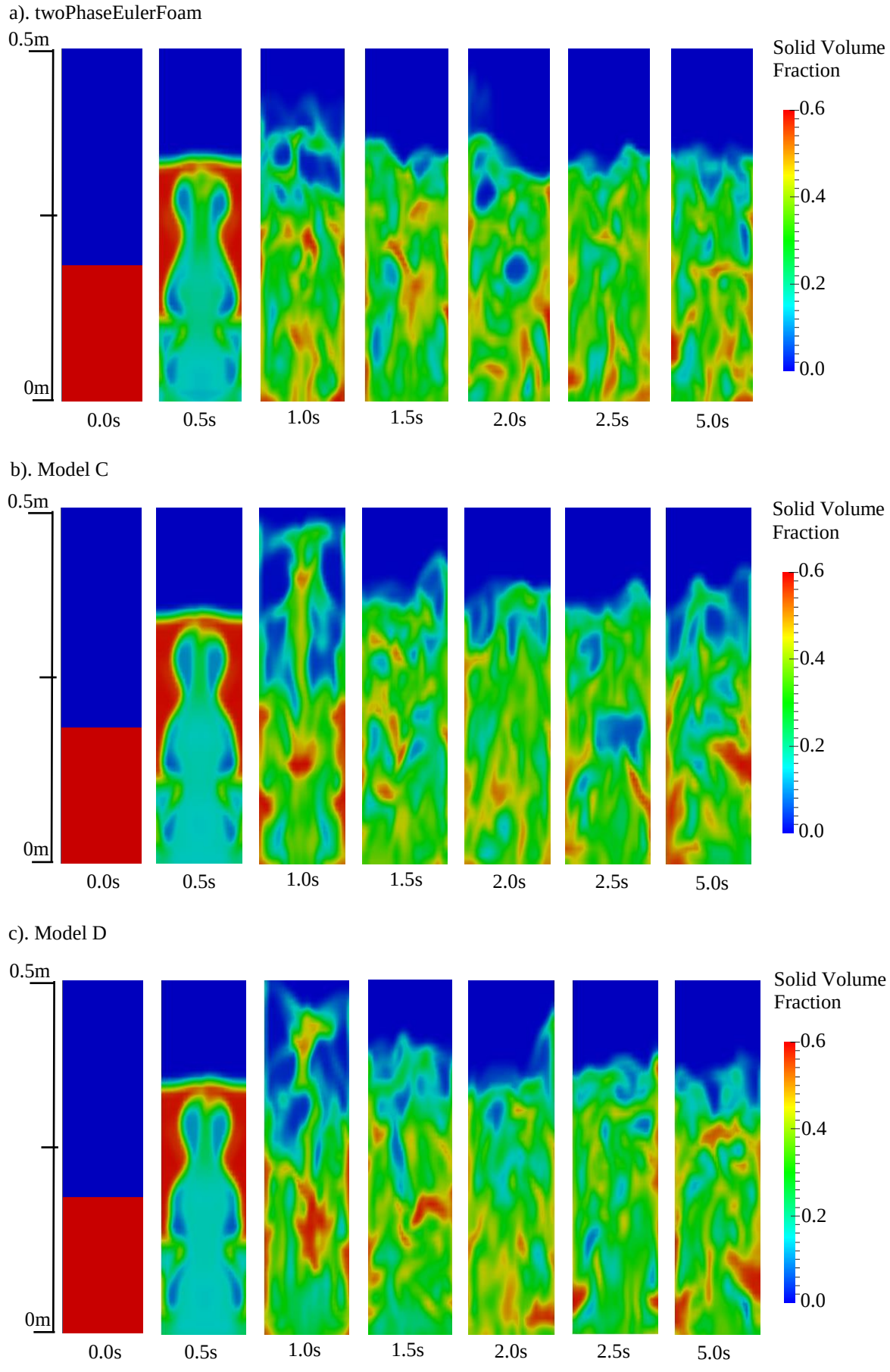

Figure 20 - Solid Volume fraction in the vertical section of the cylinder, from 0 to 5 seconds, for the Korteweg Stress models.

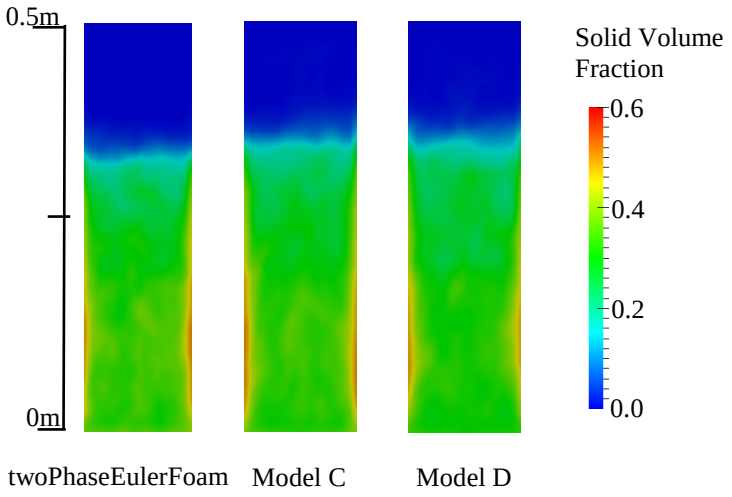

Figure 21 – Time-averaged solid volume fraction, for the Korteweg Stress models.

The final discussion is of the time-averaged solids velocity, as shown in Figure 22, where all three models show the solids circulating up in the centre and then downwards near the walls. Models C and D show an interesting flow profile just above where the average solids volume fraction is at its maximum time-averaged height. There is a small region where the particles rising and the particles falling meet and the move out towards the walls, away from the centre. This could be due to some particles travelling further up the cylinder and coming down with a greater velocity; when they meet the flow coming upwards they collide and create a small region near the cross-sectional centre of the cylinder with very little velocity of particles and tends to move towards the walls. There is also a very strong circulating motion that occurs near the walls that is greater for both models C and D, as can be seen by the larger solids velocities in Figure 19 which suggest a greater particle momentum. Therefore, the region in Figure 17 where there is a small sharp increase in solids volume fraction around 0.1m in height could be due to the increase in the particle momentum, meaning particles travel further down the cylinder before being recirculated into the main flow upwards. This creates a distinct region near the walls where there is a large velocity difference driving the circulation.

From these results using the Korteweg Stress modifications, the most significant resultant differences were found to be primarily in the circulating movement. A large velocity difference occurs near the walls, meaning that particles travel further down the cylinders near the walls before being recirculated back into the bulk flow. For the cylinder fluidized bed case there was not a significant difference in the predictions of models C and D, while there were some differences with the results from when twoPhaseEulerFoam. However, the Korteweg Stress modifications do not in general improve upon the original twoPhaseEulerFoam model in reproducing results experimental results.

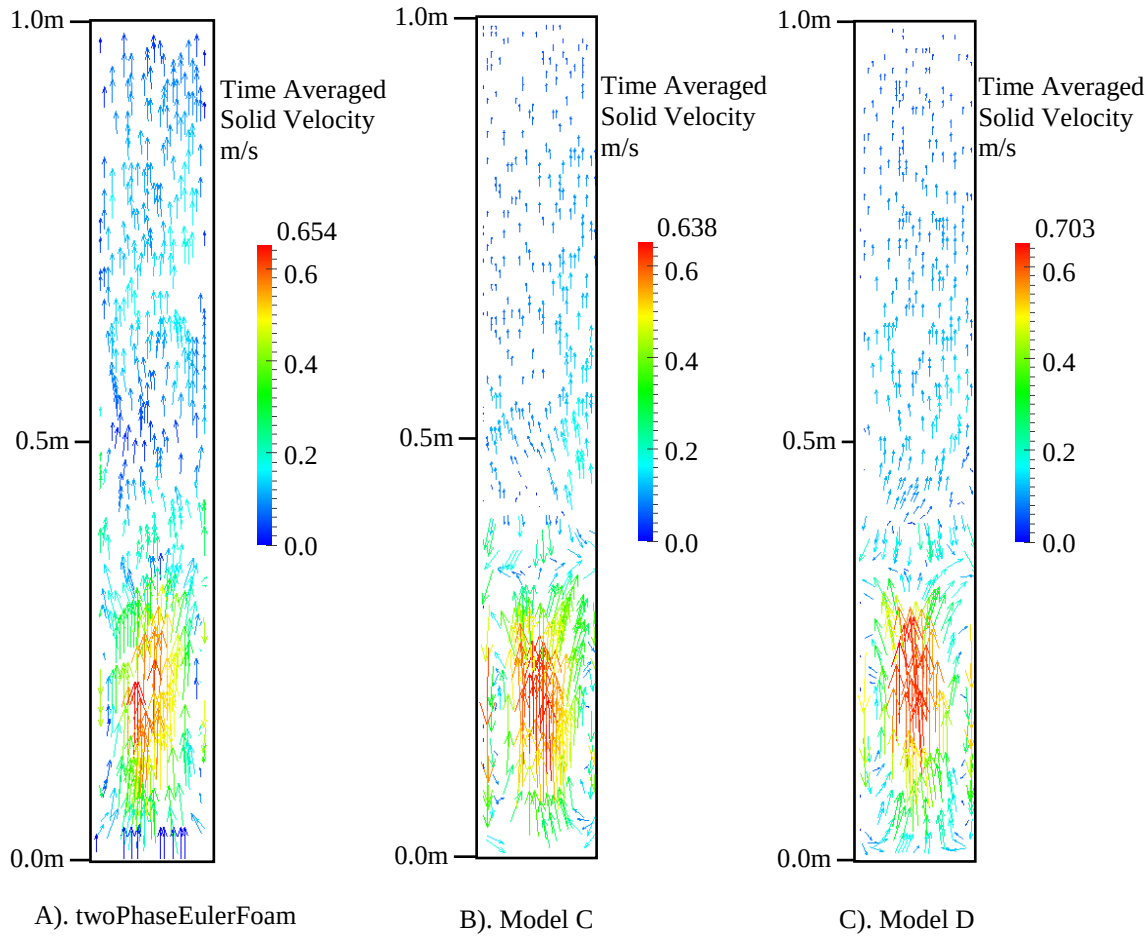

Figure 22 - Time-averaged solids velocity in a vertical cross-section of the cylinder fluidized bed case, for the Korteweg Stress models.

4.2.5 Cylinder Fluidized Bed Discussion

A cylinder fluidized bed case was used to validate various proposed physical models, and it was found that each model did show some differences with the others. The differences are due to the variations in the models, as well as how they are implemented. The study conducted here showed that none of the three models used could predict the flow characteristics of both particle diameter cases. For this work it was important to test OpenFOAM as to whether it can be a useful tool. The results showed that OpenFOAM was able to predict a certain range of flows for a particular particle diameter. It should be noted that other flow configurations will be used in this thesis to further test and validate the capabilities of OpenFOAM. A small study of the Coefficient of Restitution effects in the OpenFOAM solver was conducted, and the results were as previously reported by Loha *et al.* (2014) therefore further validating the usefulness of OpenFOAM.

The modifications to include Volume Diffusion Flux and Korteweg Stress were both tested on a single case of the cylinder flow. It is concluded that Volume Diffusion Flux

does produce some qualitative changes in the flow structure of the fluidized bed. The biggest difference was noted for Model B, which is the multiphase form of the Volume Diffusion Flux developed for this work; here, there was a larger upwards solids velocity in the centre of the cylinder and a larger downwards velocity near the walls, suggesting a faster circulation is occurring. The Korteweg Stress modifications produced a similar increase in the solids velocity but there was more of an impact on the overall circulating movement within the cylinder when compared to the Volume Diffusion Flux modification. Another configuration to test both the Volume Diffusion Flux and the Korteweg stress modifications will be described in the next section.

4.3 Recirculating Fluidised Bed Case

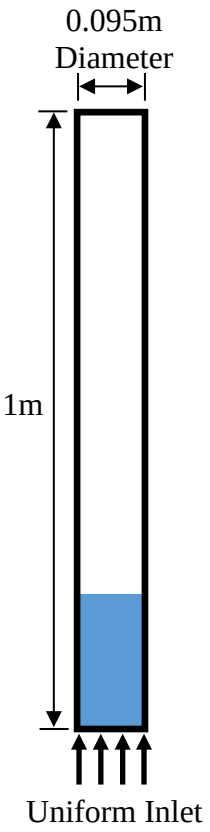

Figure 23 - Recirculating Fluidized Bed Geometry

This case is of a recirculating fluidized bed and is reported by Gao *et al.* (2012). It consists of a cylinder 1m in height, with particles allowed to exit through the top of the cylinder, and a constant solids mass at the inlet at the base of the cylinder. The paper reports both experimental and Fluent results, which will be used here to compare with OpenFOAM results. The parameters used in the simulations of both Fluent and OpenFOAM are given in Table 9, and the geometry is represented in Figure 24.

The inlet boundary is a uniform velocity inlet of 1.25m/s for both the gas and solid phase. The rate of mass entering is calculated by averaging the rate of mass leaving the domain, which in this work was completed by running OpenFOAM simulations and adjusting the solid volume fraction at the inlet until the mass rate leaving the system was the same as that entering the cylinder. This gave a solids volume fraction of 0.02 at the inlet which gave a solid phase inlet mass flow rate of 0.43kg/s. Particles are allowed to leave through the outlet at the top of the cylinder at atmospheric pressure (1.103bar). The initial conditions are such that there is a settled bed of particles up to a height of 0.204m with a random packing solids volume fraction of 0.63, and no other particles are in the system at this time. The Johnson and Jackson (1987) boundary condition are used for the wall boundaries where the gas phase has no slip and the solids phase has partial slip.

The original purpose of the paper as set out by Gao *et al.* (2012) was to compare different drag models as well as different initial bed heights at various inlet velocities. The drag model of Gao *et al.* (2012) makes use of three known drag models for different solid volume fractions. In very dilute regions ($0.99 < \alpha_g \leq 1.0$) the Schiller and Naumann (1935) drag model is used, in dilute regions ($0.94 < \alpha_g \leq 0.99$) the Wen and Yu (1966) drag model is used, and the Mckeen and Puglsey (2003) drag model is used in dense regions ($\alpha_g \leq 0.94$). With OpenFOAM this composite drag model is easily added to the solver, however, there were issues in the results it gave. Using the drag model of Gao *et al.* (2012) the bed of particles did not fluidize, instead only a little expansion occurred, with a little movement on the surface of the solid phase and no bubbles were formed. This drag model was tested again on a simpler geometry of a pseudo 2D fluidized bed, but the same results of little to no fluidization occurred. Both the Wen and Yu (1966) drag model and the Schiller and Naumann (1935) drag model were tested individually; they produced fluidized flows with particles leaving the cylinder through the top as expected. The Mckeen and Puglsey (2003) drag model was also tested alone, and the system did not fluidize, so it has been identified as the element within the composite drag model which did not work. To be able to continue, another of the drag models that was used by Gao *et al.* (2012) will be used; the Syamlal *et al.* (1993) drag model. This does limit the Fluent results that can be used for comparison to the solids volume fraction over the full height of the cylinder, as these results only were reported for this particular drag model.

Table 9 - Recirculating Cylinder Parameters (Gao *et al.*, 2012).

Parameters	
Cylinder	Diameter 0.095m, Height 1m
Gas	Air, Density 1.2kg/m^3, μ_g = 1.789 x 10^{-5}N/m^{2}s
Particles	Group B Diameter 139µm, Density 2400kg/m^3
Gas inlet Velocity	1.25m/s
Solid Volume Fraction at inlet	0.02
Particle-Particle Coefficient of Restitution	0.9
Particle-Wall Coefficient of Restitution	0.9
Max solid Fraction	0.63
Critical solid fraction	0.6
Simulation time	40s
Static Bed Height	0.204m
Measuring height at cross section	0.078m, 0.138m and 0.198m

A mesh independence study was carried out for this system configuration in the same manner as by Gao *et al.* (2012) for the Fluent simulations. Four sizes of mesh were compared; a rough mesh of 10625 cells, a medium mesh of 16200 cells, a fine mesh of 33075 cells and a very fine mesh of 44800 cells. The void fraction of each mesh across the full height of the cylinder was compared and it was found that a fine mesh with 33075

cells was the most suitable, with the very fine mesh not significantly improving the results compared to the increase in computing cost.

For the recirculating fluidized bed the original solver in OpenFOAM will be used compared with the Fluent and experimental results reported by Gao *et al.* (2012). They will form a basis to which the modifications of Volume Diffusion Flux and Korteweg Stress will be applied.

4.3.1 Volume Diffusion Flux Models

As before, the single phase model as described in section 3.2, equations (29) and (35) will be referred to as Model, A and the multiphase model as described also in section 3.2, equations (31), (35) and (34), will be Model B. The original model in OpenFOAM will be referred to by the solver's name which is twoPhaseEulerFoam. The description of each model is in Table 10.

Table 10 - Volume Diffusion Flux model descriptions for the recirculating fluidized bed.

Label	Equations for Original and Volume Diffusion Flux Modifications	
twoPhaseEulerFoam	$\tau_s = 2\mu_s D_s + \left(\lambda_i - \frac{2}{3}\mu_s\right) tr(D_s) I$	(9)
	$D_s = \frac{1}{2}(\nabla U_s + (\nabla U_s)^T$	(10)
Model A	$U_{vs} = U_m + J_{vs}$, to replace U_s in equation (10)	(26)
	$D_{vs} = \frac{\rho_s \nu_s}{(\alpha_s \rho_s) + (\alpha_g \rho_g)}$	(36)
	$J_{vs} = D_{vs} \nabla \alpha_s$	(29)
Model B	$U_{vs} = U_m + J_{vs}$, to replace U_s in equation (10)	(26)
	$D_{vs} = \frac{\rho_s \nu_s}{(\alpha_s \rho_s) + (\alpha_g \rho_g)}$	(36)
	$w_s = \frac{\alpha_s \rho_s}{\alpha_s \rho_s + \alpha_g \rho_g}$	(32)
	$J_s = -\rho_s D_{vs} \nabla w_s$	(33)
	$J_{vs} = \left(\bar{v}_s - \bar{v}_g\right) J_s$,	(34)

The time-averaging occurs after 20 seconds of simulation time, to allow for initial start-up effects to pass, and the averaging then occurs over the next 20 seconds to reduce the fluctuations in the flow. The time-averaged solid volume fraction over the full height of the cylinder can be seen in Figure 24a), where the differences between the simulation and experimental results are very apparent. This is due to the drag model used over-predicting the amount of drag occurring on the particles, therefore distributing the particles further up the cylinder (as is also seen in the original paper results). The Fluent results better predicts the solids volume fraction from about midway up the cylinder. In the lower half of the cylinder, Fluent does predict an increase in solids volume fraction in the region near the base of the cylinder, as the experimental results show, but is far smaller than the

empirical value. The unmodified OpenFOAM solver, twoPhaseEulerFoam, shows a larger solids volume fraction in the upper region of the cylinder, but does not show a significantly larger solids volume fraction near the base of the cylinder. As the particles are more evenly distributed throughout the height of the cylinder, there are not as many particles left near the base of the cylinder. Both models A and B produce the same profiles in the upper, more dilute regions, while predicting even smaller solids volume fractions in the lower part of the cylinder. It should be noted that where the results from twoPhaseEulerFoam and both models peak in the solids volume fraction in the lower section is near to the height where the experimental results also peak. The reported Fluent results show the solids volume fraction peaking at a lower height in the cylinder. Model B has the lowest solids volume fraction in the lower section. The profiles produced by the models agree with what was found in the cylinder fluidized bed case in Figure 10.

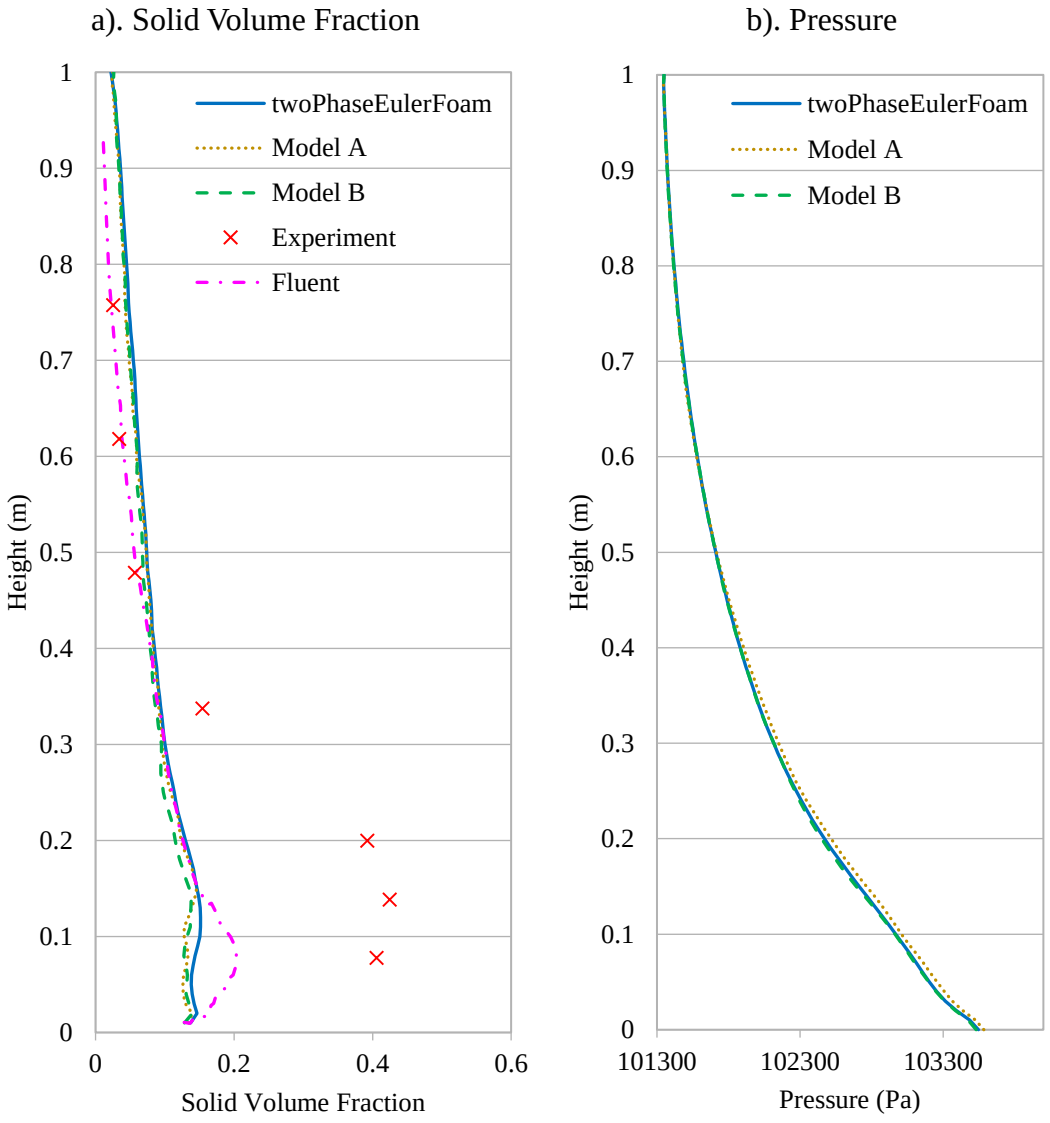

Figure 24 – Profiles through the height of the cylinder of a). Solid Volume Fraction, and b). Pressure, for the Volume Diffusion models.

The pressure profile or overall pressure drop in the recirculating cylinder was not reported by Gao *et al.* (2012), so only the twoPhaseEulerFoam results and both model results are compared in Figure 24b). Model B and twoPhaseEulerFoam have the same pressure drop profile through the height of the cylinder. Model A only matches with twoPhaseEulerFoam above 0.5m and has slightly larger pressures below this height. This is the opposite to what was observed in the cylinder fluidized bed case where Model A had a smaller pressure drop and Model B had a larger pressure drop, when compared to twoPhaseEulerFoam.

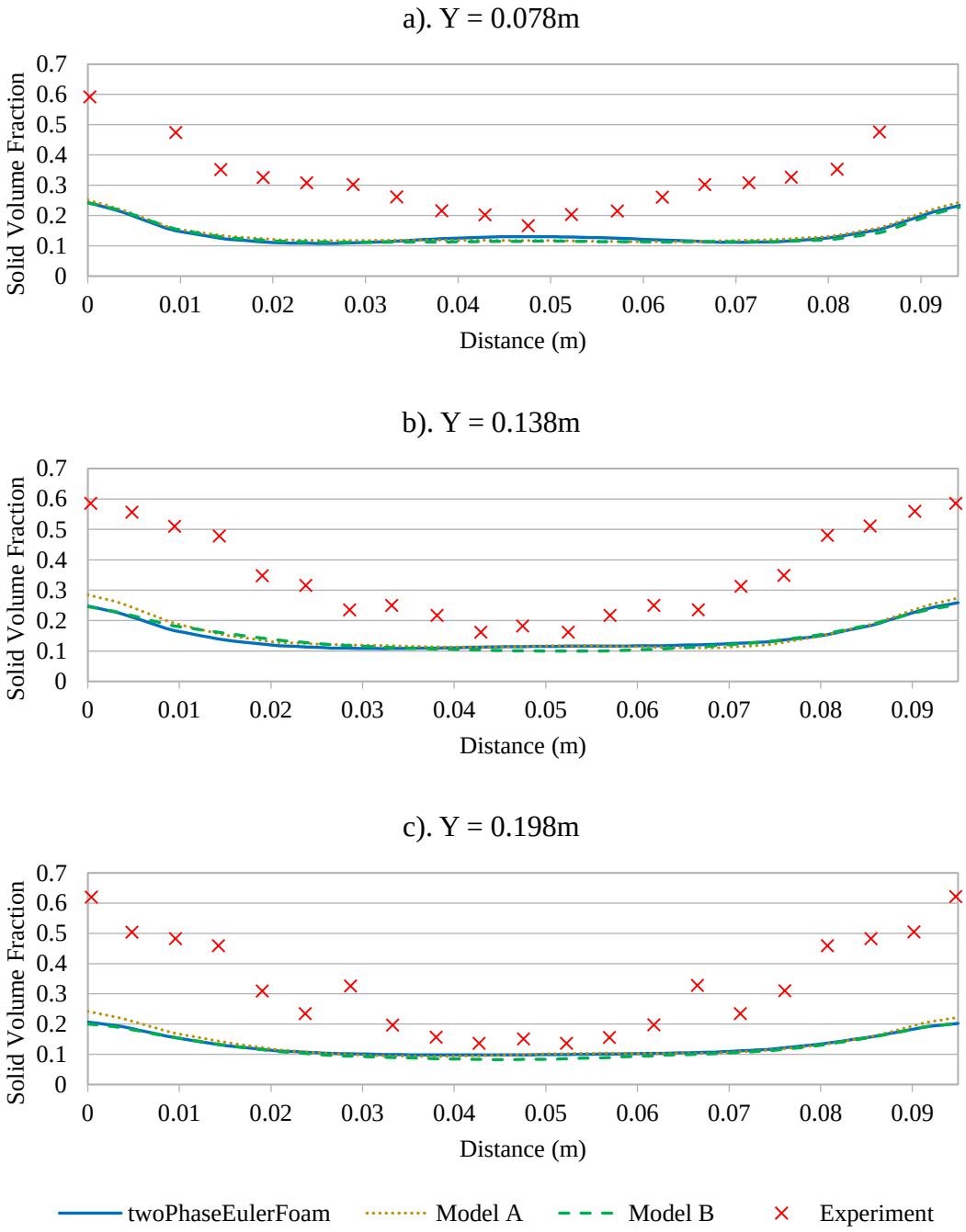

Figure 25 - Time-averaged cross-cylinder solid volume fraction at heights of a). 0.078m, b). 0.138m and c). 0.198m, for the Volume Diffusion Flux models.

The cross-sectional solid volume fraction profiles at heights of 0.078m, 0.138m and 0.198m are shown in Figure 25. At 0.078m in Figure 25a) all three models have a similar and flatter profile at a lower solids volume fraction than from experiment, with very little variation between each model. The only measurable difference is that models A and B have a lower solids volume fraction in the centre and Model A has a slight increase near the walls, in comparison to the twoPhaseEulerFoam model. The profile at 0.138m shows that Model A has a higher solids volume fraction at the walls again, and this difference is more apparent. In the centre of the flow, Model A and twoPhaseEulerFoam match closely, while there is a slight drop in the solids volume fraction for Model B. The last profile is at 0.198m where the same differences between each of the models at the height of 0.138m can be seen. Again, both Model A and twoPhaseEulerFoam have the same profile in the centre, while Model B predicts a lower solids volume fraction. Model A predicts a slightly larger solids volume fraction at the walls than for the other heights. All three models under predict the solids volume fraction across the cylinder at all the heights. While they matched experiment better towards the centre of the cylinder, towards the walls the simulations did not capture the rise in the solids volume fraction. This reflects the results in Figure 24a).

The vertical solids velocity at cross sections of the cylinder at heights of 0.078m, 0.138m and 0.198m can be seen in Figure 26. All three cross sections show a distinct difference between the predictions of the modifications and twoPhaseEulerFoam. A general trend is that Model A tends to have a smaller upwards (positive) solids velocity in the centre of the cylinder and a small downwards (negative) velocity at the walls, when compared to twoPhaseEulerFoam. This means that the particles are not rising and falling as quickly as the particles in twoPhaseEulerFoam. Model B tends to have a larger velocity in the centre and a downwards (negative) velocity similar to twoPhaseEulerFoam near the walls. So particles are rising quicker with Model B but are falling at the same velocity as twoPhaseEulerFoam. Comparing with Figure 12 for the cylinder fluidized bed case, Model B acted similarly, with an increase in the solids velocity in the centre of the flow. While Model A did not show any significant differences in the cylinder fluidized bed case, there are more significant differences shown in this case, with an overall lower solids velocity.

The snapshots of solids volume fraction at 35 seconds in Figure 27 show that twoPhaseEulerFoam has larger regions of a higher solids volume fraction compared to the Fluent results as given by Gao *et al.* (2012). Models A and B have even larger areas

with the same solids volume fraction as twoPhaseEulerFoam, along with "ribbon" like clusters of the solid phase near the top of the region, similar to the Fluent results. All the models here have a more distributed solids volume fraction throughout the height of the cylinder, which has already been attributed to the choice of drag model.

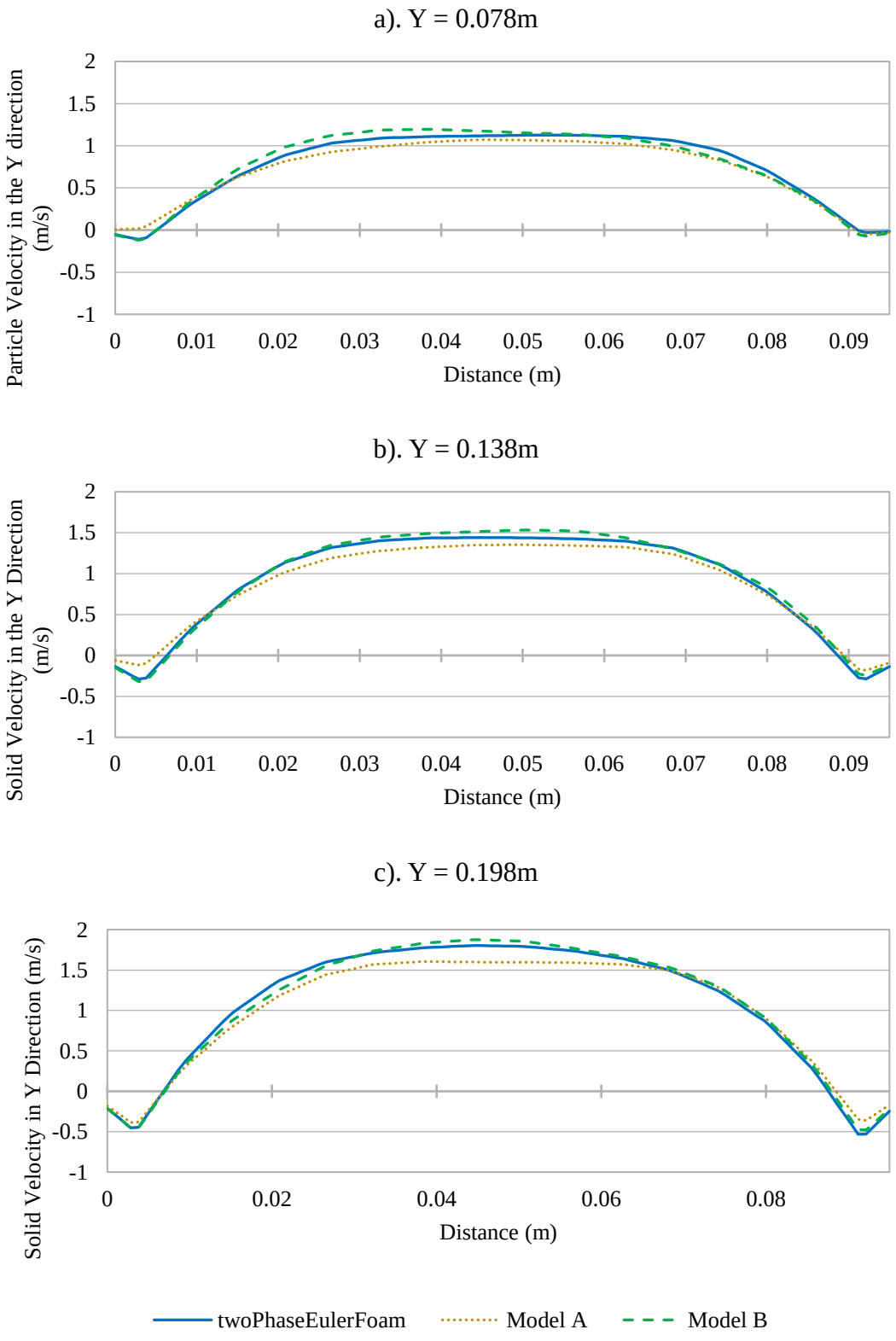

Figure 26 – Vertical solids velocity at cylinder cross-section at heights of a). 0.078m, b). 0.138m and c). 0.198m, for the Volume Diffusion Flux models.

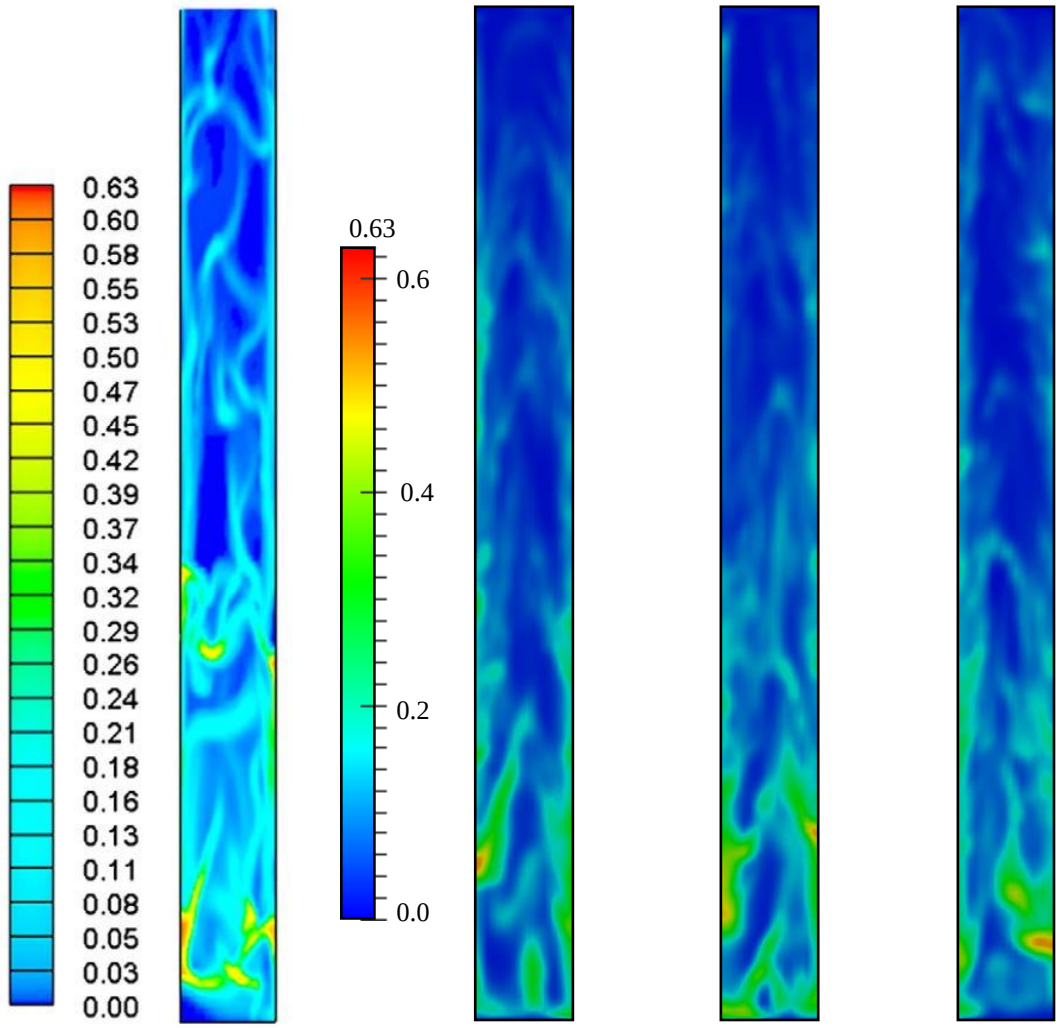

Figure 27 – Snapshots of solid volume fraction over the full height of the cylinder at 35s, for the Volume Diffusion Flux models.

The time-averaged solids volume fractions in Figure 28 show that for twoPhaseEulerFoam the densest region occurs near the base of the cylinder, with the highest solids volume fraction occurring at the walls within this region. As the flow travels up the cylinder the solids volume fraction tends to be larger near the walls, with an increasing void region towards the centre. Both models A and B show a less smooth transition up the cylinder for the solids volume fraction: there are fluctuations in the thickness of the region that the solid phase occupies near the walls. Also, both models have more dilute solid phase clustering occurring within the centre and occurs lower in the cylinder than with twoPhaseEulerFoam. Model A does have a higher solids volume fraction in the dense region near the walls than either twoPhaseEulerFoam or Model B, while there is a larger region at the base of the cylinder that has fewer particles in Model B only. This suggests that Model B is producing more or bigger bubbles near the base of the cylinder.

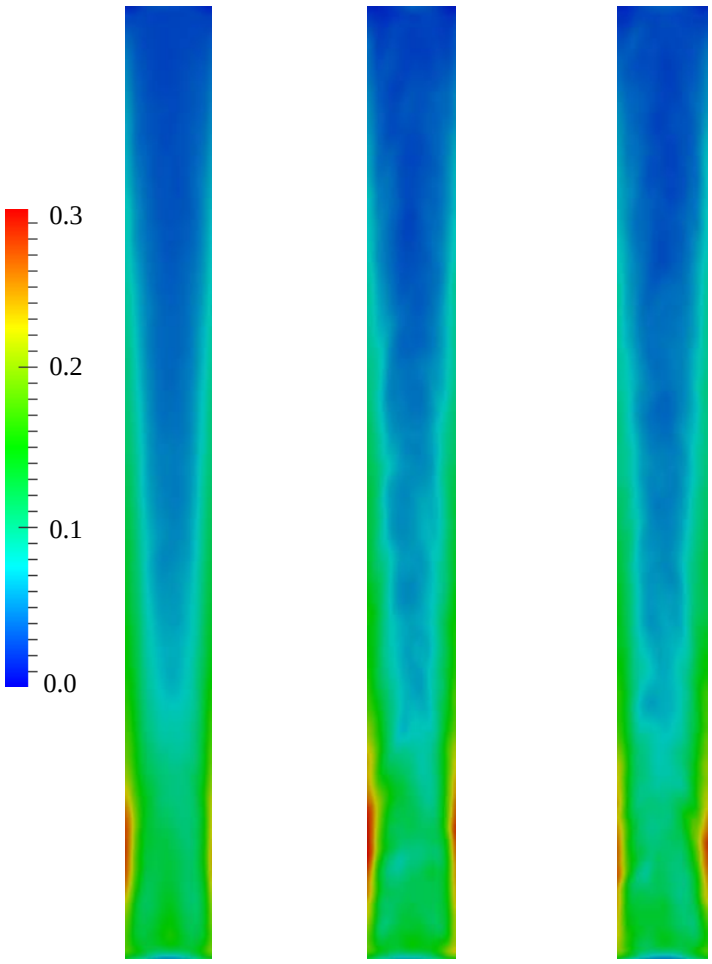

Figure 28 - Time-averaged solid volume fraction over the full height of the cylinder, for the Volume Diffusion Flux models.

From these results, the Volume Diffusion Flux modifications seem to make only a little more impact than was seen in the cylinder fluidized bed case. Also, more differences could be seen between models A and B, such as higher solids volume fraction at the walls for Model A and an increase in the solids velocity in the centre of the cylinder for Model B. As with the simple case, it should be noted that neither Model A nor Model B significantly improved the results when compared to the experiments.

4.3.2 Korteweg Stress Models

As with the previous section, results from the original OpenFOAM model twoPhaseEulerFoam will be compared to the two modifications of the Korteweg stress model that are called Model C and Model D. The summary of the models is in Table 11.

Table 11 – Korteweg Stress model descriptions for the recirculating fluidized bed.

Label	Equations for Original and Korteweg Stress Modifications	
twoPhaseEulerFoam	$\rho_s\alpha_s\left[\frac{\partial U_s}{\partial t}+U_s\cdot\nabla U_s\right]=-\alpha_s\nabla P+\nabla\cdot\alpha_s\tau_s-\nabla P_s+\alpha_g\rho_g g+\beta(U_g-U_s)$	(5)
Model C	$\rho_s\alpha_s\left[\frac{\partial U_s}{\partial t}+U_s\cdot\nabla U_s\right]=-\alpha_s\nabla \mathrm{P}+\nabla\cdot\alpha_s\tau_s-\nabla \mathrm{T}+\alpha_g\rho_g g+\beta(U_g-U_s)$	(42)
	$T=\left[-P+K\rho\nabla^2\alpha_s+\frac{1}{2}K\lvert\nabla\alpha_s\rvert^2\right]I-K\nabla\alpha_s\otimes\nabla\alpha_s$	(39)
	$K=\frac{\mu_s^2}{\rho_s}$	(40)
Model D	$\rho_s\alpha_s\left[\frac{\partial U_s}{\partial t}+U_s\cdot\nabla U_s\right]=-\alpha_s\nabla \mathrm{P}+\nabla\cdot\alpha_s\tau_s-\nabla \mathrm{T}+\alpha_g\rho_g g+\beta(U_g-U_s)$	(42)
	$T=\left[-P+K\rho\nabla^2 w_s+\frac{1}{2}K\lvert\nabla w_s\rvert^2\right]I-K\nabla w_s\otimes\nabla w_s$	(41)
	$K=\frac{\mu_s^2}{\rho_s}$	(40)
	$w_s=\frac{\alpha_s\rho_s}{\alpha_s\rho_s+\alpha_g\rho_g}$	(32)

The solids volume fraction varying with the height of the cylinder can be seen in Figure 29a). Again, both models C and D predict an overall lower solids volume fraction than both the Fluent and twoPhaseEulerFoam results. Model C produces a small variation in the profile near the base of the cylinder, while Model D predicts a more pronounced increase in the solids volume fraction at a similar height to the experimental results. The twoPhaseEulerFoam model and models C and D all have similar solid volume fractions above the midpoint of the cylinder, and these are larger than both the Fluent and the experimental results. The more pronounced curve of Model D near the base of the cylinder could be showing a difference in the dispersion of the solid phase as different clustering effects could be occurring. Model C produces the smallest solids volume fraction near the base of the cylinder, suggesting the solids phase is more distributed in this region than in the prediction of Model D.

The pressure predicted by for twoPhaseEulerFoam, and models C and D are shown in Figure 29b), where over the upper part of the cylinder there is very little difference between each of these models. The differences only become apparent below about 0.3m in height, as Model C has slightly lower pressures while the pressure in Model D increases towards the inlet of the cylinder. This gives the overall pressure drop between the inlet and outlet to be slightly larger for Model D and slightly smaller for Model C, when compared to that from the twoPhaseEulerFoam model. Around 0.1m, the greatest difference between Model D and twoPhaseEulerFoam is observed, just below the location of the highest solids volume fraction. The increase in pressure in this region suggests that the particles are slowing down and clustering more at the height in the cylinder.

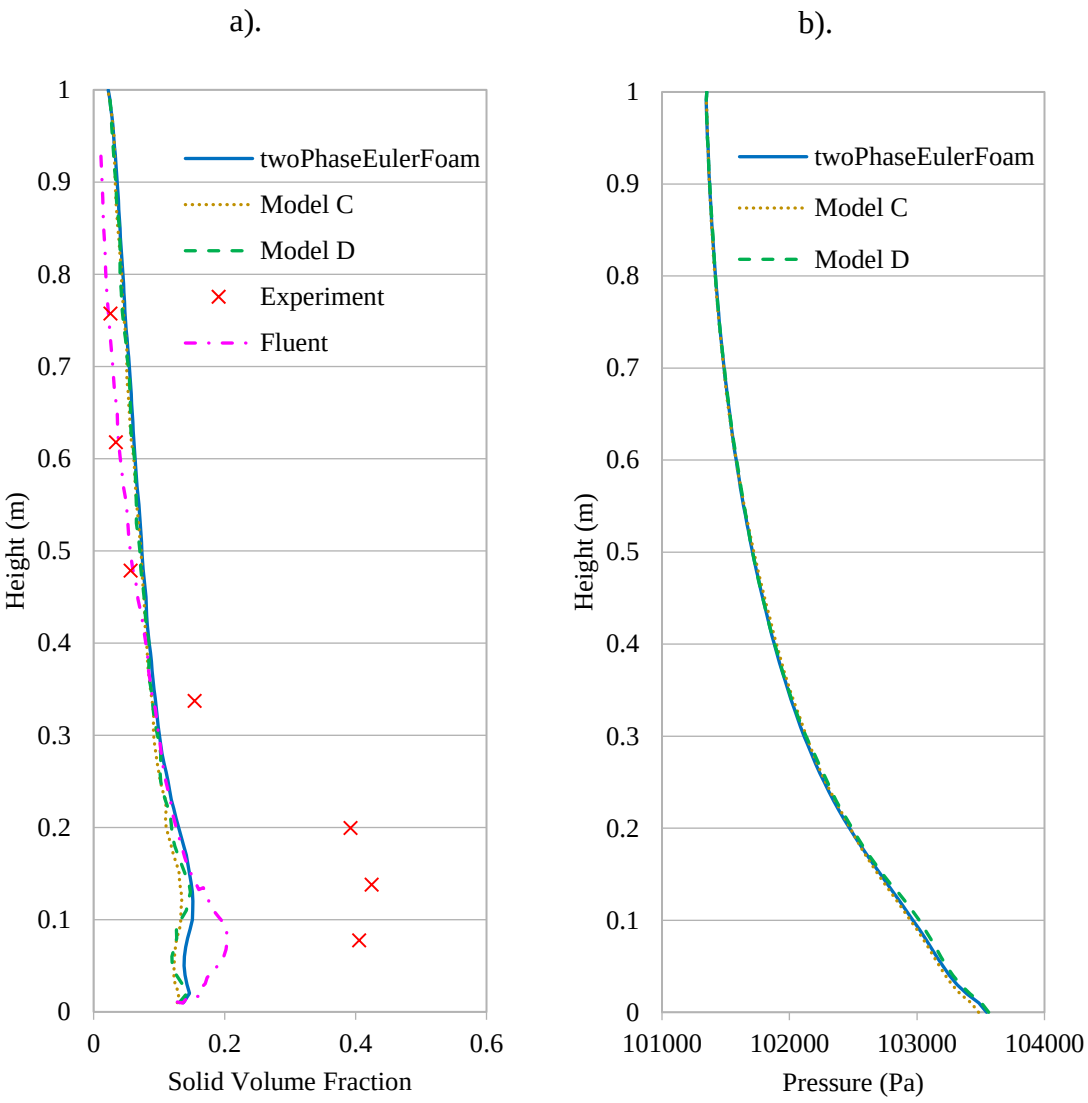

Figure 29 – Variation over the full cylinder height of a). Solid Volume Fraction and b). Pressure, for Korteweg Stress models.

The solids volume fraction profiles across the width of the cylinder at various heights are shown in Figure 30. At a height of 0.078m in Figure 30a) there is only a marginal difference between the results of models C and D with those of twoPhaseEulerFoam. Both models C and D predict a slightly lower solids volume fraction near the centre of the cylinder, while only Model C has a lower solids volume fraction near the walls. Similar observations can be made for the profile at 0.138m in Figure 30b), although Model C has a slightly higher solids volume fraction near the walls. However, there is little difference between each of the models at the centre of the cylinder, although Model D produces a larger solids volume fraction towards one side of the cylinder. This will give an overall higher solids volume fraction at this height, which can be seen in Figure 29a). The final cross-section at a height of 0.198m shows that Model C predicts a lower solids volume fraction in the centre, and now Model D has a slightly larger solids volume

fraction compared to twoPhaseEulerFoam. At this height, the results from Model D are still showing some bias to one side of the cylinder.

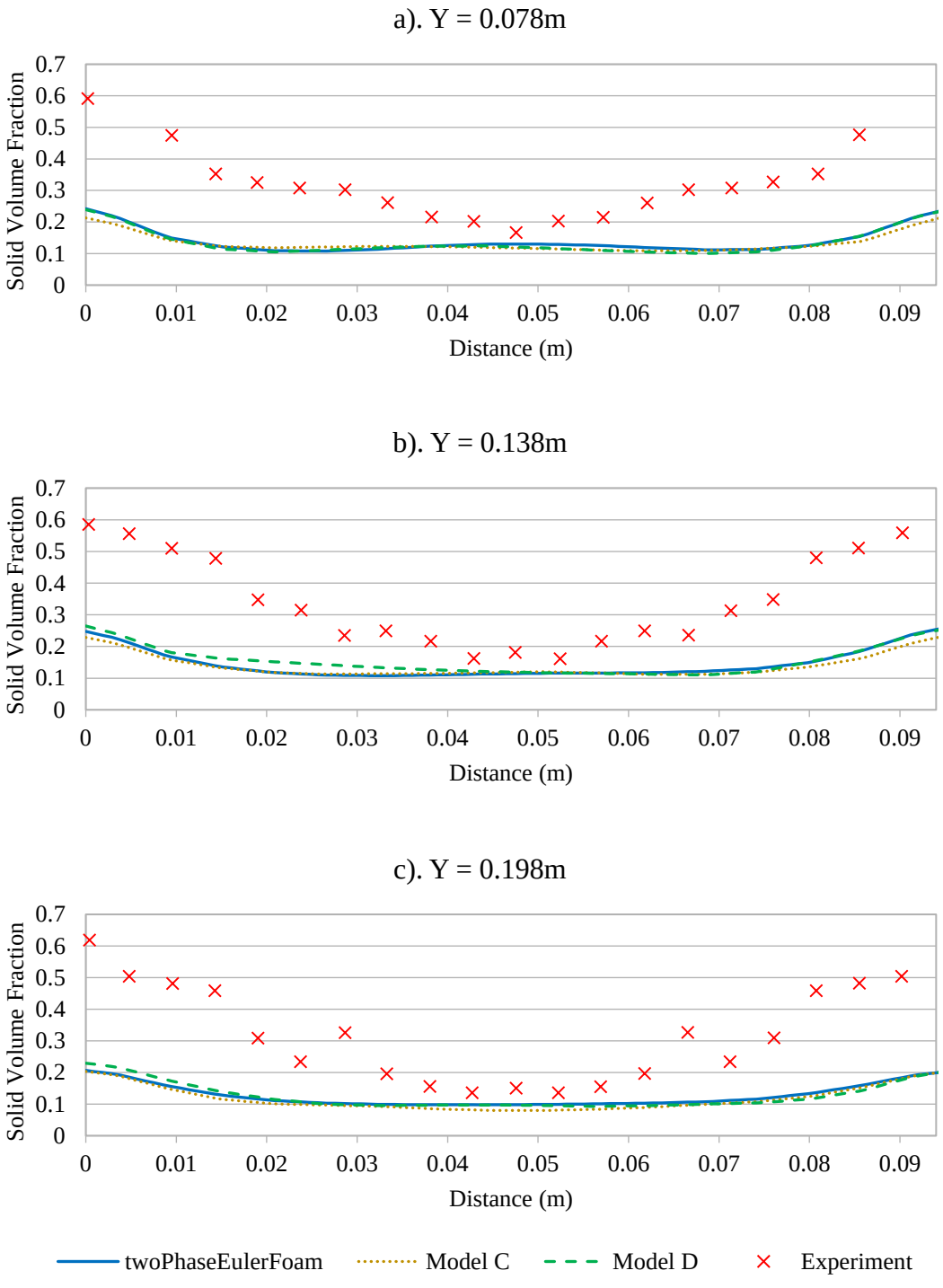

Figure 30 - Time-averaged cross-sectional solid volume fractions at heights of a). 0.078m, b). 0.138m and c). 0.198m, for Korteweg Stress models.

The cross-sectional vertical solids velocity at different heights can be seen in Figure 31. Near the base of the cylinder, at a height of 0.078m, both models C and D predict a lower solids velocity across the centre of the cylinder. Model D can be seen to dip lower in the centre, while both Model C and twoPhaseEulerFoam appear to flatten out. At the walls,

Model C produces a larger positive solids velocity in the centre than both Model D, where the particles are not moving very fast at the walls. At the next cross-sectional height of 0.138m, both models C and D have on average a smaller solids volume fraction than twoPhaseEulerFoam, and their profiles are not symmetrical about the centre. Again, Model D and twoPhaseEulerFoam have a similar solids velocity at the walls, while Model C has a smaller downwards (negative) velocity. At the height of 0.198m, the average profiles of all three models are similar to each other.

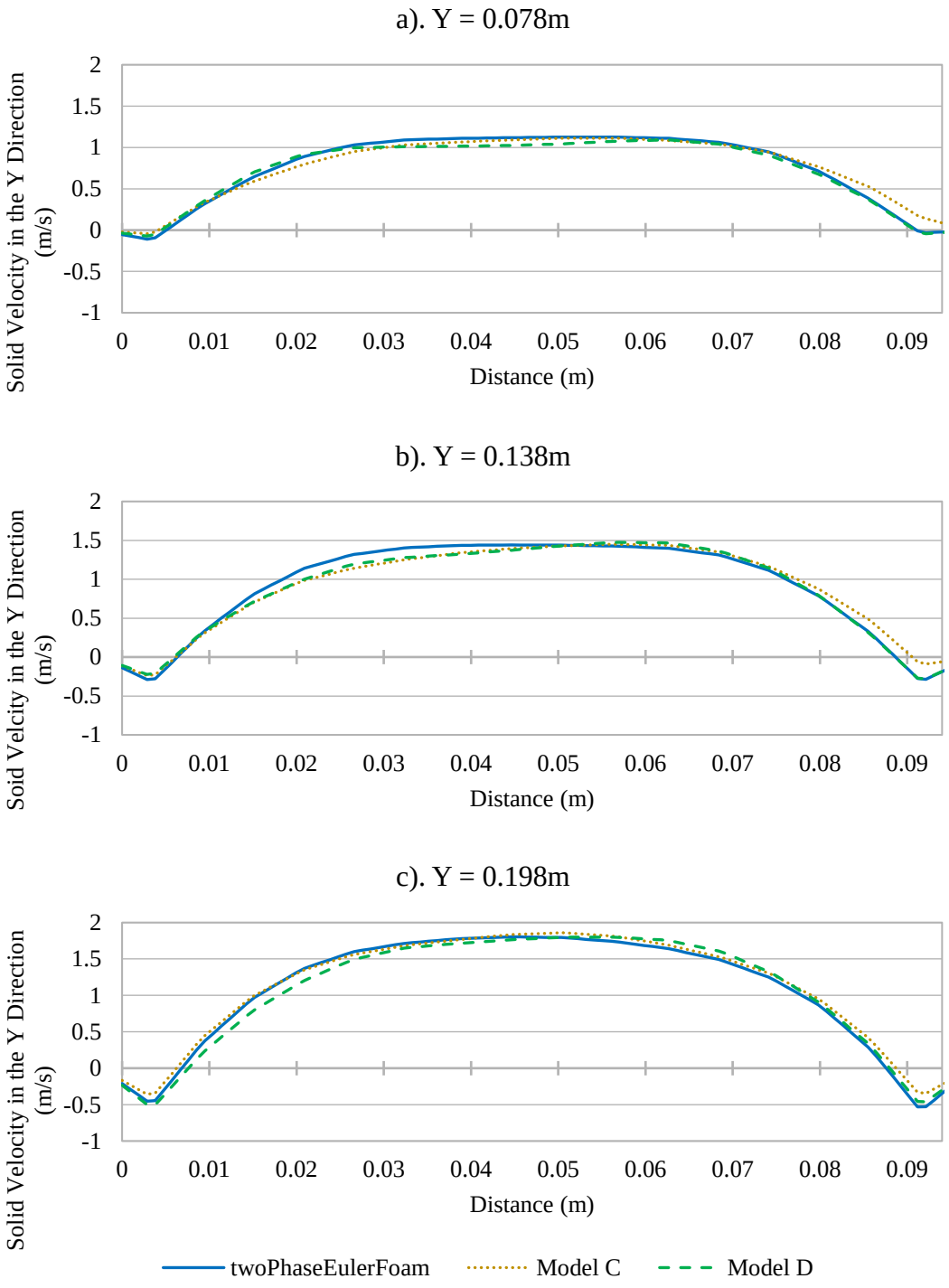

Figure 31 – Vertical solids velocity at cylinder cross-section at heights of a). 0.078m, b). 0.138m and c). 0.198m, for the Korteweg Stress models.

Snapshots of the solids volume fraction at a time of 35 seconds are shown in Figure 32. There are similar amounts of clustering of the solid phase in twoPhaseEulerFoam and models C and D. The "ribbon" effect that occurs in the upper region of the cylinder, predicted by Fluent and twoPhaseEulerFoam, is not as apparent in the models C and D results. Model D does have a greater solids volume fraction at the walls, with one wall having a significant amount. This could be what is producing a larger solids volume fraction towards one side of the cylinder as seen in Figure 30.

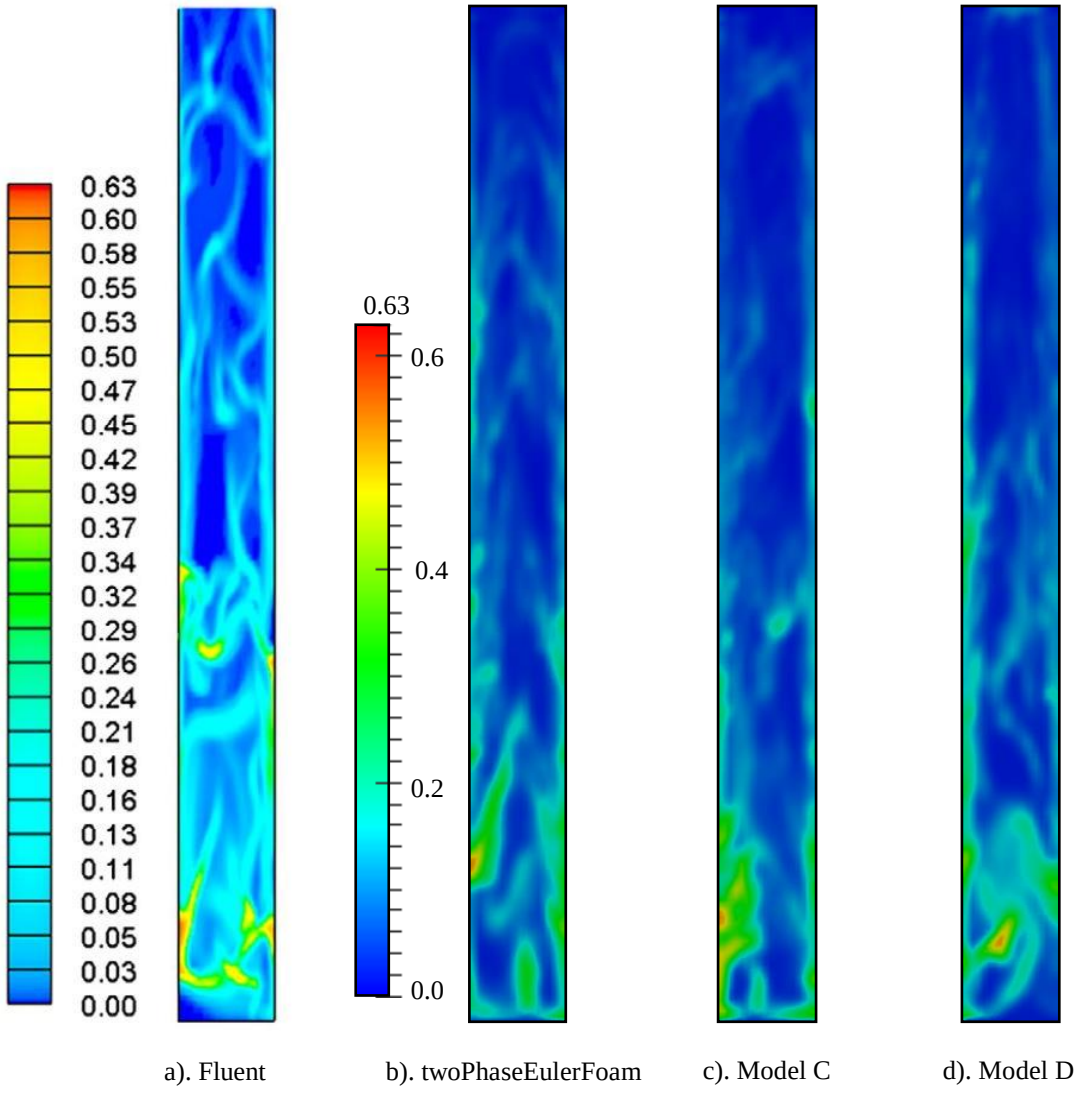

Figure 32 - Snapshots of solid volume fraction over the full height of the cylinder at 35s, for the Korteweg Stress models.

Figure 33 is the time-averaged solid volume fraction across the cylinder, over its full height. Model C has a significantly smaller solids volume fraction at the walls near the base of the cylinder, which agrees with what was seen in Figure 29a). The solid phase is more evenly distributed below 0.2m in the cylinder, especially when compared to Model D where there is a small region of lower solids volume fraction before it increases then

finally tends to zero towards the top of the cylinder. This again agrees with Figure 29a), where the solids volume fraction decreases in the centre at a lower part of the cylinder for both models C and D than twoPhaseEulerFoam. There is also more uneven clustering up the cylinder walls for the solid volume fraction at the walls.

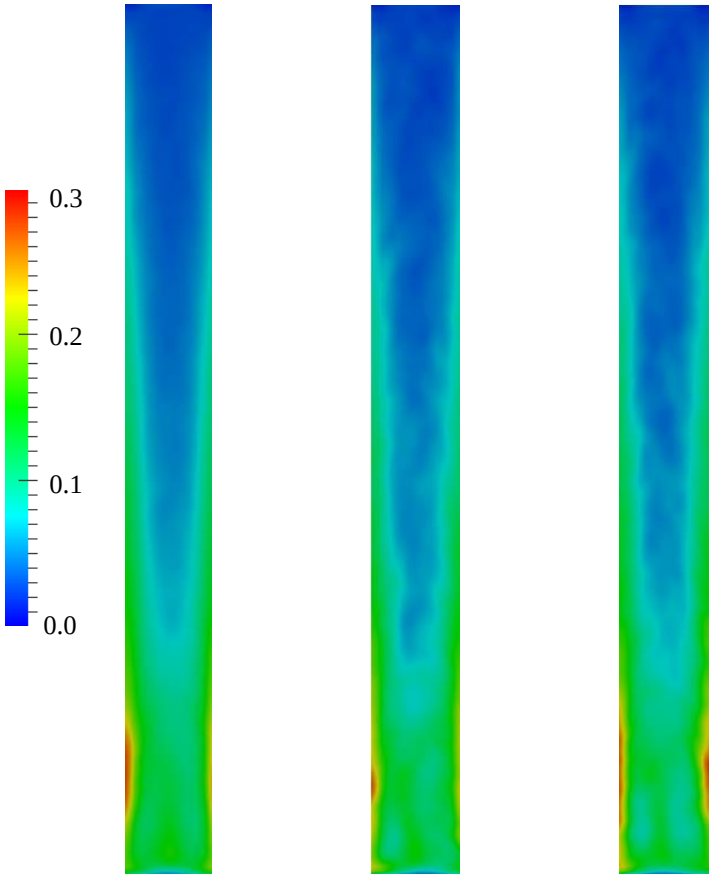

a). twoPhaseEulerFoam b). Model C c). Model D

Figure 33 - Time-averaged solid volume fraction over the full height of the cylinder, for the Korteweg Stress models.

The Korteweg Stress modifications in this case presented some differences in the results between models C and D. Model C presented worse results, in comparison to the experimental profile of the solids volume fraction, with a decrease in the solids volume fraction near the walls in Figure 30. Also, the solids volume fraction variation over the full height of the cylinder in Figure 29a) had a more even distribution of the solid phase and had less variation than the experimental results. Model D did have greater variations in solids volume fraction, as there was a clear region where there was lower solids volume fraction, which increased to its maximum at the height the experimental results also had their largest solids volume fraction. Overall there were some small differences caused by the modifications of the Korteweg Stress, but these did not improve overall the results in comparison to the experimental data.

4.3.3 Recirculating Fluidised Bed Results Discussion

The recirculating fluidized bed as investigated by Gao *et al.* (2012) was used to further study the effects of the modifications of both the Volume Diffusion Flux and the Korteweg Stress. It was not possible to use the drag model as used in the original paper due to issues in its formulation and implementation into OpenFOAM. This was due to the formulation of the combined drag model where the Mckeen and Puglsey (2003) drag model was inhibiting the formation of bubbles and allowing for fluidization to occur. Therefore, another drag model was used, which produced results that did not match as well with the experimental results but were able to be obtained from OpenFOAM. Both Fluent and OpenFOAM under-predicted the solids volume fraction near the base of the cylinder while over predicting towards the top. OpenFOAM was found to produce a more evenly distributed solid phase throughout the cylinder, with not a clear region of higher solids volume fraction near the base, as was predicated by Fluent and shown by the experimental results.

The Volume Diffusion Flux modifications have been shown to have a greater impact on the flow characteristics than was seen in the cylinder fluidized bed case, but it did not improve the overall results to closer match the experimental results. The Korteweg Stress modifications showed a larger impact when compared to the original OpenFOAM solver, twoPhaseEulerFoam. Model D showed the most distinct difference in the solids volume fraction, with a more distinct region of highest density seen in Figure 29a) occurring at the same height in the cylinder as the experimental results. However, the Korteweg Stress modifications did not significantly improve the simulation results when compared to Fluent and the experimental results. However, even though both Volume Diffusion Flux and Korteweg Stress modifications do not directly make improvements in reproducing the experimental solids volume fraction, other effects have been found that prompt further investigation.

4.4 Discussion

In this chapter, two different rapid granular-gas systems were simulated; a fluidized bed and a recirculating fluidized bed. For the simulation of these systems, various software were compared. For the fluidized bed, OpenFOAM, MFix and Fluent were compared and showed that for each solver there still needs to be improvement in modelling to account for both Geldart groups A and B type particles. OpenFOAM performed best for the smaller Geldart group A/B particles, while overpredicting the minimum fluidization of

the larger diameter group B particles. This has been reported before by Herzog *et al.* (2012) for very large particles in the Geldart group D range. Fluent did not perform as expected for Geldart group B particles, despite the same models for drag, friction and radial distribution models being selected for Fluent and OpenFOAM to match the MFix simulation. However, it did coincide very well with the MFix results for Group A/B particles without any changes to the simulation parameters other than the particle diameter and inlet gas velocity. For the cylinder fluidized bed case the results show that OpenFOAM in its current form does not perform well for larger particles, while MFix and Fluent predicts flow of larger particle better. OpenFOAM produced better predictions of the solids volume fraction, in comparison to the experimental results of the Group A/B, particles than both Fluent and MFix.

The recirculating fluidized bed as set out by Gao *et al.* (2012) was used to further study the software differences, although in this case only Fluent and experimental results were reported. It was not possible to use the drag model as used in the original paper due to issues in its formulation and implementation into OpenFOAM. This was due to the formulation of the combined drag model where the Mckeen and Puglsey (2003) drag model was inhibiting the formation of bubbles and allowing for fluidization to occur, therefore another drag model was used with OpenFOAM to produce results. The recirculating fluidized bed had Geldart group B type particles; the previous cylinder fluidized bed case results suggested that the particles would be more difficult to fluidize using the OpenFOAM software, however, this was not the case in practise. Both Fluent and OpenFOAM underpredicted the solids volume fraction near the base of the cylinder while overpredicting it towards the top. The OpenFOAM results did produce a more evenly distributed solid phase throughout the cylinder, with a less distinctive region of higher solids volume fraction near the base that was better predicted by Fluent and shown by the experimental results. The full model description was not given for the Fluent simulations, therefore there could be some unreported differences between Fluent and OpenFOAM that could be in the choice of Kinetic Theory of Granular Flow (KTGF) models such as the radial distribution function model.

From this software comparison on the fluidized cylinder bed and recirculating fluidized bed cases, none of the software used had a particular advantage over another as each performed well in some cases and poorly in others. This could be due to particular models used in KTGF within the software not being stated as different, or due to the solution techniques for the governing differential equations. OpenFOAM will, however, continue

to be used throughout this thesis as it can be easily modified and has a number of models, such as drag and friction models, already included as part of the software. OpenFOAM did not perform significantly better or worse overall when compared to MFix and Fluent.

The Coefficient of Restitution (CoR) was tested for two cases of the cylinder fluidised bed to assess the sensitivity of the OpenFOAM software to this parameter. The overall results show that OpenFOAM acts as is expected in terms of its sensitivity to the Coefficient of Restitution, with a decrease in bubble formation as the CoR increases towards 1 or fully elastic type collisions as described by Loha *et al.* (2014). This thesis concludes that a CoR of 0.8 was the best choice as it closely matched the experimental results from the range of CoR tested.

The results of the Volume Diffusion Flux modifications on the results for the cylinder fluidized bed showed that there was not a significant difference between the original OpenFOAM solver and the modifications. Some minor differences were seen for Model B in flow characteristics such as the solids velocity and start-up effects in the solids volume fraction. The lack of improvement with the Volume Diffusion Flux modifications could be due to these modifications not necessarily affecting this particular set of flow conditions as it is from compressible flow theory and the cylinder fluidized bed may not have a large enough compressible flow occurring. The recirculating fluidized bed showed only to have only a little more impact than was seen in the fluidized cylinder case. More differences were seen between models A and B, such as higher solids volume fraction at the walls for Model A and an increase in solids velocity in the centre of the cylinder for Model B. However, as with the simple case, it should be noted that neither Model A or Model B significantly improved the results when compared to experimental data.

The Korteweg Stress modifications, when applied to the cylinder fluidized bed case, produced the most significant differences primarily in the circulating movement of the particles within the bed. This could be seen as a large velocity difference occurring near the walls, so the particles are more likely to travel further before being recirculated into the centre of the flow. In this case there was not a significant difference the results of models C and D, but there were greater differences when compared to twoPhaseEulerFoam results. For the recirculating fluidized bed case the modifications presented some differences between models C and D. Model C presented a solids volume fraction profile that as worse than all other models compared to the experimental data. Also, the solids volume fraction over the full height of the cylinder was more evenly distributed and had less variability. Model D did produce more of a variability in the

solids volume fractions than Model C, as there was a clear region where there was a smaller solids volume fraction that increased to its maximum value at the height in the cylinder that the experimental results had their largest solids volume fraction. Overall there were some small differences caused by the modifications to incorporate the Korteweg Stress, but these did not improve the results significantly.

In conclusion, it appears that both the Volume Diffusion Flux and Korteweg Stress modifications do not significantly change the results of simulations to better match the experimental results. The modifications have shown some flow characteristic differences, such as an increase in the solids velocity for the Volume Diffusion Flux, and the rate of circulation for the Korteweg Stress modifications. As there are small effects occurring, it is possible that these effects will become significant in a larger system, as well as seeing the effects of combining these models into a single solver modification to observe if these effects can be larger or smaller. This will be investigated in the next chapter.

Chapter 5: Complex Fluidized System

This chapter is based on a complex geometry fluidized bed in the form of a six-cyclone recirculating fluidized bed. As was discussed in the previous chapter a larger and more complex fluidized bed could have the cumulative effect for each of the modifications. The description of the six-cyclone recirculating fluidized bed is given and both the Volume Diffusion Flux and Korteweg Stress modifications will be simulated using this configuration. From these results and the previous results in Chapter 4 will determine which version of each modification is best suited and will be combined to give a new single modification combining the effects of Volume Diffusion Flux and Korteweg Stress modifications. This final modification will be tested with the six-cyclone recirculating fluidized bed and followed by a discussion of the results. A final evaluation of each modification and their combined effects will be reviewed.

5.1 Simulation parameters

The six-cyclone recirculating fluidized bed is based on the work of Jiang *et al.* (2014) where experimental measurements are compared with simulations carried out with a Computational Particle Fluid Dynamic (CPFD) solver. The CPFD solver is a new approach to modelling granular-gas flows using a Eulerian-Lagrangian method and is based on the commercial code BARRACUDA. Two different configurations of the cyclones were tested in 'point' and 'axis' orientation with their conclusion that the 'axis' orientation gave the best distribution of the solids mass flow between each of the cyclones therefore this configuration will be used and is shown in Figure 34. It consists of a large rectangular riser section of 5.8m in height with six cyclones branching off at the top of the riser section. Stand pipes from the cyclones connect to a U-bend near the base of the riser where an additional gas inlet at the bottom of the U-bend will help circulate the particles back into the riser section, completing the circulation loop. At the base of the riser is a distributer for the gas inlet of 4m/s and another gas inlet of 0.6m/s is at the bottom of each U-bend. The pressure of the outlet of the cylinders was measured at 1000Pa less than atmospheric pressure. The initial bed height of the particles is 0.5m in the riser section only and is at a random packing solids volume fraction of 0.6. The CPFD used 500,000 particles with an average particle diameter of 500μm and density of 2620kg/m^3 which are Geldart group B type particles. A summary of the six-cyclone recirculating fluidized bed parameters are given in Table 12.

Table 12 - Six -cyclone recirculating system parameters (Jiang, Qiu and Wang, 2014).

Parameters	
Static Bed Height	0.5m
Particle density	2620kg/m^3
Gas density	1.205kg/m^3
Gas kinematic viscosity	1.85x10^{-5}m^2/s
Mean particle diameter	500μm, Geldart group B
Initial solids packing	0.6
Coefficient of Restitution	0.89
Distributer inlet velocity	4m/s
U-bend inlet velocity	0.6m/s
Simulation Time	40s

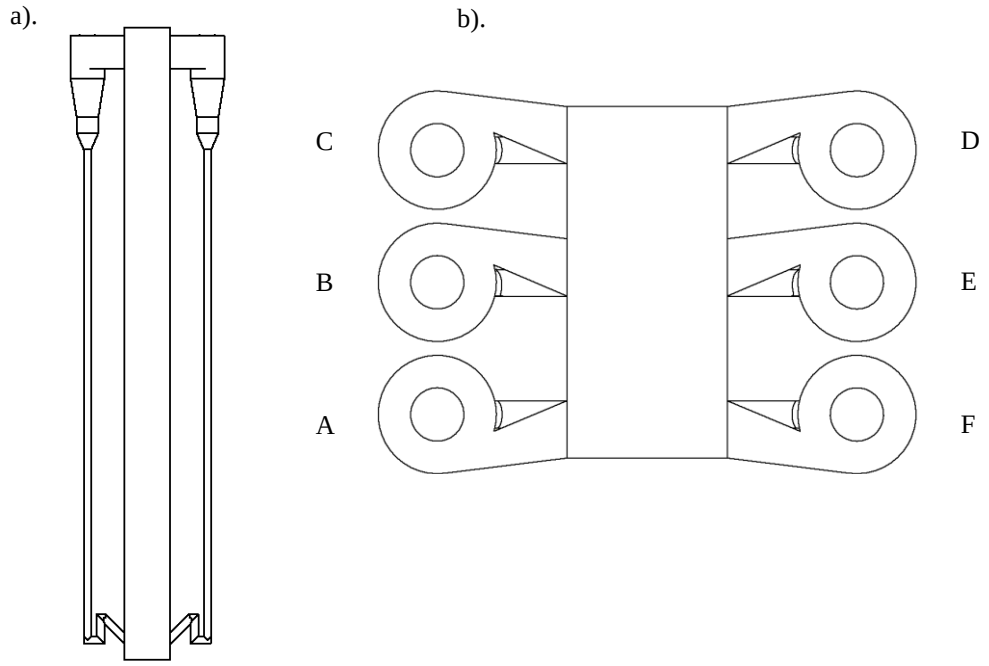

Figure 34 – Six-cyclone recirculating fluidized bed Geometry a). full riser and cyclones with U-bend loop, b). six cyclones in axis symmetry orientation.

The boundaries and models, such as drag and radial distribution models, for the CPFD solver will be as closely matched using OpenFOAM to allow for as close a comparison between the two models for simulation. The inlet of the riser section is a porous plate which is difficult to simulate as a boundary therefore a simple uniformly distributed inlet for the gas phase of 4m/s is used. The U-bend inlets will also have a uniformly distributed gas inlet of 0.6m/s. The outlet of the cyclones is set to be 1000Pa less than atmospheric and initially the whole system will be at atmospheric pressure of 101,350Pa. To simulate the start conditions accurately, the inlet of the riser section will be ramped from 0m/s to 4m/s over 1 second which is more realistic of the system being initiated. The walls will be described using the Johnson and Jackson (1987) boundary conditions with the particle-wall Coefficient of Restitution being the same as the particle-particle Coefficient of Restitution of 0.89 as it is not stated in the original work. The drag model selected is the Syamlal *et al.* (1993) drag model. The simulation will run for 40 seconds: 20 seconds for

the system to become fully developed and then time averaging occurs over the last 20 seconds.

For the mesh an OpenFOAM tool called snappyHexMesh is used to create a hexahedral mesh from geometry files. Four different mesh sizes were used for the mesh independence test; a rough mesh of around 250,000 cells, a medium mesh of around 350,000 cells, a fine mesh of around 500,000 cells, and a very fine mesh of around 800,000 cells. As with the recirculating fluidized bed, the time-averaged solids volume fraction across the full height of the riser section is used for comparison. The fine mesh was found to be most suitable and coincidentally is around the same number of cells as used for the CPFD simulations.

5.2 Volume Diffuse Flux

As with previous sections a summary of each modification for the Volume Diffusion Flux and the original solver are given in Table 13.

Table 13 - Volume Diffusion Flux model descriptions, for the six-cyclone recirculating fluidized bed.

Label	Equations for Original and Volume Diffusion Flux Modifications	
twoPhaseEulerFoam	$\tau_s = 2\mu_s D_s + \left(\lambda_i - \frac{2}{3}\mu_s\right) tr(D_s) I$	(9)
	$D_s = \frac{1}{2}(\nabla U_s + (\nabla U_s)^T$	(10)
Model A	$U_{vs} = U_m + J_{vs}$, to replace U_s in equation (10)	(26)
	$D_{vs} = \frac{\rho_s \nu_s}{(\alpha_s \rho_s) + (\alpha_g \rho_g)}$	(35)
	$J_{vs} = D_{vs} \nabla \alpha_s$	(29)
Model B	$U_{vs} = U_m + J_{vs}$, to replace U_s in equation (10)	(26)
	$D_{vs} = \frac{\rho_s \nu_s}{(\alpha_s \rho_s) + (\alpha_g \rho_g)}$	(36)
	$w_s = \frac{\alpha_s \rho_s}{\alpha_s \rho_s + \alpha_g \rho_g}$	(32)
	$J_s = -\rho_s D_{vs} \nabla w_s$	(33)
	$J_{vs} = \left(\bar{v_s} - \bar{v_g}\right) J_s$,	(34)

From chapter 4 there were some differences between the models that were observed. For the cylinder fluidized bed case there was a higher average bed height and overall a lower solids volume fraction in the denser regions. Model B showed an increase in the solids velocity with the fluidized bed while with the recirculating fluidized bed case Model A showed a decrease in magnitude of solids velocity and Model B an increase. From these observations it is expected to have some more even distribution of the solid phase throughout the riser section for both models while a smaller solids velocity for Model A and larger for Model B should be observed in this case.

5.2.1 Volume Diffuse Flux Results

The solids volume fraction and pressure drop across the full height of the riser section is shown in Figure 35. The solids volume fraction of CPFD in Figure 35a) are seen to have a more evenly distributed solids phase throughout the height than the experimental data and twoPhaseEulerFoam simulation. In the lower region of the riser CPFD under predicts the solids volume fraction, while twoPhaseEulerFoam is larger than the experimental data. The twoPhaseEulerFoam simulation shows very clearly the return of the particles from the cyclone separators near the base of the riser section with a region of high solids volume fraction which coincides with the increase shown by the experimental data. This effect is not clearly being captured with the CPFD solver.

In the upper region of the riser the CPFD simulation have a higher solids volume fraction while twoPhaseEulerFoam and the experimental results match more closely. For the Volume Diffusion Flux modifications, very little difference can be observed when compared to the twoPhaseEulerFoam simulation profile. Model A has no significant differences in solids volume fraction profile compared with twoPhaseEulerFoam. Model B has a small increase between 1m and 1.5m, while a decrease in solids volume fraction between 2m and 3.5m is seen. These solids volume fraction profile differences could be due to the dispersion occurring near the base of the riser which has been noted before in Chapter 4.

For the pressure across the riser section in Figure 35b), there is a significant difference in the overall pressure drop between the CPFD and twoPhaseEulerFoam simulations. While the profiles near the middle of the riser section are similar, the top of the riser section shows CPFD to have a smaller pressure than twoPhaseEulerFoam, and at the base there is a much larger pressure difference between CPFD and twoPhaseEulerFoam. The experimentally measured pressure drop of the riser section reports to be around 5kPa with the CPFD only reporting around 4kPa. The pressure drop for twoPhaseEulerFoam was found to be around 7kPa which is much greater than the experimental results. The lower pressure coincides with the lower solids volume fraction for the CPFD simulation which was remarked upon in the original work. The larger pressure profile of the twoPhaseEulerFoam simulation near the base of the riser does coincide with the higher solids volume fraction in Figure 35a). Neither of the modifications have made any significant differences in the pressure profile or the overall pressure drop of the riser, therefore, the modifications do not have a significant affect the pressure drop this large system.

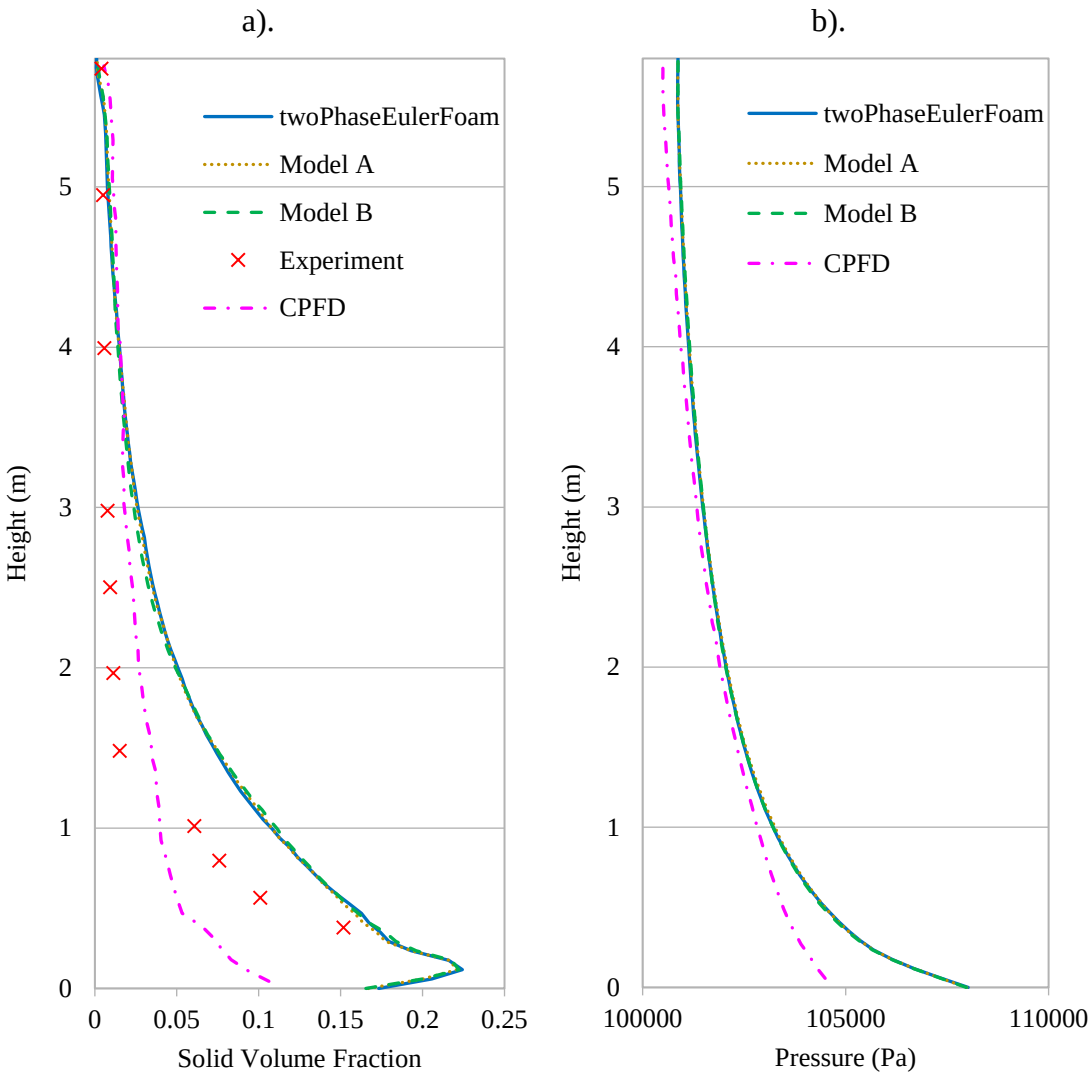

Figure 35 - Time-averaged through the height of the riser section for a). solids volume fraction, and b). pressure.

From Figure 35a) it is expected that the solids volume fraction of twoPhaseEulerFoam and the models will have significantly different cross-sectional profiles throughout the height of the riser section compared to CPFD in Figure 36. With the increase in height, the solids volume fraction profiles of CPFD and twoPhaseEulerFoam can be observed to have a gradual decrease in the difference between them with twoPhaseEulerFoam having the larger solids volume fraction. One exception is at the height of 5.5m in Figure 36f) where the solids volume fraction of CPFD is greater than twoPhaseEulerFoam which shows that CPFD has a more distributed solids phase fraction as it's larger than the experimental results near the top of the riser. More significant differences between the modifications can be seen with Model A and Model B both having a similar profile up to and including the cross-sectional profile at 1.5m in height. Both Models A and B have a lower solids volume fraction bias to one side of the riser section in Figure 36a) which could be affected by the return of the particles in to the riser section as the solids mass

not being evenly distributed through each of the six cyclones. At a height of 1.5m in Figure 36b), the solids volume fraction is slightly larger in the centre and at the walls of the riser section giving a denser region. Figures 37c) and d) start to show the differences between models A and B with Model A following very closely to the twoPhaseEulerFoam solids volume fraction profile. Model B has a lower solids volume fraction profile which matches what was observed previously in Chapter 4. For heights of 4.5m and 5.5m both models A and B have a higher solids volume fraction than twoPhaseEulerFoam and closer matches to the CPFD simulation.

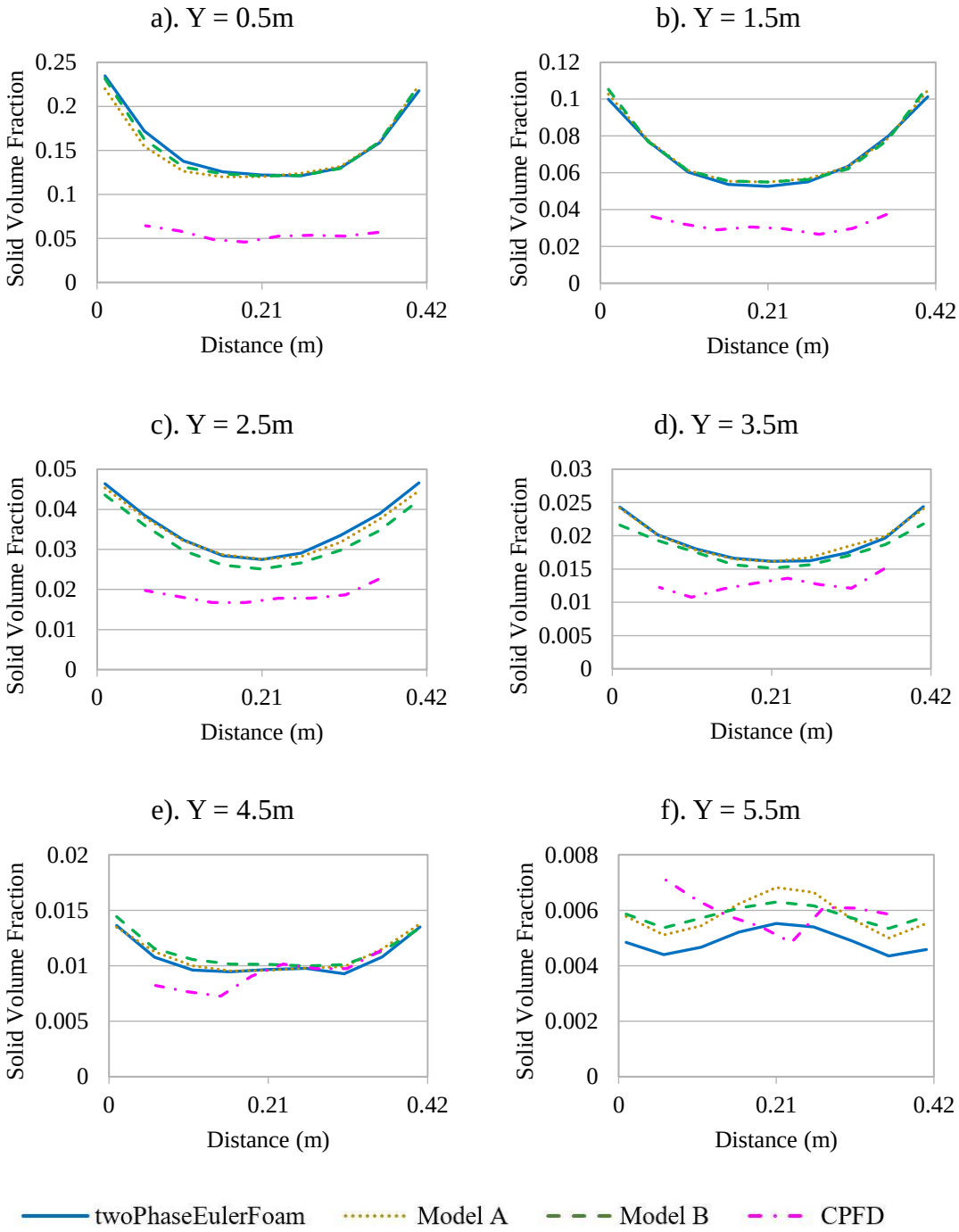

Figure 36 – Time-averaged solid volume fraction cross-section of the riser section in the x-direction.

The solids velocity between 0.5m and 3.5m in Figure 37a), b), c), and d) show that twoPhaseEulerFoam has a larger solids velocity than reported by CPFD at the centre of the riser while matches CPFD near the walls. This coincides with the pressure reported in Figure 35b) at these heights with the higher velocity coinciding with the higher pressure seen for twoPhaseEulerFoam. The cross-section at 4.5m show that both CPFD and twoPhaseEulerFoam simulations have very similar velocities and at 5.5m CPFD has the largest solids velocity. As the particles rise the twoPhaseEulerFoam simulation has faster moving particles in the centre of the flow until around 4.5m where they slow down faster at a greater rate than the CPFD simulation.

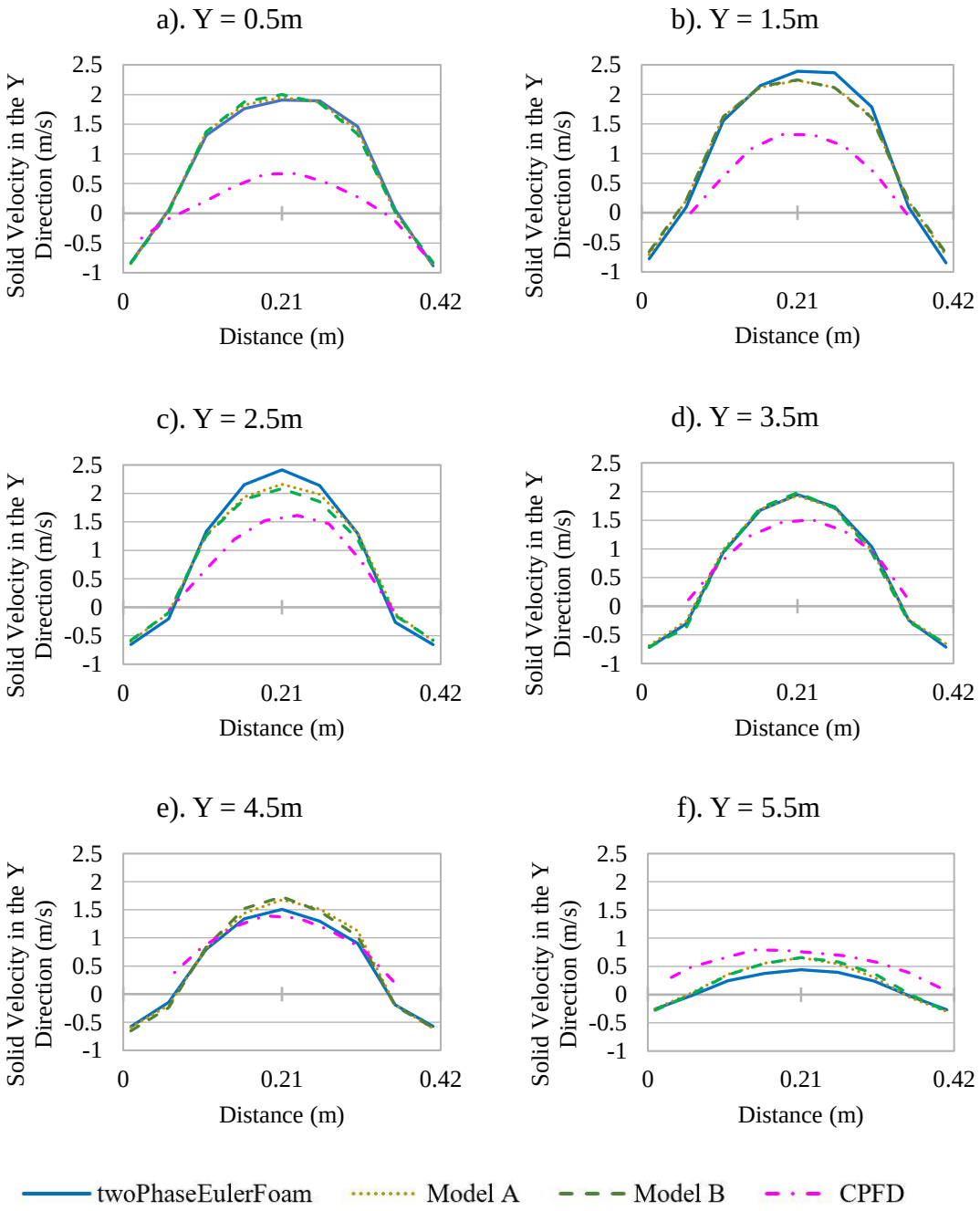

Figure 37 - Time-averaged solids velocity cross-section the riser section in the x-direction.

The solids velocity for both models A and B show a similar change at the various cross-sections at different heights. At 0.5m there is not a significant difference for both models. At the heights of 1.5m and 2.5m show Model B having a larger solid velocity and Model A matching more closely with the twoPhaseEulerFoam simulation. Models A and B match with twoPhaseEulerFoam at the height of 3.5m and then from 4.5m models A and B exceed the velocity that both CPFD and twoPhaseEulerFoam reported. Finally, at 5.5m both models are still larger than twoPhaseEulerFoam but are smaller than the CPFD simulation. From the base of the riser both models particle velocities increase at a similar rate as twoPhaseEulerFoam until 4.5m where twoPhaseEulerFoam begins to slow down its rate of increasing solids velocity compared to models A and B. Near the top of the riser at 5.5m both models still have a larger solids velocity than twoPhaseEulerFoam and is closer to the CPFD results which suggest that again the rate of change in the solids velocity is smaller for models A and B than for twoPhaseEulerFoam.

Figure 38 shows snapshots of the solids volume fraction at various times for different parts of the six-cyclone fluidized bed. The full system in Figures 39a), b) and c) show that the majority of the particles in the riser section tend to be near the base with clusters of particles travelling up the riser section to enter the cyclones. When comparing these to an instants profile of the CPFD results (not shown here for brevity), significant proportion of the particles are distributed further up the riser section and enter the cyclones than with the twoPhaseEulerFoam simulation. The cross-section of the riser section and cyclones at 5.5m in Figures 39d), e), and f) where there are clusters of particles entering the cyclones and are not evenly distributed among the cyclones. The particles are in contact with the walls of the cyclone as it curves round meaning particles are moving through the cyclone as expected. The final set of images in Figure 38 show a closer view of the base of the riser where the U-bends are to return the particles back into the riser section. There is a build-up of particles that is occurring in the U-bend and stand pipe which was also reported in the original work. An effect of the gas inlet at the bottom of the U-bend has caused fluidization to occur in the stand pipes which could be inhibiting the particles to recirculate properly for both twoPhaseEulerFoam and models which was not reported to be observed by either the experimental data or the CPFD simulation. No distinct differences between models A and B could be seen in this comparison except in the bubbling action at the bottom of the stand pipes where Model B can be seen to have smaller bubbles than Model A and twoPhaseEulerFoam. It should also be noted that during the start-up of the simulation particles were forced up into the cyclone return pipe and settled in the U-bend causing less mass to be in the riser section.

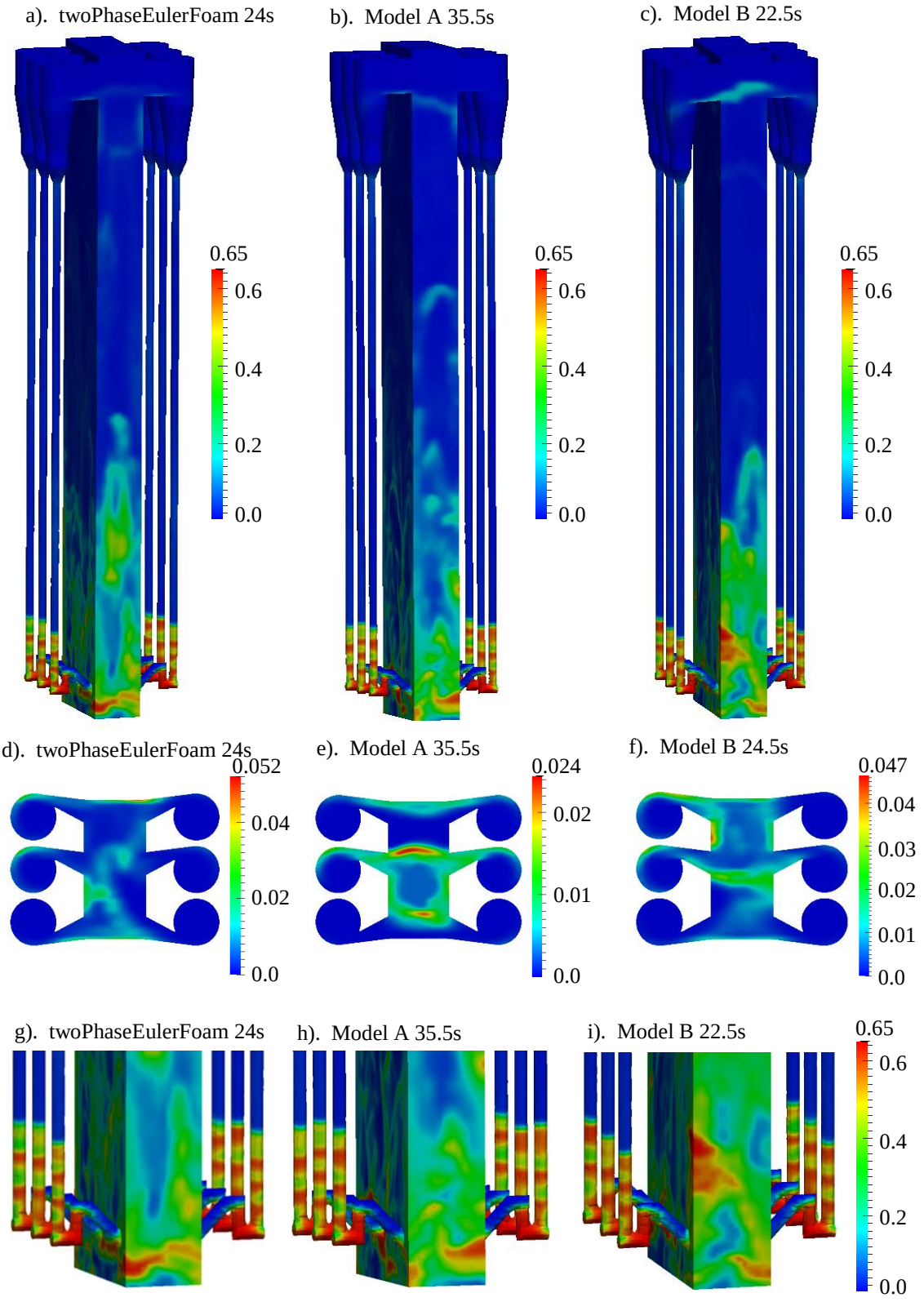

Figure 38 – Snapshots of the solids volume fraction of the six-cyclone recirculating fluidized bed at various times.

The vector fields for the gas velocity for different parts of the system is given in Figure 39. The top cross-section of cyclones B and E and the top of the riser are seen in Figures 40a), b), and c) show all three simulations have a similar flow profile where the gas phase enters the cyclones, and a very large gas velocity when exiting the cyclone through the

centre. One difference observed is the gas velocity at the inlets to the cyclones are a more evenly distributed entering into the cyclones with the twoPhaseEulerFoam simulation compared to models A and B where they have a larger gas velocity near the top of the inlet to the cyclones. The base of the riser with the U-bend and return pipe are in Figures 40d), e), and f) show the effect of the gas inlet at the bottom of the U-bend. All three simulations show that the gas velocities direction splits at the base of the U-bend with some of the flow going up the stand pipe towards the cyclones, while the rest of the flow goes through the U-bend and returns to the riser section. As there was an initial push of particles into the U-bend during the start-up with some of the gas flow travelling up the standpipe, there was some concern that there was not enough gas flow to prevent more particles being pushed back into the return pipe. This is not so as the gas velocity is in the direction of leaving the return pipe and into the main flow of the riser section. Finally, the top cross section of the cyclones and the riser section at a height of 5.5m is seen to have very little variation between each of the models.

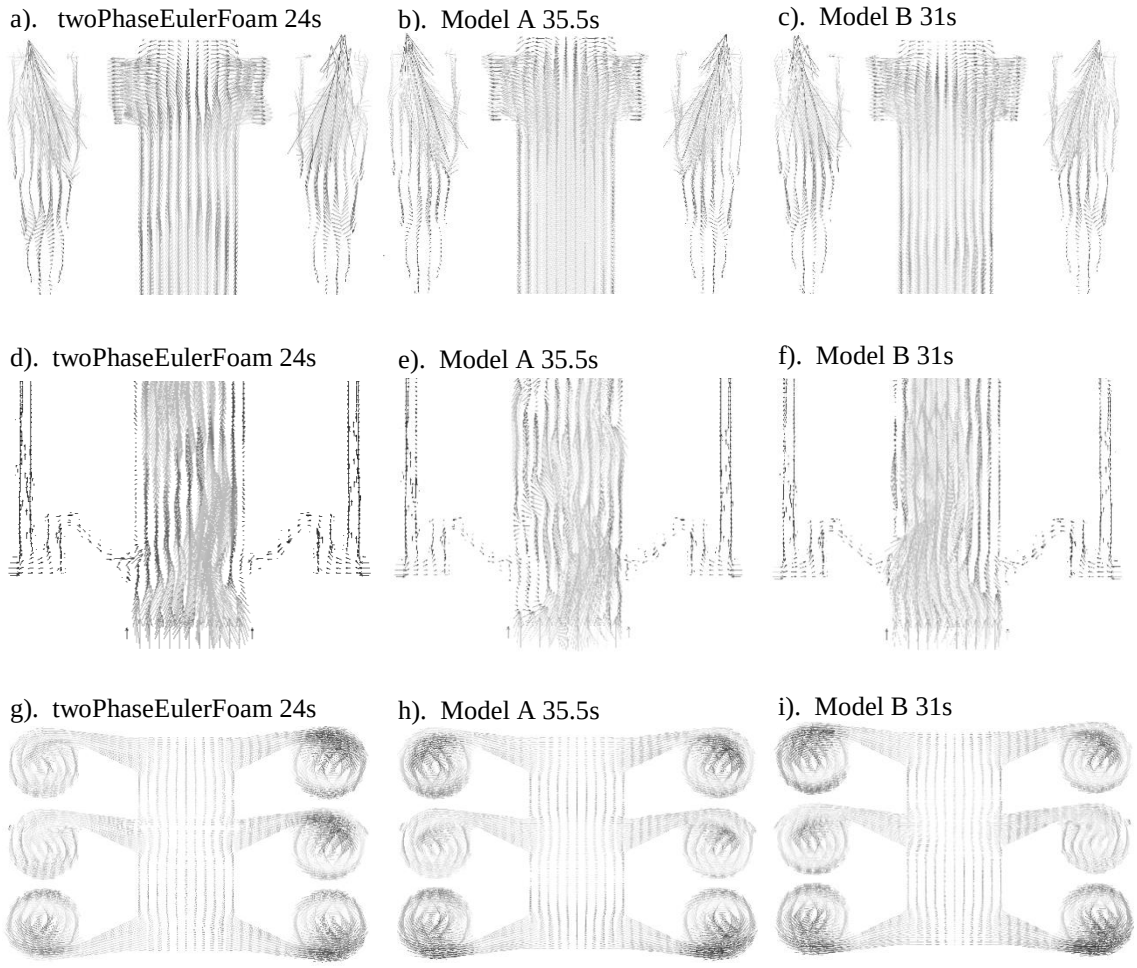

Figure 39 – Gas-velocity of the six-cyclone recirculating fluidized bed at various times.

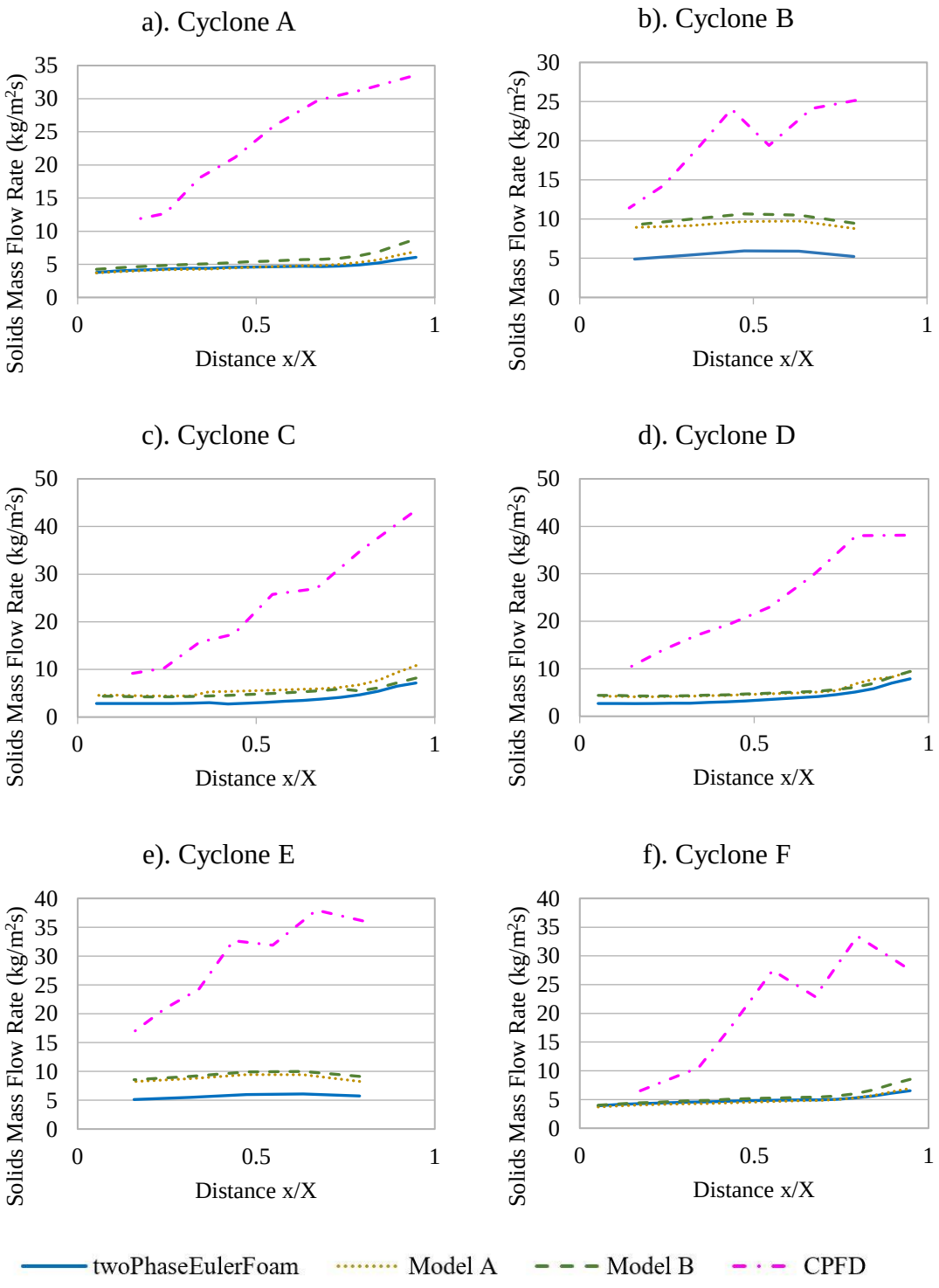

Figure 40 – Solids mass flow rate through the inlet of each Cyclone A to F in the x-direction.

The solids mass flow rate across the inlet of each cyclone are seen in Figure 40. The CPFD simulation mass flow rate through each cyclone inlet is much larger than twoPhaseEulerFoam which is to be expected. A larger number of particles are moving up the riser section in the CPFD simulations, therefore more solid phase mass phase will pass through each cyclone. There is a similar profile trend between CPFD and twoPhaseEulerFoam where the mass flow rate increases to one side of the inlet. Models

A and B both show a difference in the solids mass flow rate across each of the cyclone inlets where there is an increase in the total mass flow through the cyclones. Cyclones B and E show the greatest difference from the twoPhaseEulerFoam results with Model B having the largest mass flow rate. This increase could be in part due to the increase in solids velocity in the centre of the riser where cyclones B and E are located, and the other cyclone inlets are at the corners of the riser where the solids velocity is closer to that been reported for twoPhaseEulerFoam.

The total mass flow through each cyclone and the average of all the cyclones are in Figure 41, where the large difference between the CPFD and twoPhaseEulerFoam simulations can be clearly seen. CPFD has an even distribution of mass flow though, each cyclone while twoPhaseEulerFoam has shown a slightly higher mass flow into the centrally placed cyclones of B and E. Models A and B have a larger average solids mass rate than twoPhaseEulerFoam which occurs significantly in the centre cyclones B and E.

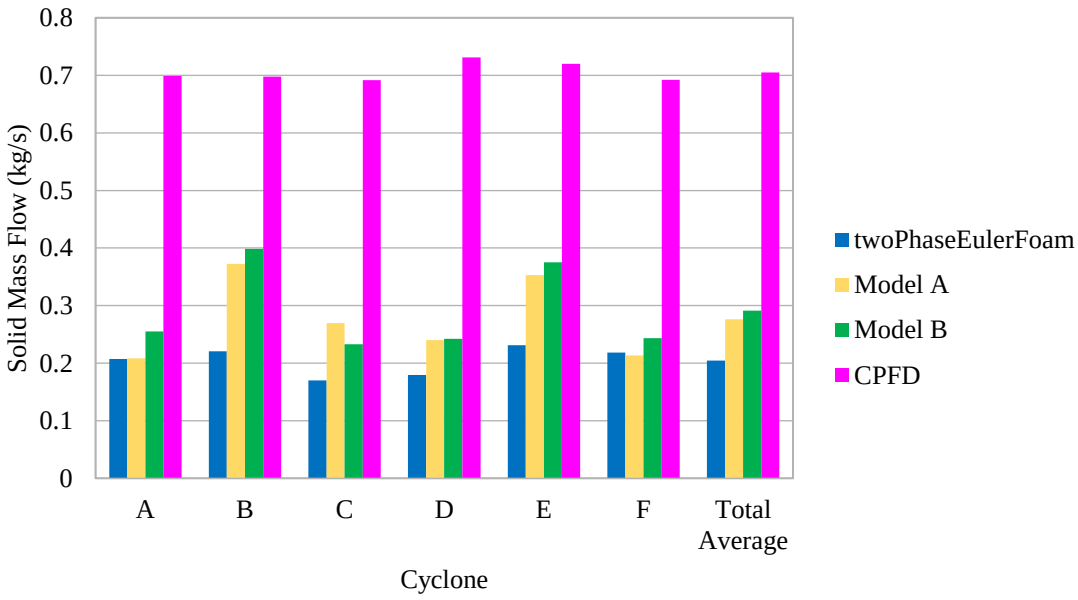

Figure 41 - Solids mass flow through each cyclone A to F and an average of all the cyclones.

As was touched on earlier the CPFD results has a more evenly distributed solids volume fraction throughout the system and the experimental results in the riser section show that there is not as an even distribution of particles. Therefore, it could be that the CPFD is over predicting the number of particles entering each cyclone resulting in a very large mass flow rate. Also, twoPhaseEulerFoam has a larger solids volume fraction region of particles near the base of the riser section and a region of high solids volume fraction in the stand pipes causing there to be less mass in the riser, overall causing the simulation to possibly be underpredicting the solids mass flow into each cyclone. Therefore, the

increase in solids mass flow caused by the modifications might be closer to a more realistic mass flow through the cyclones.

5.2.2 Volume Diffusion Flux Results Discussion

The Volume Diffusion Flux modifications have been simulated using the complex geometry of a six-cyclone recirculating fluidized bed. From these results the solid volume fraction across the height of the riser section showed very little variation between models A and B, and twoPhaseEulerFoam. Model B did show some variation in the lower section of the riser where it fluctuated between being slightly less and slightly more solids volume fraction compared to twoPhaseEulerFoam. The pressure across the height of the riser showed no difference in profile or the overall pressure drop between twoPhaseEulerFoam and the models. The cross-sectional solids volume fraction at various heights showed a difference between the models that the height's overall solids volume fraction did not. Model A did not show much variation from twoPhaseEulerFoam while model B did show a lower solids volume fraction below 4m in the denser region which was expected from the results seen in Chapter 4. In the more dilute region above 4m, the solids volume fraction is larger than twoPhaseEulerFoam for both models seen in the cross-sectional profile in the riser section. This was not seen in the previous cases as it was not measured in the dilute region of the recirculating fluidized bed case. The solids velocity also shows that there is a smaller velocity profile below 4m in height of the riser section for both models and above 4m in height a larger profile seen when compared to the twoPhaseEulerFoam simulation. This combined with the observed increase in solids volume fraction in the dilute region suggests there is more momentum of the particles for Model B. This is also reflected in the results of the solids mass flow into the cyclones with Model B producing the largest increase of solids volume fraction than either Model A or twoPhaseEulerFoam.

5.3 Korteweg Stress Models

From Chapter 4 the Korteweg Stress modifications made more of an impact on both the fluidized bed and the recirculating fluidized bed simulation cases than the Volume Diffusion Flux models. The main effects observed were a greater amount of circulation occurring with a larger upwards solids velocity in the centre of the flow and larger downwards velocity near the walls for both models. Also, the particles were more evenly distributed throughout the system compared to the twoPhaseEulerFoam simulation.

Similar effects are expected to be observed in this case. As with the previous sections, a summary of the modifications is shown in Table 14.

Table 14 – Korteweg Stress model descriptions for the six-cyclone recirculating fluidized bed.

Label	Equations for Original and Korteweg Stress Modifications	
twoPhaseEulerFoam	$\rho_s\alpha_s\left[\frac{\partial U_s}{\partial t}+U_s\cdot\nabla U_s\right]=-\alpha_s\nabla P+\nabla\cdot\alpha_s\tau_s-\nabla P_s+\alpha_g\rho_g g+\beta(U_g-U_s)$	(5)
Model C	$\rho_s\alpha_s\left[\frac{\partial U_s}{\partial t}+U_s\cdot\nabla U_s\right]=-\alpha_s\nabla \mathrm{P}+\nabla\cdot\alpha_s\tau_s-\nabla \mathrm{T}+\alpha_g\rho_g g+\beta(U_g-U_s)$	(42)
	$T=\left[-P+K\rho\nabla^2\alpha_s+\frac{1}{2}K\lvert\nabla\alpha_s\rvert^2\right]I-K\nabla\alpha_s\otimes\nabla\alpha_s$	(39)
	$K=\frac{\mu_s^2}{\rho_s}$	(40)
Model D	$\rho_s\alpha_s\left[\frac{\partial U_s}{\partial t}+U_s\cdot\nabla U_s\right]=-\alpha_s\nabla \mathrm{P}+\nabla\cdot\alpha_s\tau_s-\nabla \mathrm{T}+\alpha_g\rho_g g+\beta(U_g-U_s)$	(42)
	$T=\left[-P+K\rho\nabla^2 w_s+\frac{1}{2}K\lvert\nabla w_s\rvert^2\right]I-K\nabla w_s\otimes\nabla w_s$	(41)
	$K=\frac{\mu_s^2}{\rho_s}$	(40)
	$w_s=\frac{\alpha_s\rho_s}{\alpha_s\rho_s+\alpha_g\rho_g}$	(32)

5.3.1 Korteweg Stress Results

The solids volume fraction and pressure across the full height of the riser section are shown in Figure 42. There are some minor differences in the solids volume fraction between twoPhaseEulerFoam and each model, with Model C showing the largest difference in profiles. Approximately between 0.5m and 1.2m Model C has a larger solids volume fraction, while between 2m and 3m it then has a smaller solids volume fraction. Model D matches the twoPhaseEulerFoam results with some minor deviations between their profiles below 2m in height in the riser section where a smaller solids volume fraction is observed. Above 3m in the riser, where it is considered to be the more dilute region, both twoPhaseEulerFoam and the models match closely as the Korteweg Stress modifications do not have an effect on the dilute region.

The pressure across the riser section in Figure 42b), there is very little difference between the twoPhaseEulerFoam and models' simulations. Model C has a very slightly lower pressure between 0.5m and 1.5m which coincides with the slightly larger solids volume fraction observed in Figure 42a). Model D has a slightly larger pressure profile above 1m which then converges with the twoPhaseEulerFoam pressure near the top of the riser section. Below 0.5m it has a very slightly lower pressure profile than twoPhaseEulerFoam and then matches closely with twoPhaseEulerFoam at the base of the riser section. The overall pressure drop has not changed by each model therefore the Korteweg Stress modifications do not have a significant effect on the time-averaged pressure drop of this fluidized bed system.

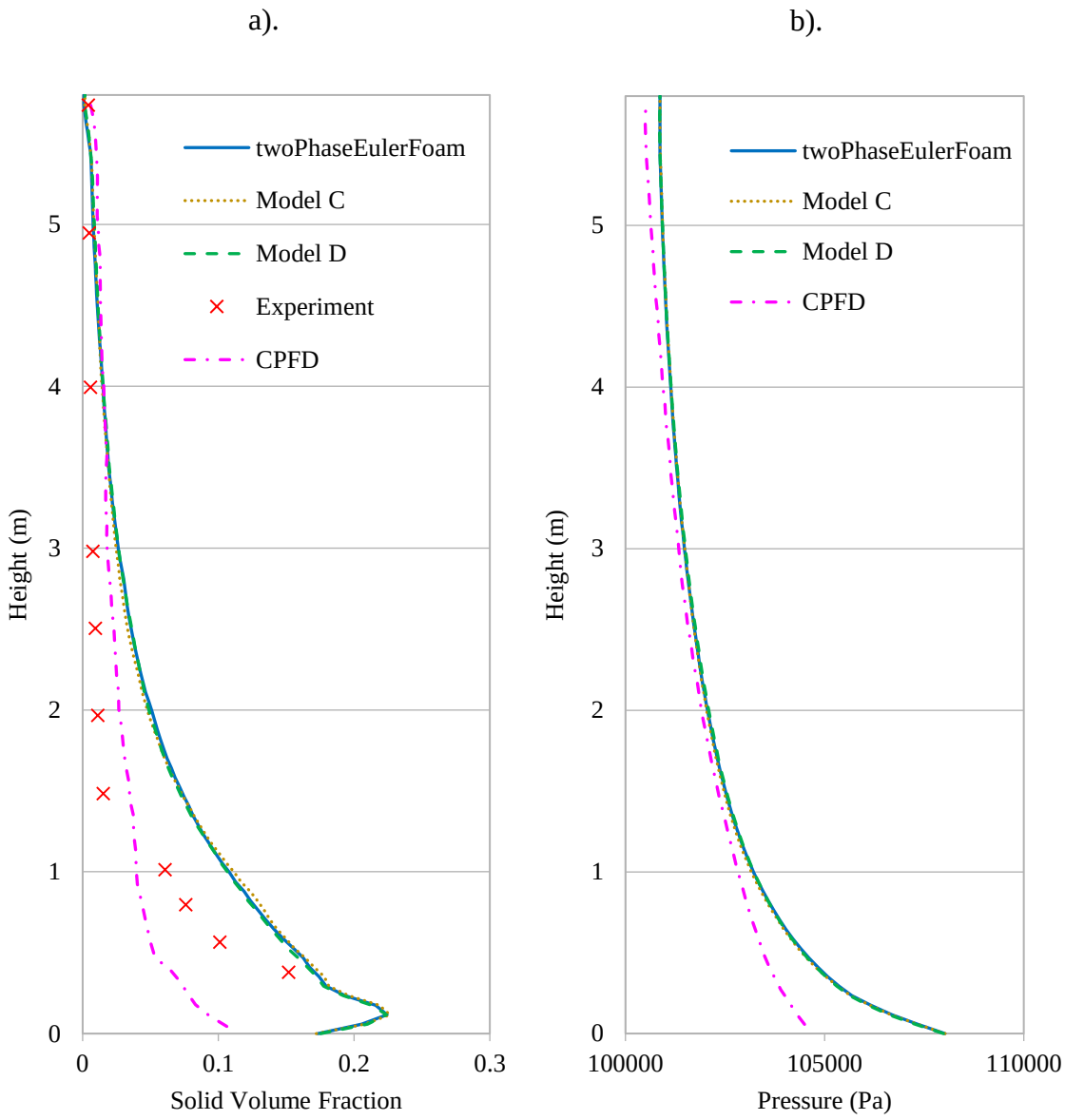

Figure 42 - Time-averaged through the height of the riser for a). solid volume fraction, and b). pressure.

The solids volume fraction at various height cross-sections of the riser section is shown in Figure 43. At 0.5m and 1.5m the models C and D show a small variation in profile compared to twoPhaseEulerFoam with Model D having a slightly lower solids volume fraction as was observed from the previous cases. Midway up the riser section at 2.5m only Model C showed a lower solids volume fraction which agrees with what was observed at that height in Figure 42a), while Model D matched well with the twoPhaseEulerFoam simulation profile. Between 3.5m and 4.5m Model D has an increase in solids volume fraction, while the Model C simulation profile either matched twoPhaseEulerFoam or also increased. Near the top of the riser at 5.5m there is not as much of a difference between twoPhaseEulerFoam and the models in the centre of the riser section, while at the walls both models C and D show an increase in solids volume fraction with the biggest increase occurring with Model D.

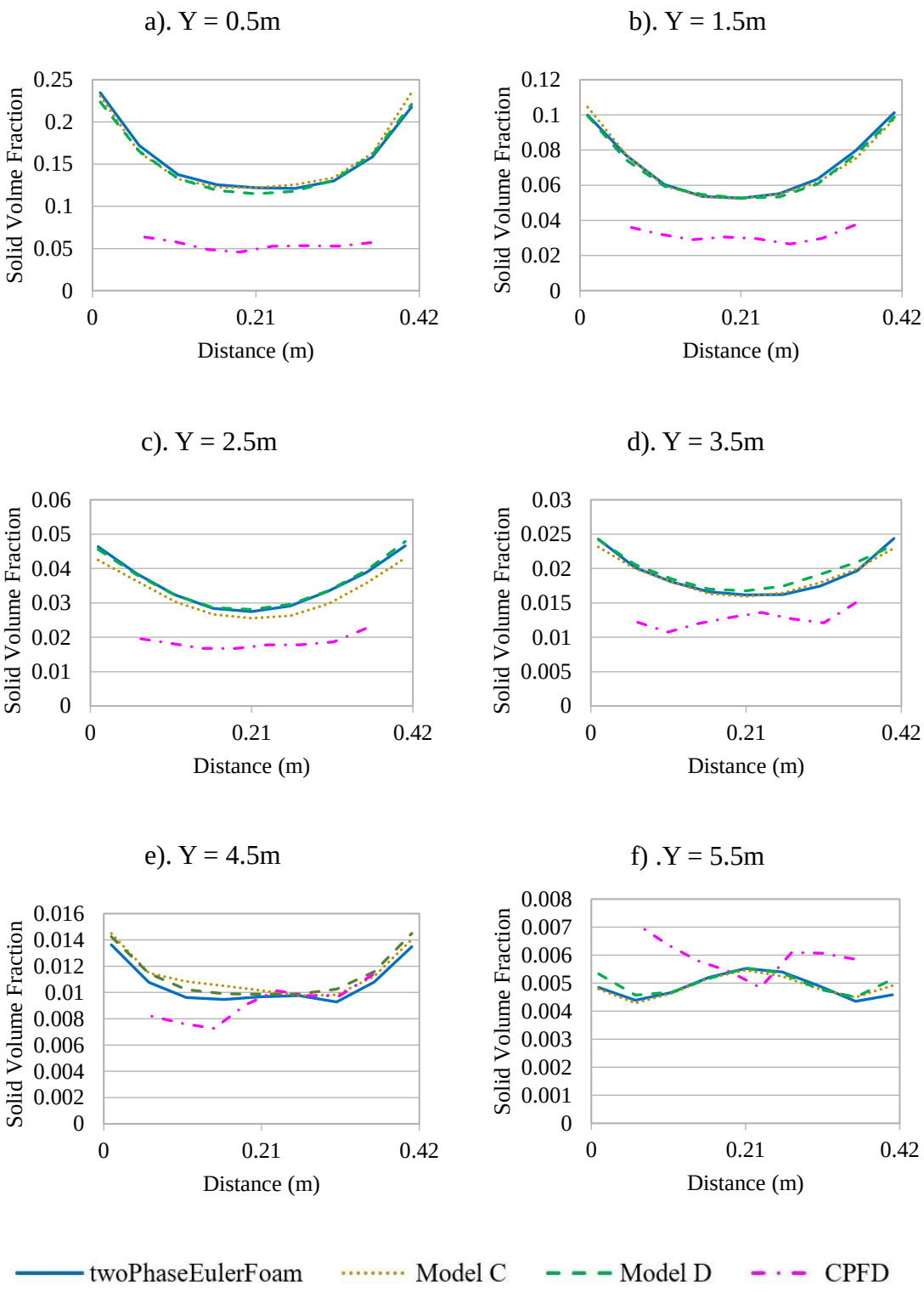

Figure 43 - Time-averaged solid volume fraction across the riser section in the x-direction.

The solids velocity at various height cross-section of the riser section in Figure 44 show that throughout the riser section the solid velocity near the walls for twoPhaseEulerFoam and both models are very similar. This suggests that the models do not affect the velocity near the walls and the main effects are seen in the centre of the flow. Initially at 0.5m models C and D have a slightly larger solids velocity than twoPhaseEulerFoam at the

centre of the riser section away from the walls. From 1.5m to 2.5m, both models C and D have a lower solids velocity than twoPhaseEulerFoam and is closer to the CPFD simulation. For the cross-section of the riser at height of 3.5m, both twoPhaseEulerFoam and the models have the same shape and magnitude solids velocity profile. Near to the top of the riser both 4.5m and 5.5m cross-sections show that models C and D have a larger peak of solids velocity in the centre of the riser than twoPhaseEulerFoam and Model Ds profile becomes larger than Model C at 5.5m.

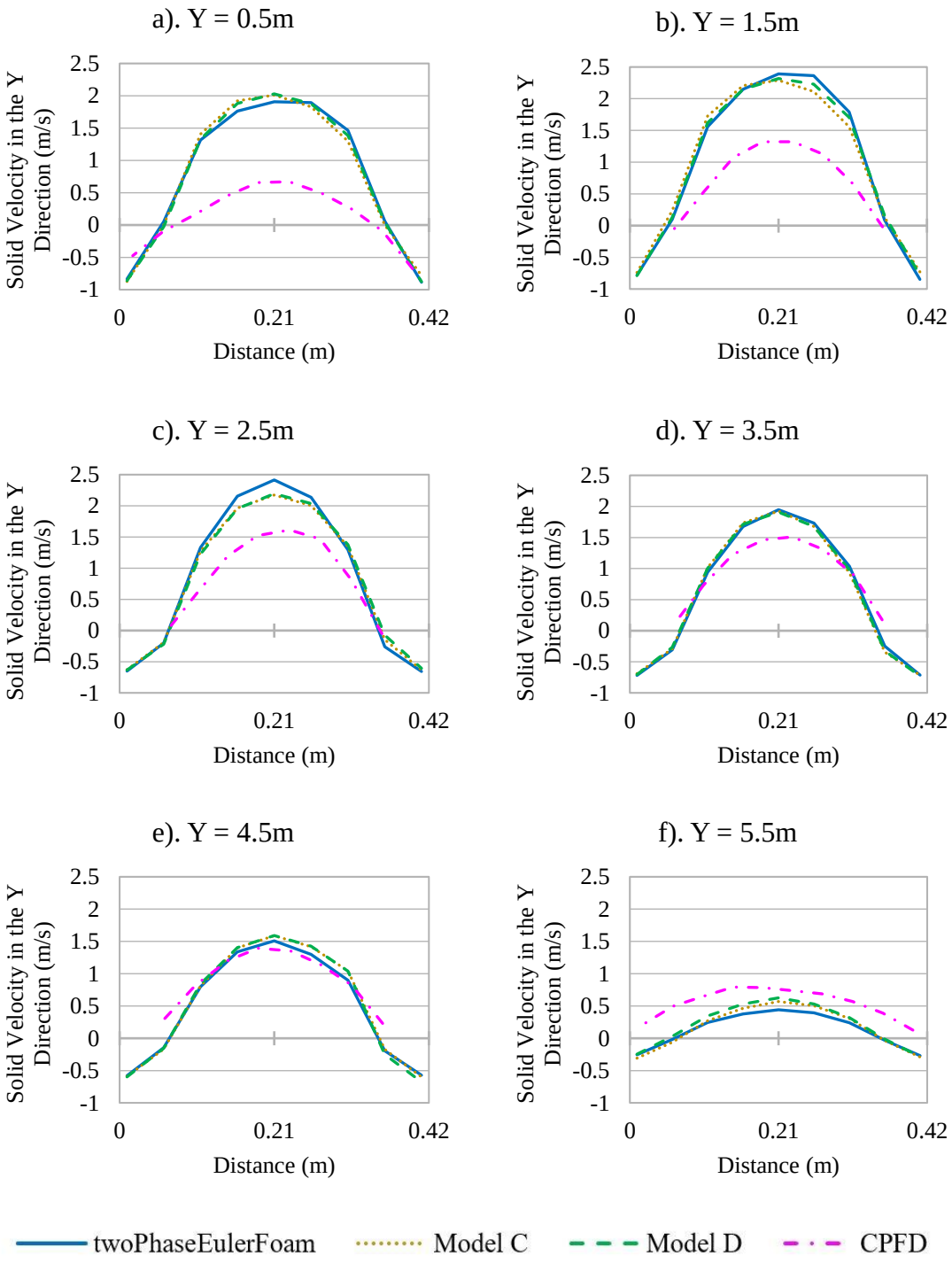

Figure 44 - Time-averaged solid velocity cross-sections at different heights of the riser section in the x-direction.

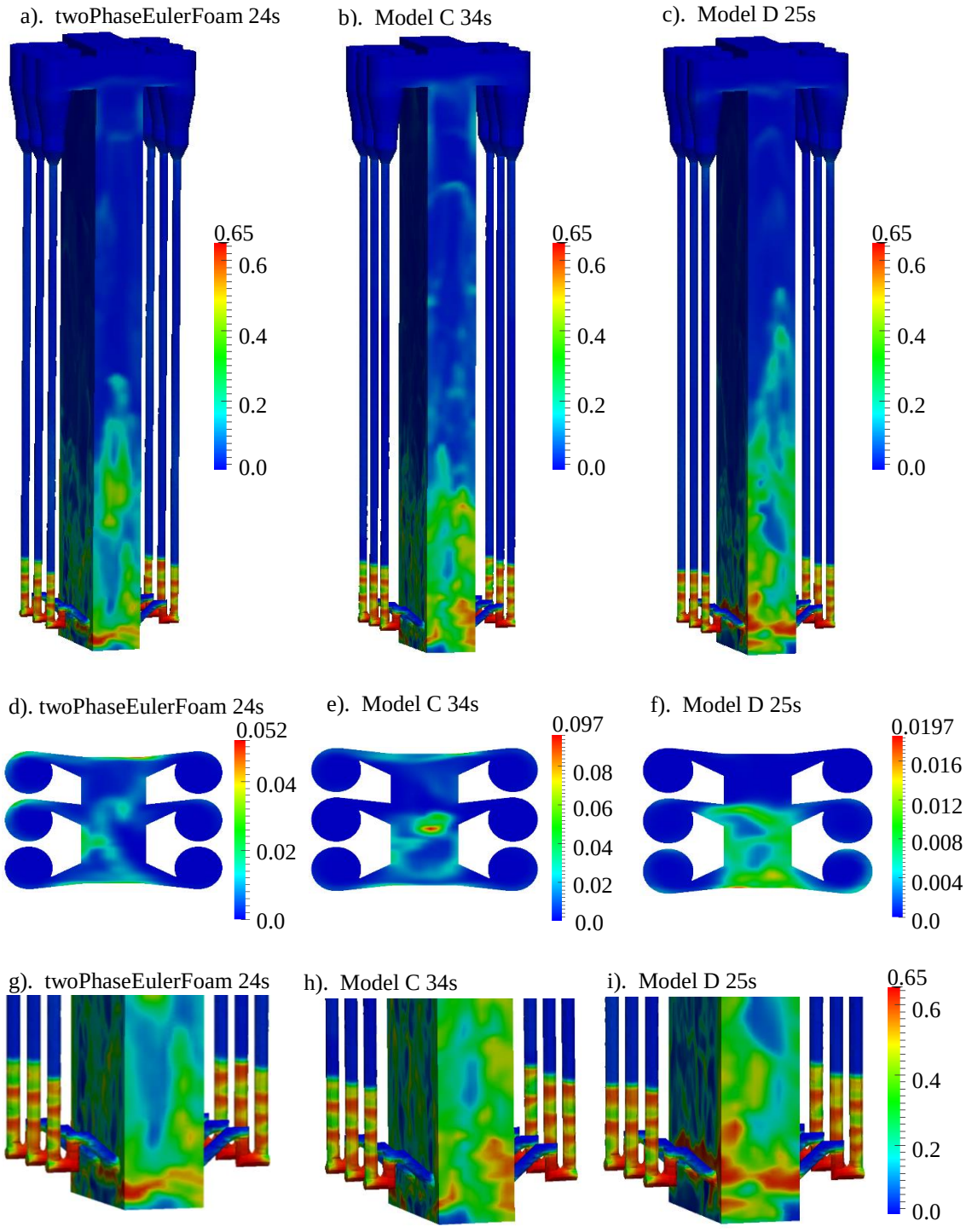

Figure 45 - Solid volume fraction of the six-cyclone recirculating fluidized bed at various times.

Figure 45 shows snapshots of the solids volume fraction for various sections of the system. The standpipes and the U-bend are still filled with particles as was observed with the Volume Diffusion Flux modifications and does not show any significant differences in the shape or size of the bubbles formed between twoPhaseEulerFoam and the models. Both twoPhaseEulerFoam and Model C show more 'ribbon' like structures of solids as they are rising in the riser section, while Model D seeming to have more rounded clusters

rising up. Also, Model D seems to have a smaller region of denser solids phase near the base of the riser.

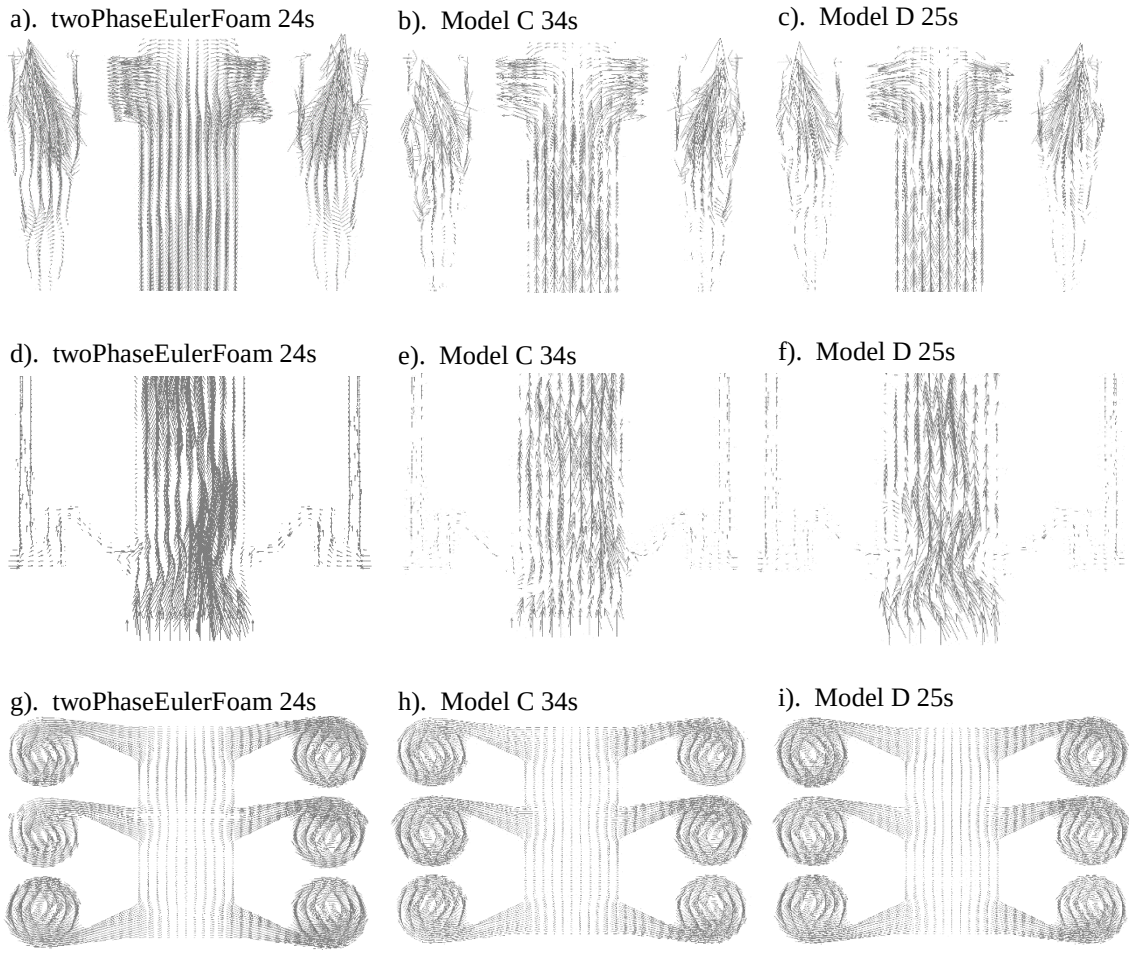

Figure 46 - Gas velocity of the six-cyclone recirculating fluidized bed at various times.

Snapshots of the vector fields of the gas velocity for various times in Figure 46, where Model C and Model D show a more evenly distributed gas velocity through the inlets of the cyclones than twoPhaseEulerFoam. As was seen with the Volume Diffusion Flux model simulations there is gas flow back into the riser section meaning the particles are also being returned with help of the gas inlet at the bottom of the U-bend and there is varying velocity profile across the cyclones. There are no significant differences that can be seen in these snapshots of the gas velocity.

A significant difference between twoPhaseEulerFoam and the models can be seen in the mass flow rate into each cyclone in Figure 47. Both models C and D either match the profiles or are greater than the twoPhaseEulerFoam mass flow rate for each cyclone and is largest in the centre cyclones B and E. The centre cyclones B and E profiles for models C and D both sharply decrease towards the twoPhaseEulerFoam mass flow rate on one side of the cyclone inlet. This is in contrast to the CPFD simulation where the mass flow

rate tends to increase from one side to the other, while models C and D solids mass flow rate profile gradually increases for the majority of the length of the inlet then a sharp decline near the wall on one side of the cyclone inlet.

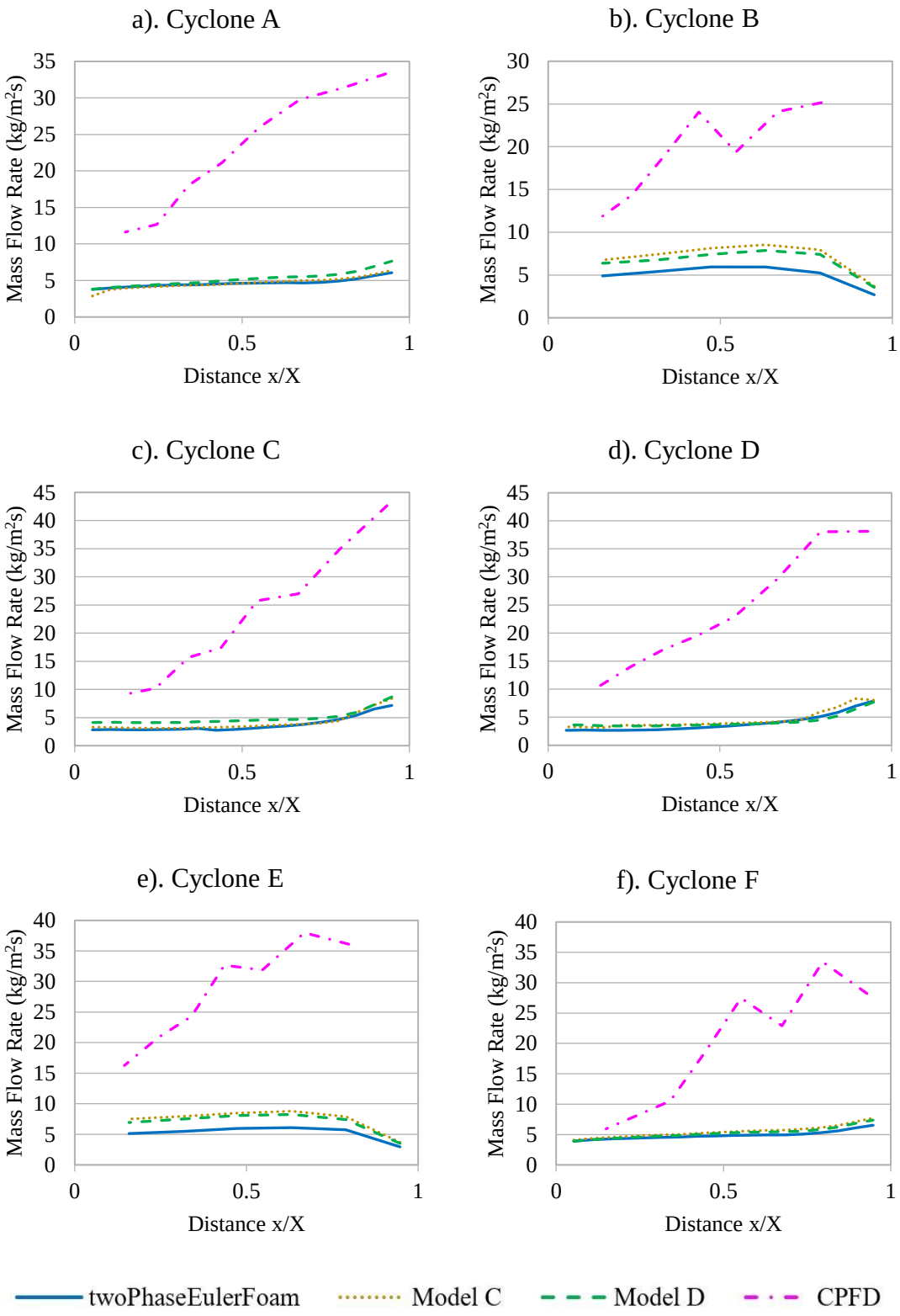

Figure 47 – Solids mass flow rate through the inlet of each cyclone A to F.

The average solids mass flux for each cyclone and the overall average are shown in Figure 48. There is an almost even distribution of whether Models C or D is larger than the other

which has resulted in very similar solids mass flow average across all the cylinders. The largest average solids mass flow occurs at the centre set of cyclones B and E, with Model C having the largest overall solids mass flow. Both models have a higher solids velocity and solids volume fraction near the centre of the riser which has resulted in an average larger solids mass flow into the cyclones, especially for the centre cyclones B and E. Overall, both models have a higher mass flow rate on average with Model C having the most significant difference across all the cyclones.

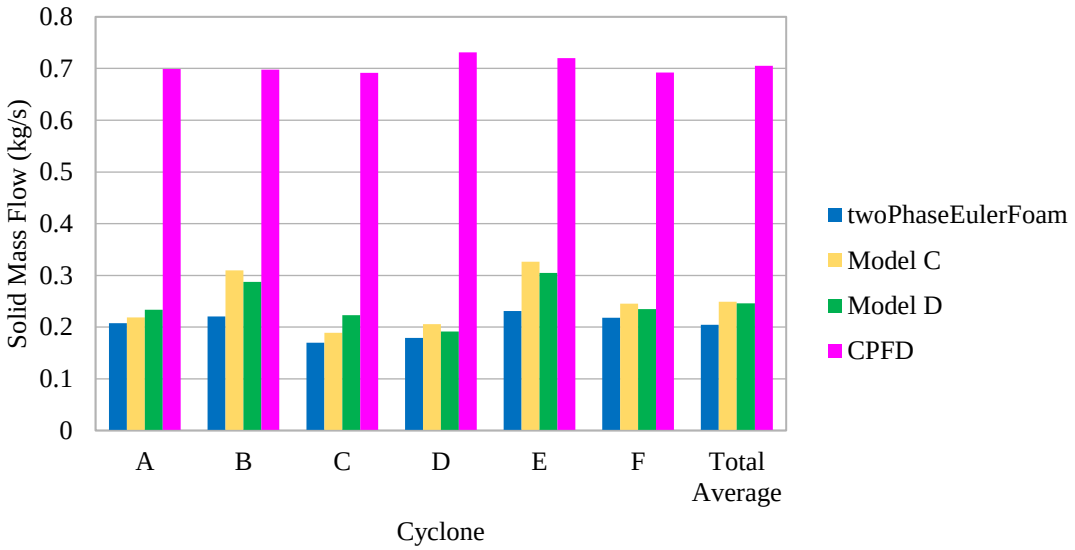

Figure 48 - Solids mass flow through each cyclone and averaged across all cyclones.

5.3.2 Korteweg Stress Results Discussion

The Korteweg Stress modifications were tested on the six-cyclone recirculating fluidized bed case and found that the larger system did not give the larger cumulative effects to be observed. Overall the results were like that of the Volume Diffusion Flux modifications in that there was a larger solids velocity in the centre of the riser section and not much effects seen near the walls. Both models C and D do show more distribution of the solids phase at different cross-sections throughout the riser section but was not significant in the solids volume fraction profile across the full height. Model C has shown to have the lowest solids volume fraction in the cross-sections of the riser while Model D was closer to the twoPhaseEulerFoam simulation profile. The solids volume fraction profile across the full height of the riser for Model C shows that it has a slightly larger proportion of the solids phase in the lower, denser region and slightly less midway up the riser section. This is a less distributed profile which was not observed in previous cases. Model D was more somewhere between Model C and twoPhaseEulerFoam simulation profiles in terms of solids volume fraction distribution throughout the height. For the distribution of mass

flow rate across the cyclones is the centre cyclones B and E have the higher solids volume fraction for both models while on average Model C had a slightly larger solids mass flow than Model D.

5.4 Combined Modification

With the data gotten so far from each model individually a discussion as to which model for each modification will be used to make a new combined model will be completed. For the Volume Diffusion Flux modifications, Model A is based on a single-phase formulation which gave very little significant results. and Model B takes into account the effect of the overall density change across both solid and gas phases in its formulation which gave a more significant effect on the solids velocity and a more distributed solids volume fraction throughout the domain. Model B is selected to be combined with the Korteweg Stress modification because of its formulation for multiphase flows and that it has a greater effect on the flow though it is noted here that Model B did not closer matched the experimental data provided in the previous sections. For the Korteweg stress modification Model D outperformed Model C by having a less distributed solids volume fraction in the recirculating fluidized bed and more circulation effects occurring in the main flow which better compared to experimental data. By combining the Volume Diffusion Flux and the Korteweg Stress the effects of both will be tested with the six-cyclone recirculating fluidized bed case. A summary models are given in Table 15.

Table 15 – Model descriptions for the six-cyclone recirculating fluidized bed.

Label	Equations for Original and new modifications	
twoPhaseEulerFoam	$\rho_s\alpha_s\left[\frac{\partial U_s}{\partial t}+U_s\cdot\nabla U_s\right]=-\alpha_s\nabla P+\nabla\cdot\alpha_s\tau_s-\nabla P_s+\alpha_g\rho_g g+\beta(U_g-U_s)$	(5)
Model B	$U_{vs}=U_m+J_{vs}$, to replace U_s in equation (10)	(26)
	$D_{vs}=\frac{\rho_s v_s}{(\alpha_s\rho_s)+(\alpha_g\rho_g)}$	(36)
	$w_s=\frac{\alpha_s\rho_s}{\alpha_s\rho_s+\alpha_g\rho_g}$	(32)
	$J_s=-\rho_s D_{vs}\nabla w_s$	(33)
	$J_{vs}=\left(\bar{v}_s-\bar{v}_g\right)J_s$	(34)
Model D	$\rho_s\alpha_s\left[\frac{\partial U_s}{\partial t}+U_s\cdot\nabla U_s\right]=-\alpha_s\nabla\mathrm{P}+\nabla\cdot\alpha_s\tau_s-\nabla\mathrm{T}+\alpha_g\rho_g g+\beta(U_g-U_s)$	(42)
	$T=\left[-P+K\rho\nabla^2 w_s+\frac{1}{2}K\lvert\nabla w_s\rvert^2\right]I-K\nabla w_s\otimes\nabla w_s$	(41)
	$K=\frac{\mu_s^2}{\rho_s}$	(40)
	$w_s=\frac{\alpha_s\rho_s}{\alpha_s\rho_s+\alpha_g\rho_g}$	(32)
Model B+D	$T=\left[-P+K\rho\nabla^2 w_s+\frac{1}{2}K\lvert\nabla w_s\rvert^2\right]I-K\nabla w_s\otimes\nabla w_s$	(41)
	$K=\frac{\mu_s^2}{\rho_s}$	(40)
	$w_s=\frac{\alpha_s\rho_s}{\alpha_s\rho_s+\alpha_g\rho_g}$	(32)

5.4.1 Combined Modification Results

The solids volume fraction and pressure across the full height of the riser section is shown in Figure 49. For the solids volume fraction in Figure 49a), the combined Model B+D has the largest distinction in profile compared to the individual models and twoPhaseEulerFoam. The combined model has a denser region near the base, while further up the riser the solids volume fraction profile becomes less than that of twoPhaseEulerFoam and closer to the experimental data. The overall profile of the combined model is closer to the experimental results in that there is a denser region near the base of the riser and then becomes fairly dilute very quickly further up the riser. So far, by combining models B and D the overall solids volume fraction is less distributed throughout the riser section than the models individually reported. Near the top of the riser section there is no distinction between Model B+D, individual models and twoPhaseEulerFoam.

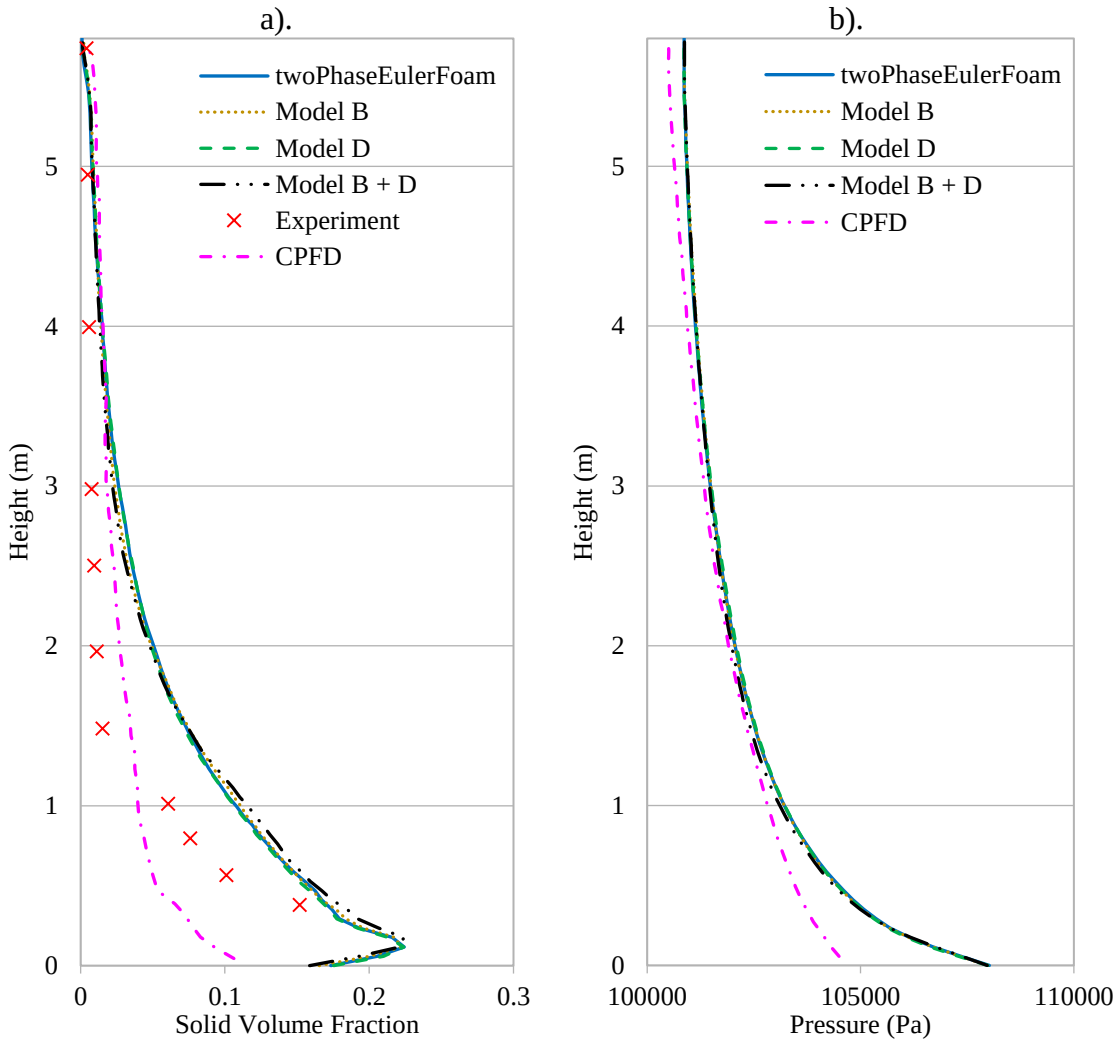

Figure 49 - Time-averaged through the height of the Riser section for a). solid volume fraction, and b). pressure.

The pressure through the height of the riser in Figure 49b) show that models B and D have very little differences between their profiles while the combined model has a more significant difference between 0.5m and 3m of the riser section. This coincides with the larger solids volume fraction in Figure 49a) which suggests the Model B+D simulation is closer to the CPFD results in this section. Even with the difference in the pressure profile near the base of the riser, the pressure drop at the base and at the top of the riser are the same for all models and twoPhaseEulerFoam tested giving no significant difference in pressure drop over the riser section.

The solids volume fraction cross sections at various heights of the riser are given in Figure 50. Between 0.5m and 1.5m in height Model B+D closely matches the twoPhaseEulerFoam profile at the centre of the riser and has a larger solids volume fraction at the walls. Model B has the effect of a higher solid volume fraction across the whole section, while Model D has a lower solids volume fraction than twoPhaseEulerFoam. At the cross-sectional heights of 2.5m and 3.5m Model B+D has a much lower solids volume fraction than the other models and twoPhaseEulerFoam. This matches what was seen in the solid volume fraction across the height of the riser in Figure 49a). Model B also has this trend, but Model D has a larger solids volume fraction across the riser section. At 4.5m both models B and D individually have a larger solids volume fraction while the combined model has a much lower solids volume fraction. Finally, at the height of 5.5m Model B+D is closer in profile to Model B with a slightly higher solids volume fraction near the walls similar to the increase seen with Model D. Overall the combined Model B+D has shown a decrease in the solids volume fraction as was expected from the models individually and from previous simulation cases. It is interesting to note that larger effects occurred by combining the models than that of each model has shown individually.

The solids velocity cross-sections of the riser section at different heights are reported in Figure 51. Near the base of the riser at 0.5m the solids velocity for the combined model matches that of both models B and D individually which are slightly larger than the solids velocity profile of twoPhaseEulerFoam. At the heights of 1.5m and 2.5m of the riser, models B, D and B+D show a lower solids velocity in the centre of the flow with a slightly larger velocity at the walls. By 3.5m in height the individual and combined models match with twoPhaseEulerFoam as the particles are no longer accelerating upwards. In the dilute region near the top of the riser at heights of 4.5m and 5.5m Model B+D matches Model B at the centre of the riser while having a slightly larger solids velocity near the walls

which are all larger than the twoPhaseEulerFoam and CPFD simulation. Overall the solids velocity seems to be most closely following the same effects as was observed by Model B where a much larger solids velocity was seen through all previous cases. The particles have a larger momentum as was slower to accelerate up the riser section and slower to decelerate near the top, which has been noted before with both Volume Diffusion Flux and Korteweg Stress modifications individually in previous cases.

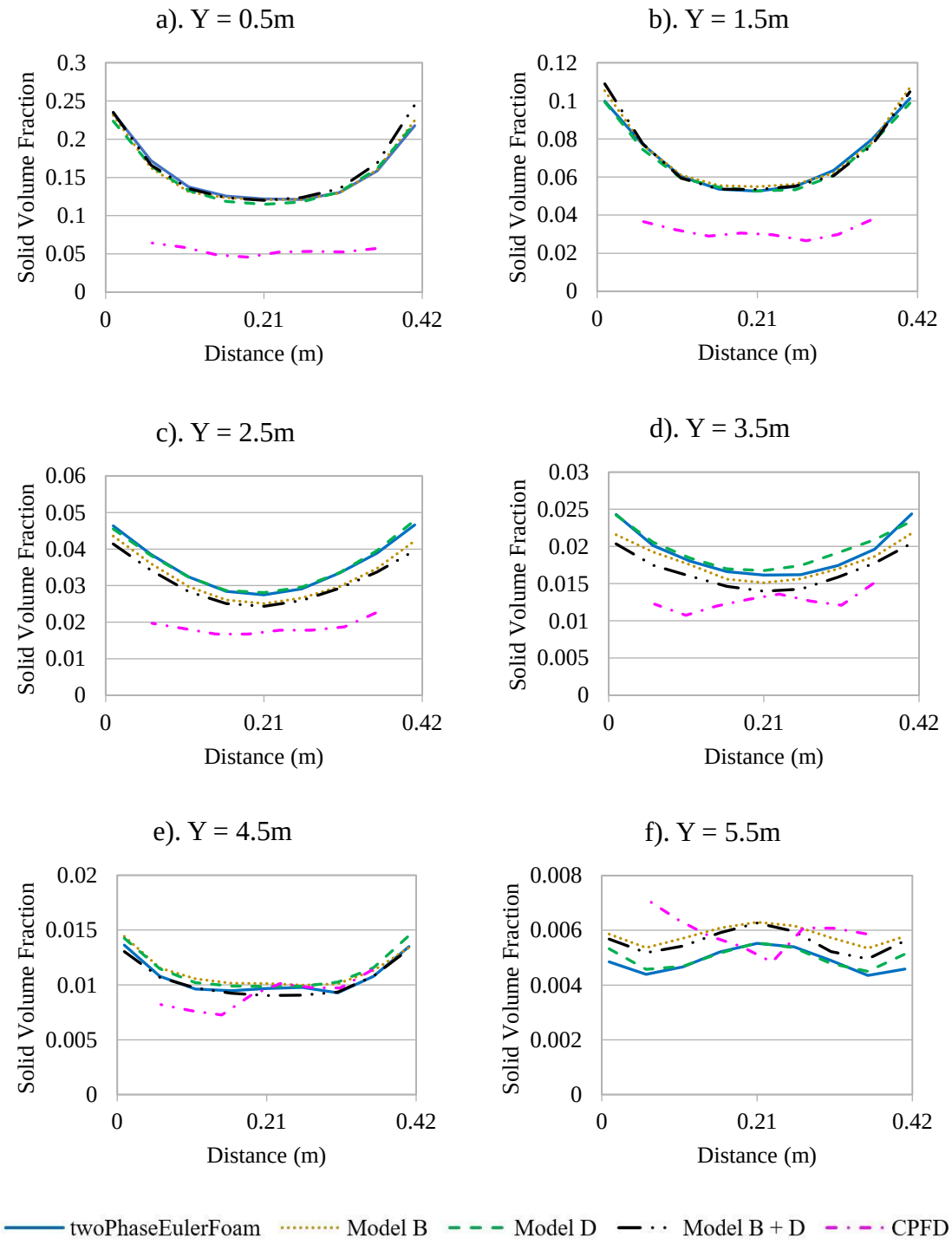

Figure 50 - Time-averaged solid volume fraction cross-section of the riser section in the x direction.

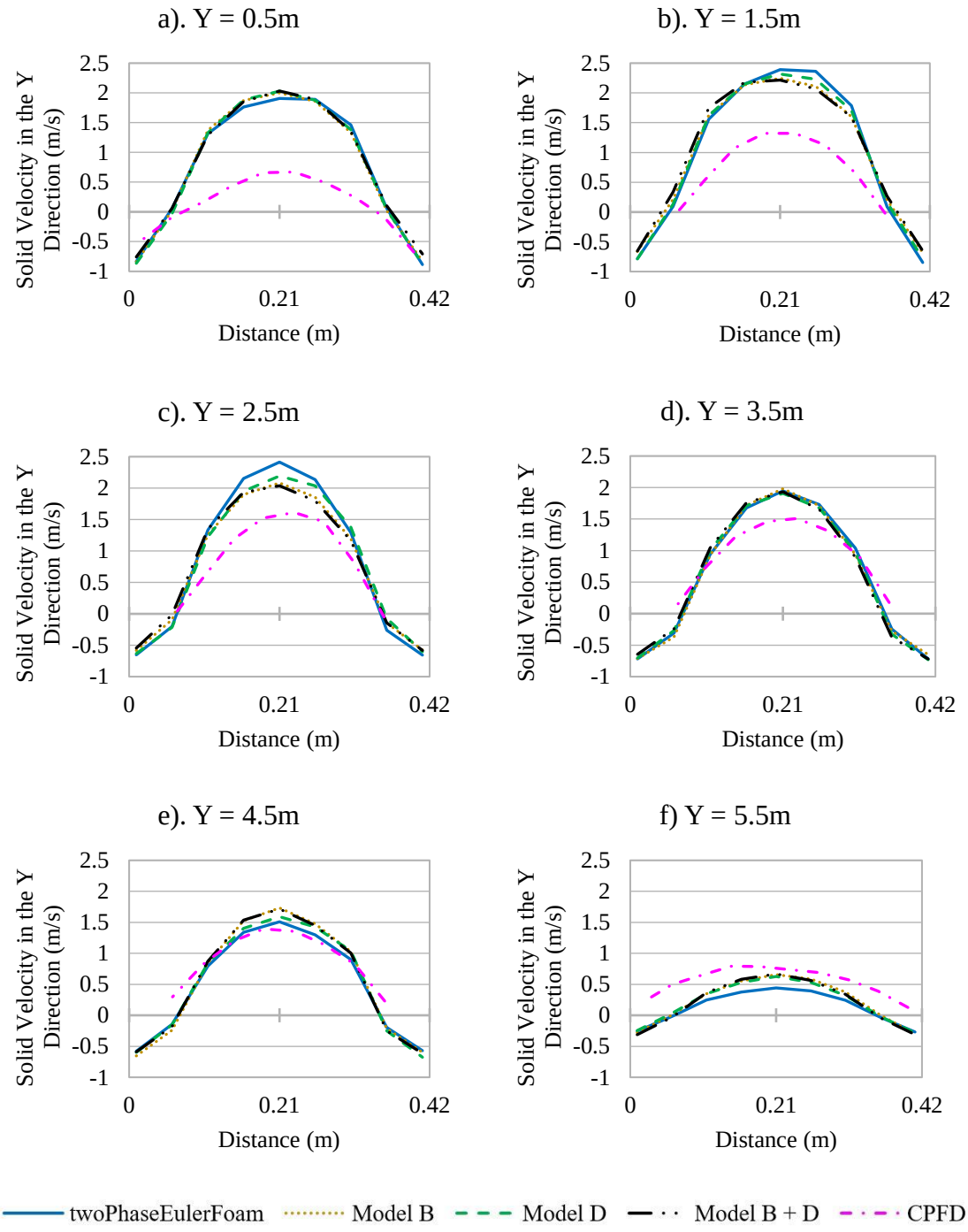

Figure 51 - Time-averaged solid velocity cross-sections of the riser section in the y-direction.

Figure 52 has snapshots of the solids volume fraction for the individual and combined models. Model B+D in Figure 52c) show that there is a smaller, more dense region near the base of the riser section which agrees with the average solids volume fraction seen in both Figures 50 and 51. Model B does not show any distinct clusters of particles rising to the top the riser section, while Model D has large clusters of particles near the middle. The combination of the models shows more what was observed with the recirculating fluidized bed are where 'ribbon'-like clusters of less dense particles are rise upwards. This could account for the less even distribution of particles time-averaged through the

height of the riser section for Model B+D. At the base of the riser section with the U-bend return pipes in Figures 53g), h), and i) Model B+D has smaller and more numerous clusters which are less dense than models B or D.

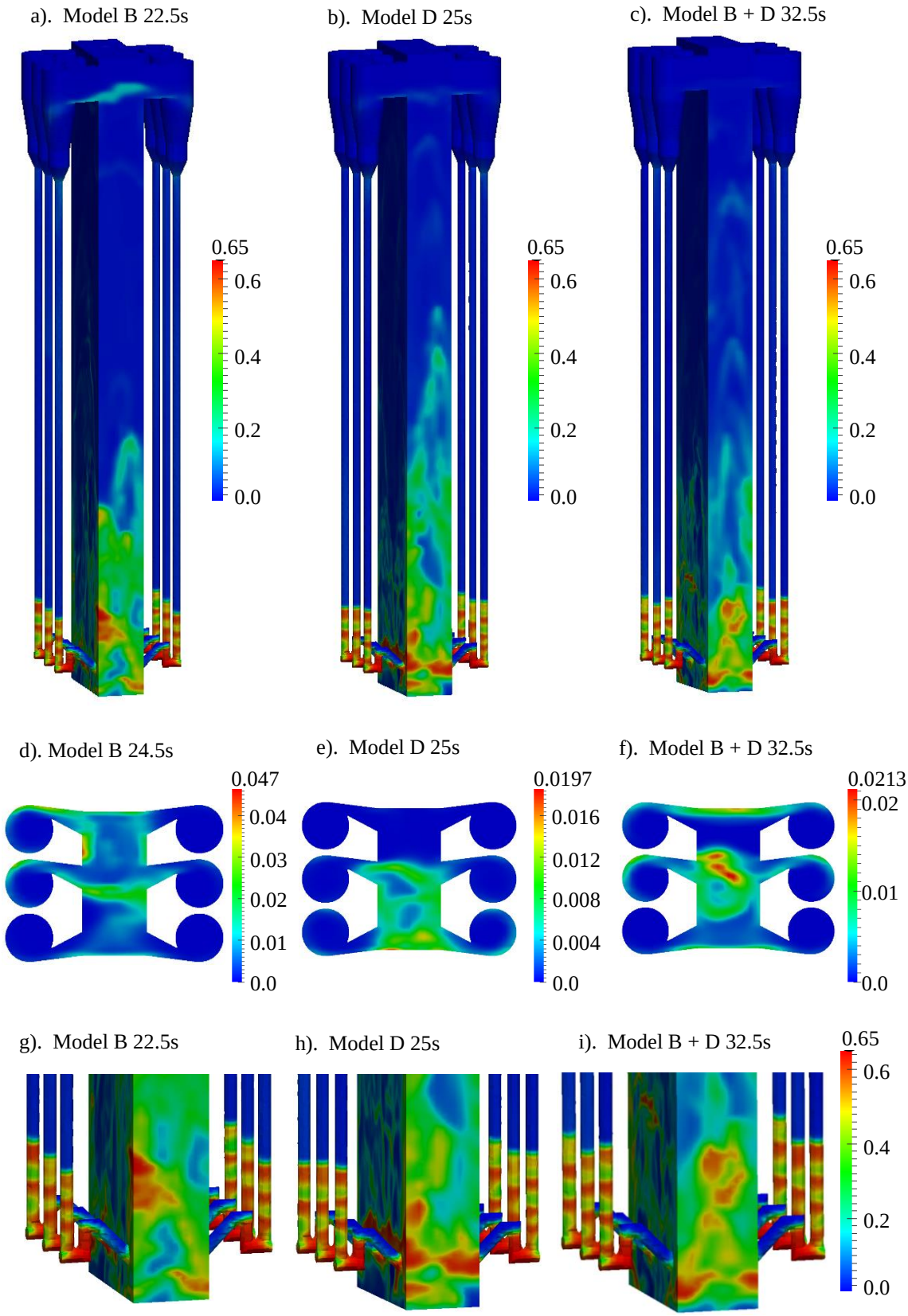

Figure 52 - Solid volume fraction of the six-cyclone recirculating fluidized bed at various times.

The vector fields of the gas velocity for various times can be seen in Figure 53 where there is not much distinction between the various models. Model B shows there is a slight difference in the gas velocity entering the cyclones where it is largest near the top of the inlet. This is not seen with Model D, and with Model B+D there is only a slight increase towards top of the cyclone inlets which will have been influenced by Model B. Overall there are no significant differences that can be seen in these snapshots.

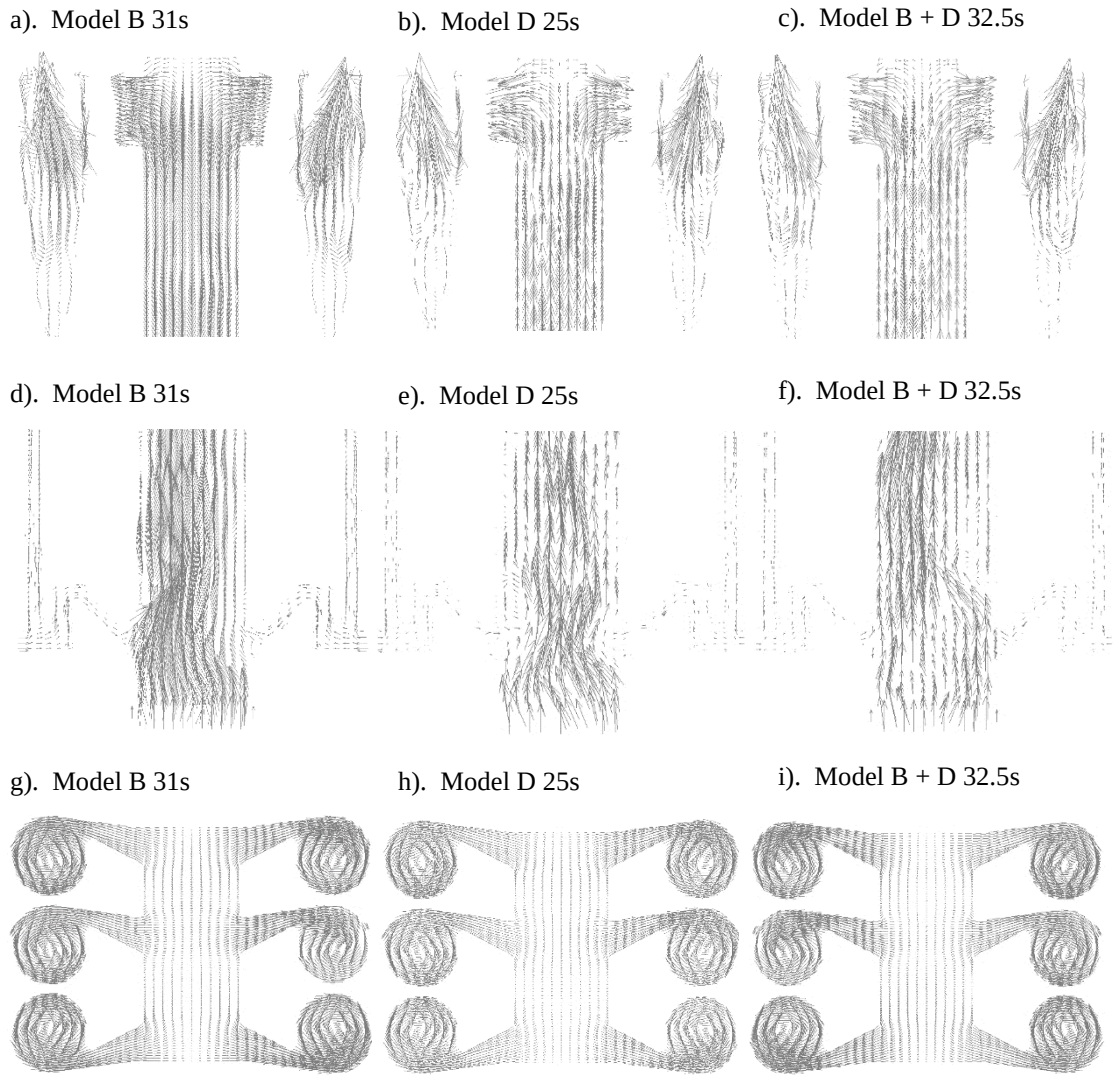

Figure 53 - Gas velocity of the six-cyclone recirculating fluidized bed at various times.

The solids mass flow rate across the inlet of each cyclone is shown in Figure 54 where Model B has the highest mass flow rate profile, while Model D is closer to the twoPhaseEulerFoam simulation profile. The combined Model B+D simulation profile occurs generally between the individual profiles models B and D. For model B+D the profile tends to be closer to Model D for the lowest mass flow rate and will increase nearly to the mass flow rate of Model B. As with models B and D individually, Model B+D has a larger solids mass flow through the middle cyclones B and E than twoPhaseEulerFoam.

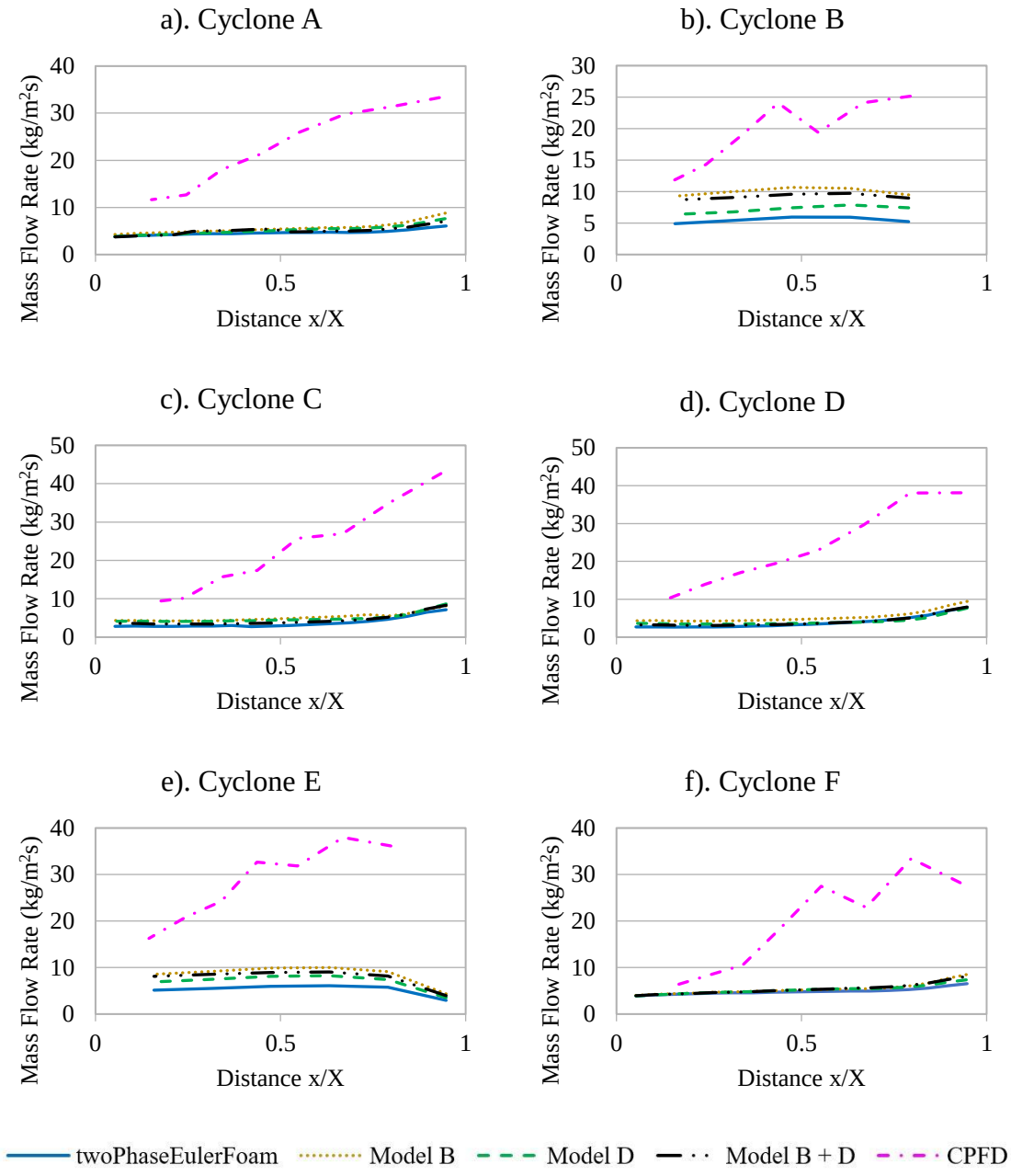

Figure 54 – Solids mass flow rate across the inlet of each cyclone A to F.

The total time-averaged solids mass flow through each cyclone and their average has been reported in Figure 55. It can be clearly seen that by time-averaging the mass flow Model B+D has less solids mass flow across the farthest set of cyclones C and D. For all other cyclones the mass flow Model B+D tends to have a much larger profile than twoPhaseEulerFoam and tends to be close to or larger than whichever individual model is largest. Model B+D has the least evenly distributed solids mass flow between the cyclones and the average of all the cyclones gives a mass flow rate somewhere between the models B and D solids mass flow rate. This shows that there is a link to the effects of both the Korteweg Stress and Volume Diffusion Flux modifications.

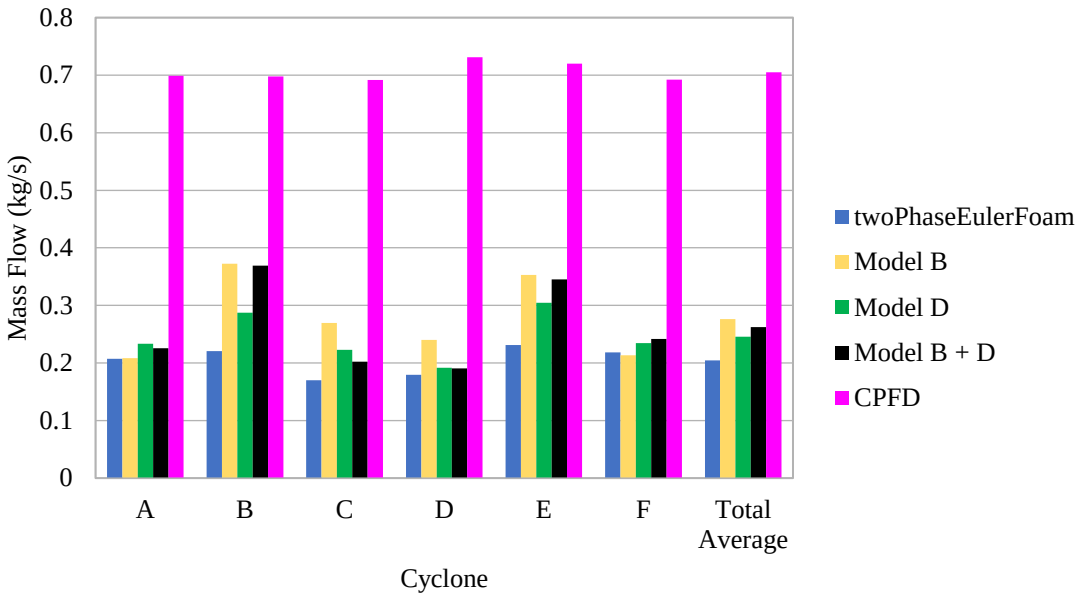

Figure 55 - Solids mass flow through each cyclone and the average across all cyclones.

5.4.2 Combined Modification Discussion

In this section a modification was selected from both the Volume Diffusion Flux and Korteweg Stress models and was combined to see the effects of both modifications on the six-cyclone recirculating fluidized bed. Model B was selected for the Volume Diffusion Flux for its larger effects on the flow observed and its formulation. The Korteweg Stress model used was Model D for its similar formulation to Model B as well as it gave better results compared to experimental data. This section also allowed for the comparison between the Volume Diffusion Flux and Korteweg Stress modifications to be made directly.

For the solids volume fraction in the riser section Model B had very little effect and Model D had slight change in its profile when compared to the twoPhaseEulerFoam simulation. The combined Model B+D had a significantly different profile than either Model B or Model D individually, or twoPhaseEulerFoam. There was a larger solids volume fraction near the base of the riser section and less in the middle region for Model B+D which better matches the profile shape of the experimental data. This was interesting as Model B has such a little effect on its own but the difference when combined with Model D was so that the profile became more distinct in the same directions as was suggested by Model D on its own. Also, the particles in the riser section seemed to be slower to accelerate and slower to decelerate near the top for Model B+D than twoPhaseEulerFoam. It looks like both models B and D had a cumulative effect on the overall solids velocity in the riser section. For the mass flow rate through the cyclones on average Model B+D is between

models B and D individually as there was a higher solids velocity but less mass of particles travelling up to the cyclones causing this difference to occur.

5.5 Discussion

This chapter looked at simulating a more complex flow system consisting of a six-cyclone recirculating fluidized bed. Each model for Volume Diffusion Flux and Korteweg Stress modifications were tested independently and then one model was selected for each modification, combined into a single solver and tested on the six-cyclone recirculating fluidized bed.

Firstly, a discussion on the comparison between the experimental results, CPFD simulations and the original OpenFOAM solver twoPhaseEulerFoam is completed here. The solids volume fraction through the full height of the riser showed the most significant differences between the different software. The solids volume fraction of CPFD had a more evenly distributed solids phase throughout the height of the riser section than both the experimental data and twoPhaseEulerFoam simulation. The twoPhaseEulerFoam simulation captures the effect of the return of particles from the cyclone separators which coincides with the increase shown by the experimental data at the same height in the riser section. For the pressure across the riser section both CPFD and twoPhaseEulerFoam simulations had a similar shaped profile, however, the experimentally measured pressure drop of the riser section was reported to be about 5kPa with the CPFD only reporting around 4kPa which coincides with the more distributed solids phase. The pressure drop for twoPhaseEulerFoam was found to be closer to 7kPa and coincides with a larger solids volume fraction near the base of the riser section. There was a build-up of particles that occurred in the U-bend and stand pipe which fluidized with bubbles travelling up the pipe towards the cyclones. The build-up of particles was also captured by the CPFD simulations, but the fluidization and bubbles were not distinctly identified. Therefore, it is possible that this effect was able to be predicted by twoPhaseEulerFoam and not by CPFD. There was a significant difference between the solids mass flow rates into the cyclones which is due to the larger distribution of particles with CPFD, therefore, the mass flow predicted by CPFD could be too high. It is of the authors opinion that as twoPhaseEulerFoam, with the larger pressure drop and the less distribution of the solids, either under predicts or is closer to the real solids mass flow of the system than the CPFD simulation showed. From the literature review it was found that typically Lagrangian based methods used for simulations will better capture effects of complex dense flows. In this case there are merits for using both the CPFD and twoPhaseEulerFoam as CPFD

had far more distribution of particles across the height of the riser section then the experimental data showed. The twoPhaseEulerFoam simulation had a better matching solids volume fraction profile but overpredicted the solids volume fraction in the lower region of the riser when compared to the experimental data.

The Volume Diffusion Flux modifications were then compared to the reported results and twoPhaseEulerFoam. From these results the solid volume fraction across the height of the riser section showed very little variation between each model and twoPhaseEulerFoam. The pressure across the height of the riser showed no difference in profile or the overall pressure drop between each model and twoPhaseEulerFoam. There was some differences noted for the solids velocity in the riser section where both models had an increase in solids velocity near the centre of the riser. This combined with the increase in solids volume fraction in the upper, more dilute region of the riser with Model B suggests there is more momentum in the solid phase. This is more apparent from the solids mass flow into the cyclones with Model B producing the largest average increase of mass flow rate through all the cyclones compared to both Model A and twoPhaseEulerFoam.

The Korteweg Stress modifications were also tested on the six-cyclone recirculating fluidized bed system. Overall the results were similar to that of the Volume Diffusion Flux modifications in that there was a larger solids velocity in the centre of the flow and very little differences seen at the walls of the riser section. Both models C and D did show more even distribution of the solids phase at different cross-sections throughout the riser section. Model C has shown to have the lowest solids volume fraction in cross-sections of the riser section, while Model D was closer to the twoPhaseEulerFoam simulation. The solids volume fraction profile across the full height of the riser was less evenly distributed for Model C as it had a slightly larger proportion of the solids phase in the lower, denser region and slightly less in the middle of the riser. The solids volume fraction profile for Model D was more somewhere between Model C and twoPhaseEulerFoam simulation profiles. For the distribution of mass flow rate across the cyclones it was seen that the centre cyclones B and E have the highest solids mass flow rate for both models. On average across all cyclones Model C had a slightly larger solids mass flow than Model D.

For the Volume Diffusion Flux modification, Model B is selected as it accounted for the effect of the overall density change across both solid and gas phases in its formulation. This gave a more significant effect on the solids velocity and more even distribution of the solids phase throughout the riser section which gave the largest solids mass flow into the cyclones. For the Korteweg Stress modification, Model D outperformed Model C by

having a less evenly distributed solids mass in the recirculating fluidized bed and more circulation effects occurring in the main flow. The combination of Model B from the Volume Diffusion Flux modifications and Model D from the Korteweg Stress modifications were made into a single combined model using the OpenFOAM software and then tested with the six-cyclone recirculating fluidized bed. Also, with these results we could compare directly the Volume Diffusion Flux and Korteweg Stress modifications individually. The combined Model B+D had a significantly different profile than models B or D, or twoPhaseEulerFoam. This is interesting as Model B had not much effect on its own but when combined with Model D the profile became more distinct from that of the individual models and twoPhaseEulerFoam. The profile tended more towards the experimental data with a denser region lower in the riser and becoming more dilute further up the riser section than twoPhaseEulerFoam. The combined Model B+D had an additive effect on the overall solids velocity in the riser section. For the mass flow rate through the cyclones on average Model B+D was between Models B and D individually as there was a higher solids velocity but less particles travelling up to the cyclones causing this difference.

The conclusion from the simulations carried out here shows that the Volume Diffusion Flux and Korteweg Stress modifications individually do make some small differences in the overall flow characteristics but not necessarily improve them. By combining the Volume Diffusion Flux and Korteweg Stress modifications into a combined model, greater effects occurred such as a shift in where the regions of dense and dilute solid phase occurs therefore, less even distribution of the solid phase occurred. By using the larger, more complex system it could be seen that the Volume Diffusion Flux did not have as large an effect to make it a useful modification on its own. With the combination with the Korteweg Stress modification the simulation did result in a more closer profile to the solids volume fraction of the experimental data for this case though still not significant.

Chapter 6: Conclusions

Currently there are two main methods for simulating rapid granular-gas flows which are based on Eulerian and Lagrangian methods. Lagrangian methods such as Computational Fluid Dynamics – Discrete Element Method (CFD-DEM) do simulate granular-gas flows effectively but have a very high computing costs. The Eulerian method of the Two Fluid Model (TFM) has been modified to treat the granular phase like a fluid by a method called the Kinetic Theory of Granular Flows (KTGF). This method has far less computing cost as the information on the particle scale is averaged out. Some of the short comings have been highlighted when KTGF has been compared with Lagrangian models. It shows that generally the description of the particle phase is incomplete, and more research and development needed to be done to improve this. This is important as currently the models that have a better overall comparability to experimental results are based on more computationally demanding solvers such as CFD-DEM and direct numerical models. Therefore, an accurate KTGF solver is still required to reduce the computing costs. Currently there is a trade-off between the accuracy needed and the efficiency of a solver. These issues are being addressed with more detailed analysis of the ways in which particles interact at different flow regimes. By simulating flows with solvers such as CFD-DEM it can become clear at which point certain interactions become important such as particle rotation and its role in friction and energy dissipation. More recently, studies of differing particle shape are bringing forward the need for including particle shape effects into the KTGF for more realistic flows and is an expanding area of research. Overall there are a lot of individual areas of research in which more integration could be done as well as more complex and realistic flows need to be tested and validated. The Lagrangian methods can be used to test and validate new Eularian models as they have been shown to model rapid granular-gas flows well.

In this thesis a new set of modifications to the Kinetic Theory of Granular Flows (KTGF) was developed and tested with different fluidized bed systems. The first modification considered here is based on Volume Diffusion Flux or also known as Bi-velocity as first set out by Brenner (2005). He states that the Navier-Stokes equations for fluid flow need to consider that two different velocities exist for both volume and mass fluxes in compressible flows. The reason for this is that the velocity of the fluid considered in the Navier-Stokes equations are based on the mass flux only. When flows become compressible the mass flux will not change but the volume flux will. This affects the viscosity of the fluid, therefore, two different velocities need to be considered: mass

velocity and volume velocity of the fluid. The Volume Diffusion Flux is used to determine the volume velocity of a fluid based on the gradient of density produced by a compressed fluid. For use with KTGF the solids density does not change but its ratio of the solids phase to the total volume known as the solids volume fraction is used as the first modification. This does not consider the effects of mass changes with the combined phases, another modification that takes this into account has been made. The second modification uses what was developed as a mass fraction where the mass of the phase is divided by the total mass of both phases. This allows for the relative difference between the mass and volume between the phases to be taken into account. Both these modifications have been tested for several fluidized beds to see whether the need to account for both phases in the Volume Diffusion Flux modification or only considering the single phase is a sufficient enough fluid description.

The second modification to the KTGF model was to include Korteweg Stress as part of the solid phase stress. Korteweg (1901) proposed a model in which phase transitional phenomena in fluids can be simulated. It was noted that when there are two fluids with different densities and viscosities, additional stresses are created. This model is similar to the Volume Diffusion Flux where it relies on part of the stress tensor being dependent on the gradient of the density of the fluid. As with the previous modification, the gradient of the solids volume fraction is used here. Again, it does not consider the overall mass changes occurring within the system, therefore to better represent the average mass changes that occur across both phases, a mass fraction was developed. In this both phases have been considered and as the total mass of the system will be different at any time throughout the particle-gas flow system the mass fraction will represent that change.

Three different fluidized bed configurations have been used to compare each of the modifications described above. The first was a cylinder fluidized bed and the second was a recirculating fluidized bed. Both fluidized beds were cylindrical, only 1m in height and were of a lab scale with experimental and simulated data reported. This allowed for a comparison of the software used in this thesis to be compared to published results and allow for effects of the modifications to be seen. The last simulation was on a larger, more complex fluidized bed system of a six-cyclone recirculating fluidized bed. The particles used in all three simulations were of Geldart group B type particles which tends to be the most common particle size and density group.

6.1 Software Discussion

Each of the fluidized bed cases and solver modifications were tested using an open source software called OpenFOAM which is a freely available software that can be downloaded and changed to implement new models easily. As OpenFOAM is an open source software there is no guarantee of the quality of results given so a comparison between OpenFOAM, other available commercial and non-commercial software, and reported experimental data has been undertaken. This was done in detail for the first simulation of a cylinder fluidized bed in detail with a brief discussion with the other cases presented here. The paper by Makkawi *et al.* (2006) presented experimental data and simulations completed using another open source code MFix. Additional simulations were carried out using the commercial software of Ansys Fluent and the open source OpenFOAM software. All three software simulations did not predict the flows across both sizes of particles effectivly. OpenFOAM performed best for the smaller particles while overpredicting the minimum fluidization for the much larger Geldart Group B particles. This has been reported before by Herzog *et al.* (2012) for very large particles in the Geldart Group D range. Fluent matched the reported MFix simulations well for the smaller particles but they did not compare as well as the OpenFOAM simulations did to the experimental data. For the larger particles, Fluent performed very poorly with over predicting the amount of solids being entrained into the main flow. For the cylinder fluidized bed case the results show that OpenFOAM in its current form does not predict well for larger particles while MFix and Fluent predicts the larger particle flows better. OpenFOAM did better predict the solids volume fraction when compared the experimental results of the Geldart group A/B type particles than both the Fluent and MFix software simulations.

The recirculating fluidized bed had Fluent and experimental data reported by Gao *et al.* (2012) and OpenFOAM was used to compare results. It was hoped that the drag model used, which agreed very well with the experimental results in the original paper would be implemented into the OpenFOAM code but was not able reproduce the same results to any degree of usefulness, therefore, another drag model was used that also simulated with Fluent in the original work. Both Fluent and OpenFOAM software under predict the solids volume fraction near the base of the cylinder while over predicting towards the top. The OpenFOAM simulation was found to have a more evenly distributed solid phase throughout the cylinder with not as distinguished a region of higher solids volume fraction near the base as was predicated by Fluent and shown by the experimental data. This is

similar to what was found with the larger Geldart group B type particles in the cylinder fluidized bed case.

The six-cyclone recirculating fluidized bed is the only case where a Lagrangian based solver is used with experimental data as reptorted by Jiang *et al.* (2014) where they used their own code using the Computational Particle Fluid Dynamic (CPFD) method. The solids volume fraction across the full height of the riser showed the most significant differences between the CPFD and OpenFOAM solvers. The solids volume fraction of CPFD had a more distributed solids phase profile throughout the height of the riser than either experimental and OpenFOAM results. OpenFOAM was able to capture the increase in solids volume fraction from the return of particles from the cyclone separators which coincides with the increase shown by the experimental results. There was a build-up of particles that occurred in the U-bend and stand pipe where with OpenFOAM was seen to fluidize. CPFD also reported a build-up of particles in the stand pipes but the fluidization behaviour was not identified. Therefore, it is possible that this effect was able to be predicted by OpenFOAM and not by CPFD. There was a significant difference between the mass flow rates into the cyclones which is due to the larger distribution of solids with CPFD therefore, the mass flow predicted by CPFD is too high. OpenFOAM could be either under predicting or is much closer to the real mass flow through the cyclones. From the literature review it was found that typically Lagrangian methods used for simulations will better capture effects of complex dense flows. In this case OpenFOAM seemed to be capturing more effects around the system that CPFD had not.

From the various simulations OpenFOAM tends to perform well as a KTGF solver for most of the cases studied here. The drawbacks seem to be more due to the selection of models such as the radial distribution and drag models giving the largest differences. As stated before, more researchers are using OpenFOAM as a useful modelling tool with its ease of accessing the code directly and being able to modify for own needs.

6.2 Kinetic Theory of Granular Flows Modifications Discussion

The Volume Diffusion Flux modifications were implemented into the OpenFOAM software and then tested on all three simulation cases. For the cylinder fluidized bed case it was seen that there were some differences between the original solver and the modifications for the solids volume fraction. Overall both Volume Diffusion Flux models had a higher average bed height and the multiphase form (Model B) had the largest decrease in the solids volume fraction profile across the cylinder. The multiphase form

also had a larger solids velocity in the upwards direction in the centre of the bed and downwards direction near the walls compared to the original solver. Neither of the models improved upon the results from the original solver when compared to the experimental results with the multiphase form producing the least comparable results. For the recirculating fluidized bed case the Volume Diffusion Flux modifications seemed to have only a little more impact than was seen in the cylinder fluidized bed case. The single-phase form of the modification showed an increase in the solids volume fraction at the walls and a lower solids velocity than the original OpenFOAM solver. The multiphase form the modification only showed an increase in the solids volume fraction in the centre of the cylinder. As with the cylinder fluidized bed case the modifications did not improve the overall results to better match that of the experimental data. From the larger, more complex flow system of the six-cyclone recirculating fluidized bed case the solid volume fraction across the height of the riser section showed very little variation between the single-phase model and the original OpenFOAM solver. The multiphase form of the modification did show some variation in the lower section of the riser where it fluctuated between being slightly less and slightly more solids volume fraction. The solids velocity for the multiphase model also showed a different progression up the riser section with particles slower near the base and faster near the top compared with the original solver and CPFD for the six-cyclone recirculating fluidized bed. This combined with the increase in solids volume fraction in the dilute region suggests there is more momentum in the solid phase for the multiphase model. This is more apparent from the solids mass flow into the cyclones with the multiphase model producing the largest average solids mass flow rate. From all three simulations the multiphase form gives the biggest change although, overall it is not very significant compared to the differences seen between the simulated and experimental results. Also, the small effects that the modifications do show are not closer matching to the experimental data except in the case of the six-cyclone recirculating fluidized bed with the increase of mass flow rate through the cyclones for the multiphase form of the modification.

The Korteweg Stress modifications were also implemented into the OpenFOAM software and tested on all the fluidized bed cases. For the cylinder fluidized bed case these modifications reported a similar increase in the solids velocity as the Volume Diffusion Flux modifications, but it could be seen that there was more of an impact on the overall flow circulating movement within the cylinder. This could be seen as a large velocity difference that occurs near the walls and that the solid phase was more likely to travel further before being recirculated back into the centre of the flow. For the cylinder

fluidized bed case there was not a significant difference between either of the modifications. There were larger differences that could be seen between the Korteweg Stress modifications and the original solver than with the Volume Diffusion Flux modifications. For the recirculating fluidized bed case the modifications presented some differences between each of the models. The single-phase model (Model C) presented a worse profile of the solids volume fraction with a decrease in the solids volume fraction near the walls when compared to the experimental data. Also, the solids volume fraction across the full height of the cylinder had a more evenly distributed solid phase and had a distinctly less variable profile near the base as was shown by the experimental data. The multiphase model (Model D) did have more of a change in solids volume fraction profile through the height of the cylinder where a clear region can be seen to have less solids volume fraction. Though it has still under predicted the solids volume fraction the profile, the shape was closer to that reported by the experimental data than the single-phase model. Finally, for the complex flow system of the six-cyclone recirculating fluidized bed case the results were, again, like that of the Volume Diffusion Flux modifications in that there was a larger solids velocity in the centre of the flow for both models. The single-phase model has shown to have the lowest solids volume fraction in the cross-sections of the riser while the multiphase model was closer to the original solver. The solids volume fraction profile through the full height of the riser for the single-phase model shows that it had a slightly larger proportion of the solids phase in the lower, denser region and slightly less in the middle of the riser. This was a less evenly distributed profile which was not as distinct as with previous cases. The multiphase model was somewhere between the single-phase model and the original OpenFOAM simulation for the solid volume fraction distribution throughout the height of the riser. For the average mass flow rate into the cyclones the single-phase model had a slightly larger solids mass flow rate than the other models. From the simulations using the Korteweg Stress modifications the multiphase model had less evenly distributed solids mass in the recirculating fluidized bed and more circulation effects occurring in the main flow as well as a better solids volume fraction profile across the riser section of the recirculating fluidized bed case.

The final step was to combine the best of the Volume Diffusion Flux and Korteweg Stress modifications into a single solver and then test using the the six-cyclone recirculating fluidized bed case. The multiphase form of the Volume Diffusion Flux modifications considered the effect of the overall density change across both solid and gas phases in its formulation which gave a more significant effect on the solids velocity and more distributed solids throughout the domain, therefore, it was used. For the multiphase form

of the Korteweg Stress modifications, it outperformed the single-phase form by having a less distributed solids mass in the recirculating fluidized bed and more circulation effects occurring in the main flow. So, by combining the multiphase forms of both the Volume Diffusion Flux and the Korteweg Stress modifications, the over prediction of the solids volume fraction profile might be corrected by the other and see what other combined effects will be for the six-cyclone recirculating fluidized bed case.

The combined model had a more distinctly different profile than either the Volume Diffusion Flux or the Korteweg Stress model individually compared to sthe original, unmodified Kinetic Theory for Granular Flows solver. A larger solids volume fraction occurred near the base of the riser and less in the middle region which better matches the profile shape of the experimental results. This was interesting as the Volume Diffusion Flux model had so little effect on its own but the difference with the Korteweg Stress included, the profile became more distinct in the same directions as suggested by the experimental data. Also, the momentum of the particles in the riser section seemed to be slower to accelerate and decelerate. It looks like both models had an additive effect of the overall solids velocity in the riser section. For the mass flow rate through the cyclones on average the combined model is between each modification individually as there was a higher solids velocity but less particles travelling up to the cyclones causing this difference.

6.3 Final Remarks and Future Work

In conclusion the Volume Diffusion Flux model in its current form does not affect the flows enough towards a more accurate result therefore further development should be considered. It should be noted that the formulation for the Volume Diffusion Flux was only applied to the viscosity stress of the momentum equations for the solid phase only. Future work should look at recasting the continuum and momentum equations in terms of volume velocity instead of its current form with mass velocity. The sensitivity to the material properties of the solid phase in the Volume Diffusion Flux should be investigated as only dimensional analysis was used to find the material properties required. Further discussion of how the solid phase should be treated if it has compressible effects needs to be continued. The Korteweg Stress general form has been incorporated into a multiphase form to work with the Kinetic Theory of Granular Flows (KTGF). The form of this equation is still not settled, and the required constants of the material properties is still a matter of debate. Both modifications made here only apply to the KTGF equations therefore have only been applied to the solid phase. The combined Volume Diffusion

Flux and Korteweg Stress solver showed some interesting effects making it better matching with the experimental data than either modification on its own. This should be investigated further to find how much the modifications are influencing each other. Further work should also include applying the Volume Diffusion Flux and Korteweg Stress to both the gas and the solid phase in a single solver. It would also be interesting to see the effects of the modifications given here on the gas phase only. So far, the modifications have only been made to the momentum equations without considering the energy equations. This will need to be considered and added to the equation set to form a complete description of the energy and the momentum interactions. The simulations that were carried out were all fluidized bed type system which the only kind of rapid granular-gas type system are not. These modifications should be tested with more varied configurations such as pneumatic conveying and more on cyclone performance. Also, all the fluidized bed cases studied here have a distributed inlet which is not used by all fluidized bed systems, there are such inlets as jet, impinging or spouting gas inlets which should also be tested.

Overall the modifications presented here are a first step in correcting the Navier-Stokes equations which will be an ongoing process not just within multiphase flows but with all fluid flows in general. The area of rapid granular gas flows is still an active area of research and will continue to be for some time. Its complexity, from the interaction of the particles that can behave like a liquid or a gas while still having properties of a solid within the same flow system, means there is still significant areas to research. The Kinetic Theory of Granular Flow (KTGF) is still flawed as it is based on certain assumptions from gas dynamics and further modifications need to be made to make the method work. Also, a lot of models are more based on empirical data rather than an actual understanding of the physics involved. While Lagrangian methods such as Computational Fluid Dynamics – Discrete Element Method have shown to give better results, the high computing cost still make this method prohibitively expensive and can only be currently used for lab-scale investigations and as a model validation tool. Until computing advances further, KTGF will still need to be continued to be developed as a large-scale simulation method.

REFERENCES

Abrahamsson, P. J., Sasic, S. and Rasmuson, A. (2014) 'On the continuum modeling of dense granular flow in high shear granulation', *Powder Technology*, 268, pp. 339-346.

Almohammed, N., Alobaid, F., Breuer, M. and Epple, B. (2014) 'A comparative study on the influence of the gas flow rate on the hydrodynamics of a gas–solid spouted fluidized bed using Euler–Euler and Euler–Lagrange/DEM models', *Powder Technology*, 264, pp. 343-364.

Anderson, D. M., McFadden, G. B. and Wheeler, A. A. (1997) 'Diffuse-Interface Methods in Fluid Mechanics', *National Institute if Standards and Technology*.

ANSYS® Academic Research Mechanical (2017) 'ANSYS Fluent 17.0 Theory Guide', *ANSYS, Inc.*, Release 17.0.

Berzi, D. (2014) 'Extended kinetic theory applied to dense, granular, simple shear flows', *Acta Mechanica*, 225(8), pp. 2191-2198.

Bird, R. B., Stewart, W. E. and Lightfoot, E. N. (2002) *Transport Phenomena*. 2nd Edition edn. New York: Wiley.

Bocquet, L., Losert, W., Schalk, D., Lubensky, T. C. and Gollub, J. P. (2001) 'Granular shear flow dynamics and forces: Experiment and continuum theory', *Physics Review E.*, 65, pp. 1-19.

Bokkers, G. A., van Sint Annaland, M. and Kuipers, J. A. M. (2004) 'Mixing and segregation in a bidisperse gas–solid fluidised bed: a numerical and experimental study', *Powder Technology*, 140(3), pp. 176-186.

Braun, M., Srinivasa, M. and Gohel, S. (2012) 'Validation of an efficient CFD-DEM model for large scale fluidized beds', ***Ninth International Conference on CFD in the Minirals and Process Industries***. CSIRO, Melbourne, Australia.

Brenner, H. (2005) 'Kinematics of volume transport', *Physica A: Statistical Mechanics and its Applications*, 349(1-2), pp. 11-59.

Brenner, H. (2009a) 'Bi-velocity hydrodynamics', *Physica A: Statistical Mechanics and its Applications*, 388(17), pp. 3391-3398.

Brenner, H. (2009b) 'Bi-velocity hydrodynamics. Multicomponent fluids', *International Journal of Engineering Science*, 47(9), pp. 902-929.

Brenner, H. (2010a) 'A critical test of bivelocity hydrodynamics for mixtures', *J Chem Phys*, 133(15), p. 154102.

Brenner, H. (2010b) 'Bi-velocity transport processes. Single-component liquid and gaseous continua', *Physica A: Statistical Mechanics and its Applications*, 389(7), pp. 1297-1316.

Brenner, H. (2012) 'Beyond Navier–Stokes', *International Journal of Engineering Science*, 54, pp. 67-98.

Brenner, H. (2013) 'Bivelocity hydrodynamics. Diffuse mass flux vs. diffuse volume flux', *Physica A: Statistical Mechanics and its Applications*, 392(4), pp. 558-566.

Campbell, C. S. (2006) 'Granular material flows – An overview', *Powder Technology*, 162(3), pp. 208-229.

Chen, X. and Wang, J. (2014) 'A comparison of two-fluid model, dense discrete particle model and CFD-DEM method for modeling impinging gas–solid flows', *Powder Technology*, 254, pp. 94-102.

Chialvo, S. and Sundaresan, S. (2013) 'A modified kinetic theory for frictional granular flows in dense and dilute regimes', *Physics of Fluids*, 25(7), p. 070603.

Crowe, C., Sommerfeld, M. and Tsuji, Y. (1998) *Multiphase Flows with Droplets and Particles*. London: CRC Press LLC.

Deen, N. G., Van Sint Annaland, M., Van der Hoef, M. A. and Kuipers, J. A. M. (2007) 'Review of discrete particle modeling of fluidized beds', *Chemical Engineering Science*, 62(1-2), pp. 28-44.

Elghobashi, S. (1994) 'On prediciting particle-laden turbuent flows', *Applied Scientific Research*, 52(4), pp. 309-329.

Enwald, H., Periano, E. and Almstedt, A.-E. (1996) 'Eularian two-phase flow theory applied to fluidization', *International Journal of Multiphase Flow*, 22, pp. 21-66.

Ergun, S. (1952) 'Fluid flow through packed columns', *Chemical Engineering and Processing*, 48, pp. 89-94.

Farzaneh, M., Almstedt, A.-E., Johnsson, F., Pallares, D. and Sasic, S. (2015) 'The crucial role of frictional stress models for simulation of bubbling fluidized beds', *Powder Technology*, 270, pp. 68-82.

Feng, Y. Q. and Yu, A. B. (2004a) 'Assessment of model formulations in the discrete particle simulation gas-solid flow', *Industrial and Engineering Chemistry Research*, 43, pp. 8378-8390.

Feng, Y. Q. and Yu, A. B. (2004b) 'Comments on “Discrete particle-continuum fluid modelling of gas–solid fluidised beds” by Kafui et al. [Chemical Engineering Scinece 57 (2002) 2395–2410]', *Chemical Engineering Science*, 59(3), pp. 719-722.

Gao, X., Wu, C., Cheng, Y.-w., Wang, L.-j. and Li, X. (2012) 'Experimental and numerical investigation of solid behavior in a gas-solid turbulent fluidized bed', *Powder Technology*, 228, pp. 1-13.

Geldart, D. (1973) 'Types of gas fluidization', *Powder Technology*, 7, pp. 285-292.

Gidaspow, D. (1994) *Multiphase Flow and Fluidization*. San Diego, USA: Academic Press.

Goldschmidt, M. J. V., Beetstra, R. and Kuipers, J. A. M. (2004) 'Hydrodynamic modelling of dense gas-fluidised beds: comparison and validation of 3D discrete particle and continuum models', *Powder Technology*, 142(1), pp. 23-47.

Goldschmidt, M. J. V., Kuipers, J. A. M. and Van Swaaij, W. P. M. (2001) 'Hydrodynamic modelling of dense gas-fluidised beds using the kinetic theory of granular flow: effect of coefficient of restitution on bed dynamics', *Chemical Engineering Science*, 56, pp. 571-578.

Goldschmidt, M. J. V., Link, J. M., Mellema, S. and Kuipers, J. A. M. (2003) 'Digital image analysis measurements of bed expansion and segregation dynamics in dense gas-fluidised beds', *Powder Technology*, 138(2-3), pp. 135-159.

Gorham, D. A. and Kharaz, A. H. (2000) 'The measurement of particle rebound characteristics', *Powder Technology*, 112, pp. 193-202.

Greenshields, C. J. and Reese, J. M. (2007) 'The structure of shock waves as a test of Brenner's modifications to the Navier–Stokes equations', *Journal of Fluid Mechanics*, 580, p. 407.

Guo, Y., Wassgren, C., Hancock, B., Ketterhagen, W. and Curtis, J. (2013) 'Granular shear flows of flat disks and elongated rods without and with friction', *Physics of Fluids*, 25(6), p. 063304.

Guo, Y., Wassgren, C., Ketterhagen, W., Hancock, B. and Curtis, J. (2012a) 'Some computational considerations associated with discrete element modeling of cylindrical particles', *Powder Technology*, 228, pp. 193-198.

Guo, Y., Wassgren, C., Ketterhagen, W., Hancock, B., James, B. and Curtis, J. (2012b) 'A numerical study of granular shear flows of rod-like particles using the discrete element method', *Journal of Fluid Mechanics*, 713, pp. 1-26.

Heida, M. and Málek, J. (2010) 'On compressible Korteweg fluid-like materials', *International Journal of Engineering Science*, 48(11), pp. 1313-1324.

Herzog, N., Schreiber, M., Egbers, C. and Krautz, H. J. (2012) 'A comparative study of different CFD-codes for numerical simulation of gas–solid fluidized bed hydrodynamics', *Computers & Chemical Engineering*, 39, pp. 41-46.

Hoomans, B. P. B., Kuipers, J. A. M. and Van Swaaij, W. P. M. (2000) 'Granular dynamics of segregation phenomena in bubbling gas-fluidized beds', *Powder Technology*, 109, pp. 41-48.

Hölzer, A. and Sommerfeld, M. (2008) 'New simple correlation formula for the drag coefficient of non-spherical particles', *Powder Technology*, 184(3), pp. 361-365.

Hölzer, A. and Sommerfeld, M. (2009) 'Lattice Boltzmann simulations to determine drag, lift and torque acting on non-spherical particles', *Computers & Fluids*, 38(3), pp. 572-589.

Jenkins, J. T. and Zhang, C. (2002) 'Kinetic theory for identical, frictional, nearly elastic spheres', *Physics of Fluids*, 14, pp. 1228-1235.

Jiang, Y., Qiu, G. and Wang, H. (2014) 'Modelling and experimental investigation of the full-loop gas–solid flow in a circulating fluidized bed with six cyclone separators', *Chemical Engineering Science*, 109, pp. 85-97.

Johnson, P. C. and Jackson, R. (1987) 'Frictional-collisional constitutive relations for granular materials, with application to plane shearing', *Journal of Fluid Mechanics*, 176, pp. 67-93.

Jop, P., Forterre, Y. and Pouliquen, O. (2006) 'A constitutive law for dense granular flows', *Nature*, 441, pp. 727-730.

Khalilitehrani, M., Abrahamsson, P. J. and Rasmuson, A. (2014) 'Modeling dilute and dense granular flows in a high shear granulator', *Powder Technology*, 263, pp. 45-49.

Kharaz, A. H., Gorham, D. A. and Salman, A. D. (2001) 'An experimental study of the elastic rebound of spheres', *Powder Technology*, 120, pp. 281-291.

Kodam, M., Bharadwaj, R., Curtis, J., Hancock, B. and Wassgren, C. (2009) 'Force model considerations for glued-sphere discrete element method simulations', *Chemical Engineering Science*, 64(15), pp. 3466-3475.

Korteweg, D. J. (1901) 'Sur la forme que prennent les équations du mouvement des fluides si l'on tient compte des forces capillaires causées par des variations de densité considérables mais continues et sur la théorie de la capillarité dans l'hypothèse d'une variation continue de la densité', *Archives Néerlandaises des sciences exactes et naturelles*, 2(6), pp. 1-24.

Kosinski, P., Balakin, B. V., Middha, P. and Hoffmann, A. C. (2014) 'Collisions between particles in multiphase flows: Focus on contact mechanics and heat conduction', *International Journal of Heat and Mass Transfer*, 70, pp. 674-687.

Li, T., Pannala, S. and Shahnam, M. (2014) 'CFD simulations of circulating fluidized bed risers, part II, evaluation of differences between 2D and 3D simulations', *Powder Technology*, 254, pp. 115-124.

Liu, X., Metzger, M. and Glasser, B. J. (2008) 'Granular and gas–particle flows in a channel with a bidisperse particle mixture', *Chemical Engineering Science*, 63(23), pp. 5696-5713.

Loha, C., Chattopadhyay, H. and Chatterjee, P. K. (2014) 'Effect of coefficient of restitution in Euler–Euler CFD simulation of fluidized-bed hydrodynamics', *Particuology*, 15, pp. 170-177.

Louge, M. Y., Mastorakos, E. and Jenkins, J. T. (1991) 'The role of particle collisions in pneumatic transport', *Journal of Fluid Mechanics*, 231, pp. 345-359.

Lun, C. K. K. and Savage, S. B. (1986) 'The effects of an impact velocity dependent coefficient of restitution on stresses developed by shear granular materials', *Acta Mechanica*, 63, pp. 15-44.

Lun, C. K. K., Savage, S. B., Jeffrey, D. J. and Chepurnity, N. (1984) 'Kinetic Theory for Granuler Flow: Inelastic Particles in Couette Flow and Slightly Inelastic Particles in a General Flow Field', *J. Fluid Mech.*, 140, pp. 223-256.

Makkawi, Y. T., Wright, P. C. and Ocone, R. (2006) 'The effect of friction and inter-particle cohesive forces on the hydrodynamics of gas–solid flow: A comparative analysis of theoretical predictions and experiments', *Powder Technology*, 163(1-2), pp. 69-79.

Massoudi, M. and Boyle, E. J. (2001) 'A continuum-kinetic theory approach to the rapid flow of granular materials: the effects of volume fraction gradient', *International Journal of Non-Linear Mechanics*, 36, pp. 637-648.

Mathiesen, V., Solberg, T. and Hjertager, B. H. (2000) 'Predictions of gas/particle flow with an Eulerian model including a realistic particle size distribution', *Powder Technology*, 112(34-45).

McKeen, T. and Pugsley, T. (2003) 'Simulation and experimental validation of a freely bubbling bed of FCC catalyst', *Powder Technology*, 129, pp. 139-152.

Mitrano, P. P., Dahl, S. R., Hilger, A. M., Ewasko, C. J. and Hrenya, C. M. (2013) 'Dual role of friction in granular flows: attenuation versus enhancement of instabilities', *Journal of Fluid Mechanics*, 729, pp. 484-495.

Murray, J. A., Benyahia, S., Metzger, P. and Hrenya, C. M. (2012) 'Continuum representation of a continuous size distribution of particles engaged in rapid granular flow', *Physics of Fluids*, 24(8), p. 083303.

Njobuenwu, D. O. and Fairweather, M. (2015) 'Dynamics of single, non-spherical ellipsoidal particles in a turbulent channel flow', *Chemical Engineering Science*, 123, pp. 265-282.

Oschmann, T., Hold, J. and Kruggel-Emden, H. (2014) 'Numerical investigation of mixing and orientation of non-spherical particles in a model type fluidized bed', *Powder Technology*, 258, pp. 304-323.

Ozahi, E., Gundogdu, M. Y. and Carpinlioglu, M. Ö. (2008) 'A Modification on Ergun's Correlation for Use in Cylindrical Packed Beds With Non-spherical Particles', *Advanced Powder Technology*, 19(4), pp. 369-381.

Passalacqua, A. and Fox, R. O. (2010) 'Numerical simulation of turnulent gas-particle flow in a riser using a quadrature-based moment method', *Chemical and Biological Engineering Conference Presentations and Proceedings*, 6.

Passalacqua, A. and Fox, R. O. (2011) 'Advanced continuum modelling of gas-particle flows beyond the hydrodynamic limit', *Applied Mathematical Modelling*, 35(4), pp. 1616-1627.

Peirano, E. and Leckner, B. (1998) 'Fundamentals of turbulent gas-solid flows applied to circulating fluidized bed combustion', *Progress in Energy and Combustion Science*, 24, pp. 259-296.

Rusche, H. (2002) *Dispersed two-phase flows at high phase fractions*. Doctor of Philosophy of the University of London and Diploma of Imperial College thesis. Imperial College of Science, Technology & Medicine.

Sau, D. C. and Biswal, K. C. (2011) 'Computational fluid dynamics and experimental study of the hydrodynamics of a gas-solid tapered fluidized bed', *Applied Mathematical Modelling*, 35, pp. 2265-2278.

Schiller, L. and Naumann, A. (1935) 'A drag coefficient correlation', *Zeitschrift des Vereins Deutscher Ingenieure*, 77, pp. 318-320.

Shuai, W., Zhenhua, H., Huilin, L., Goudong, L., Jiaxing, W. and Pengfei, X. (2012) 'A bubbling fluidization model using kinetic theory of rough spheres', *AIChE Journal*, 58(2), pp. 440-455.

Sun, J. and Battaglia, F. (2006) 'Hydrodynamic modeling of particle rotation for segregation in bubbling gas-fluidized beds', *Chemical Engineering Science*, 61(5), pp. 1470-1479.

Syamlal, M., Rogers, W. and O'Brien, T. J. (1993) 'MFIX documentation: Theory guide', *National Energy Technology Laboratory, Department of Energy, Technical Note DOE/METC-95/1013 and NTIS/DE95000031*.

Taghipour, F., Ellis, N. and Wong, C. (2005) 'Experimental and computational study of gas–solid fluidized bed hydrodynamics', *Chemical Engineering Science*, 60(24), pp. 6857-6867.

Truzzolillo, D. and Cipelletti, L. (2017) 'Off-equilibrium surface tension in miscible fluids', *The Royal Society of Chemistry*, 13, pp. 13-21.

Van Wachem, B. G. M. (2000) *Derivation, Implementation, and Validation of Computer Simulation Models for Gas-Solid Fluidized Beds*. Doctorate Degree thesis. Technical University of Delft.

Wen, C. Y. and Yu, Y. H. (1966) 'Mechanics of fluidization', *A.I.Ch.E*, 62, pp. 100-111.

Xu, B. H. and Yu, A. B. (1997) 'Numerical simulation of the gas-solid flow in a fluidized bed by combining discrete particle method with computational fluid dynamics', *Chemical Engineering Science*, 52(16), pp. 2785-2809.

Yang, L., Padding, J. T. and Kuipers, J. A. M. (2016) 'Modification of kinetic theory of granular flow for frictional spheres, Part 1: Two-fluid model derivation and numerical implimentation', *Chemical Engineering Science*, 152, pp. 767-782.

Yang, L., Padding, J. T. J. and Kuipers, J. A. M. H. (2017) 'Investigation of collisional parametersfor rough spheres in fluidized beds', *Powder Technology*, 316, pp. 256-264.

Zastawny, M., Mallouppas, G., Zhao, F. and van Wachem, B. (2012) 'Derivation of drag and lift force and torque coefficients for non-spherical particles in flows', *International Journal of Multiphase Flow*, 39, pp. 227-239.

Zhang, Y. and Reese, J. M. (2000) 'The influence of the drag force due to the interstitial gas on granular flows down a chute', *International Journal of Multiphase Flow*, 26, pp. 2049-2072.

Zhang, Y. and Reese, J. M. (2001) 'Particle-gas turbulence interactions in a kinetic theory approach to granular flows', *International Journal of Multiphase Flow*, 27, pp. 1945-1964.

Zhang, Y. and Reese, J. M. (2003) 'The drag force in two-fluid models of gas–solid flows', *Chemical Engineering Science*, 58(8), pp. 1641-1644.

Zhao, F. and van Wachem, B. G. M. (2013) 'Direct numerical simulation of ellipsoidal particles in turbulent channel flow', *Acta Mechanica*, 224(10), pp. 2331-2358.

Zhao, Y., Lu, B. and Zhong, Y. (2013) 'Euler–Euler modeling of a gas–solid bubbling fluidized bed with kinetic theory of rough particles', *Chemical Engineering Science*, 104, pp. 767-779.

Zhao, Y., Lu, B. and Zhong, Y. (2015) 'Influence of collisional parameters for rough particles on simulation of a gas-fluidized bed using a two-fluid model', *International Journal of Multiphase Flow*, 71, pp. 1-13.

Zhou, Z. Y., Kuang, S. B., Chu, K. W. and Yu, A. B. (2010) 'Discrete particle simulation of particle–fluid flow: model formulations and their applicability', *Journal of Fluid Mechanics*, 661, pp. 482-510.

Zhou, Z. Y., Pinson, D., Zou, R. P. and Yu, A. B. (2011) 'Discrete particle simulation of gas fluidization of ellipsoidal particles', *Chemical Engineering Science*, 66(23), pp. 6128-6145.

Zhu, H. P., Zhou, Z. Y., Yang, R. Y. and Yu, A. B. (2007) 'Discrete particle simulation of particulate systems: Theoretical developments', *Chemical Engineering Science*, 62(13), pp. 3378-3396.

Zhu, H. P., Zhou, Z. Y., Yang, R. Y. and Yu, A. B. (2008) 'Discrete particle simulation of particulate systems: A review of major applications and findings', *Chemical Engineering Science*, 63(23), pp. 5728-5770.